COMPOSITE HIGGS AND PHYSICS BEYOND THE STANDARD MODEL

By

AVIK BANERJEE

PHYS05201504020

Saha Institute of Nuclear Physics, Kolkata

A thesis submitted to the

Board of Studies in Physical Sciences

In partial fulfillment of requirements

for the Degree of

DOCTOR OF PHILOSOPHY

of

HOMI BHABHA NATIONAL INSTITUTE

November, 2020

Homi Bhabha National Institute

Recommendations of the Viva Voce Committee

As members of the Viva Voce Committee, we certify that we have read the dissertation prepared by **Avik Banerjee** entitled **"Composite Higgs and Physics Beyond the Standard Model"** and recommend that it maybe accepted as fulfilling the thesis requirement for the award of Degree of Doctor of Philosophy.

____ Date:

Chairman - Professor Prakash Mathews

____ Date:

Guide / Convener - Professor Gautam Bhattacharyya

____ Date:

Examiner - Prof. Amitava Raychaudhuri

____ Date:

Member 1 - Dr. Arnab Kundu

____ Date:

Member 2 - Dr. Koushik Dutta

____ Date:

Member 3 - Professor Anirban Kundu

Final approval and acceptance of this thesis is contingent upon the candidate's submission of the final copies of the thesis to HBNI.

I/We hereby certify that I/we have read this thesis prepared under my/our direction and recommend that it may be accepted as fulfilling the thesis requirement.

Date: 23/11/20
Place: Kolkata

Guide: Gautam Bhattacharyya

STATEMENT BY AUTHOR

This dissertation has been submitted in partial fulfillment of requirements for an advanced degree at Homi Bhabha National Institute (HBNI) and is deposited in the Library to be made available to borrowers under rules of the HBNI.

Brief quotations from this dissertation are allowable without special permission, provided that accurate acknowledgment of source is made. Requests for permission for extended quotation from or reproduction of this manuscript in whole or in part may be granted by the Competent Authority of HBNI when in his or her judgment the proposed use of the material is in the interests of scholarship. In all other instances, however, permission must be obtained from the author.

Avik Banerjee

Avik Banerjee

DECLARATION

I, hereby declare that the investigation presented in the thesis has been carried out by me. The work is original and has not been submitted earlier as a whole or in part for a degree / diploma at this or any other Institution / University.

Avik Banerjee

Avik Banerjee

LIST OF PUBLICATIONS

Publications included in the thesis

Journal:

1. "Improving Fine-tuning in Composite Higgs Models", Avik Banerjee, Gautam Bhattacharyya and Tirtha Sankar Ray, *Phys. Rev. D*, **2017**, *96*, 035040, [1703.08011].

2. "Constraining Composite Higgs Models using LHC data", Avik Banerjee, Gautam Bhattacharyya, Nilanjana Kumar and Tirtha Sankar Ray, *JHEP*, **2018**, *1803*, 062, [1712.07494].

3. "Impact of Yukawa-like dimension-five operators on the Georgi-Machacek model", Avik Banerjee, Gautam Bhattacharyya and Nilanjana Kumar, *Phys. Rev. D*, **2019**, *99*, 035028, [1901.01725].

4. "Dark matter seeping through dynamic gauge kinetic mixing", Avik Banerjee, Gautam Bhattacharyya, Debtosh Chowdhury and Yann Mambrini, *JCAP*, **2019**, *1912*, 009, [1905.11407].

5. "Probing the Higgs boson through Yukawa force", Avik Banerjee and Gautam Bhattacharyya, *to appear in Nucl. Phys. B*, [2006.01164].

Other publications (not included in the thesis)

1. "Clockworked VEVs and Neutrino Mass", Avik Banerjee, Subhajit Ghosh and Tirtha Sankar Ray, *JHEP*, **2018**, *1811*, 075, [1808.04010].

2. "SO(10) unification with horizontal symmetry", Avik Banerjee, Gautam Bhattacharyya and Palash B. Pal, *Phys. Rev. D*, **2020**, *102*, 015018, [2001.08762].

Avik Banerjee

Avik Banerjee

Dedicated to my parents

ACKNOWLEDGMENTS

I gratefully acknowledge the support and guidance received from my supervisor Prof. Gautam Bhattacharyya. I have learned a great many things from him about physics and beyond. His many suggestions on various academic issues or otherwise have led me towards a better career and life. I cherish the memories of our numerous discussion sessions. He has been, in the truest sense, a friend, philosopher and guide to me.

I am extremely grateful to have Dr. Tirtha Sankar Ray, Dr. Nilanjana Kumar, Prof. Yann Mambrini, Dr. Debtosh Chowdhury, Prof. Palash Baran Pal and Mr. (soon to be Dr.) Subhajit Ghosh as collaborators. Working with them have been a pleasurable and enlightening experience. I am especially indebted to Tirtha Da who formally introduced me to the world of particle physics during my Master's. I take this opportunity to thank everyone who taught me at some point of my academic life. I thank all the members of my doctoral committee for patiently evaluating my progress and providing me with important suggestions. I acknowledge the financial support from the Department of Atomic Energy, Govt of India, as well as funding from the J.C. Bose National Fellowship (SERB Grant No. SB/S2/JCB-062/2016) of Prof. Gautam Bhattacharyya from the Department of Science and Technology, Govt of India, and the Indo-French Center for Promotion of Advanced Research (IFCPAR/CEFIPRA Project No. 5404-2), in many occasions.

I thank all members of the Saha Institute of Nuclear Physics, in particular the Theory division, including the faculties, students, post-doctoral fellows and the non-academic staffs. I am especially thankful to Prof. Palash Baran Pal, Prof. Asit Kumar De and Dr. Koushik Dutta who were always available for any discussions. It would be an injustice not to mention the help received from Dola Di, Prodyut Da, Sangita Di, Arun Da and Pradip

Da on every official matters. I appreciate the help and support received from Dipankar Da, Amit Da, Aritra Da, Gautam Da, Aminul Da, Naosad Da, Chiru Da, Kuntal Da, Kumar Da, Mugdha Da, Sukannya Di, Rohit Da, Avik Da, Udit Da, Rome Da and Roopam Da. I am proud to have Augniva, Madhurima, Sajad, Aritra and Sourav as my Post-M.Sc. batchmates. I wish all the best to my academic junior-turned-friends Aranya, Bithika, Supriyo, Ritesh, Ayan, Arunima, Pritam, Khurshid, Sabyasachi, Avik, Upala and Sayan. I will always miss the vibrant atmosphere of the Theory scholar room and our frequent debates and discussions. I fondly remember the hours spent with Triparno Da, Mayukh Da, Ujjal Da, Tarak Da, Samadrita, Sneha, Nivedita Di, Siddhartha Da, Mathew, and all the SERC school batchmates at various conferences and workshops.

It is said that things are never quite as scary when you have friends beside you. The bunch of crazy persons with whom I can share every moments of joy and sorrow without a second thought are Sayan, Samik, Priyabrata, Rup, Koushik, Jeet, Arjun, Shankha Da, Archi Di and Sumeru. Over the years, some friends become part of our family. Subhajit and Ranita are always special in that sense. I gleefully cherish all the memories with them starting from my undergraduate days and wish them all the best in their own life. I am privileged to have the friendship and continued support from Srija, who has been tirelessly tolerating all of my scruples over a decade. Without their presence and never ending inspiration, a part of me would have been incomplete.

Finally all I can say about my family is that my parents and my loving brother are the backbone of my life and this thesis would not be completed without their endless support.

Avik Banerjee

CONTENTS

List of Figures

List of Tables

CHAPTER 7

CONCLUSIONS AND OUTLOOK

The Standard Model, despite its success at the LHC, is at best an effective field theory describing the physics at the electroweak scale. Among the major limitations of the SM, we have primarily concentrated on the issue of stability of the weak scale under quantum corrections, also known as the hierarchy problem. In the **Introduction**, we have outlined different popular attempts to address this problem. For the major part of this thesis, we have focused on a particular approach assuming the Higgs as a composite pseudo Nambu-Goldstone boson. The prototype of such a possibility already exists in nature in the form of pions in QCD. In the **Chapter 2**, we have reviewed how the ideas of QCD are extended to a larger setup describing the Higgs boson and electroweak interactions. With the example of minimal composite Higgs scenario, given by SO(5)/SO(4) coset, we observe that the radiatively generated Higgs potential is shielded from large UV corrections by the confining strong dynamics together with the approximate shift symmetry of the pNGBs, thereby solving the 'big' hierarchy problem. The matter sector of the SM is assumed to be elementary. In the partial compositeness paradigm they communicate with the strong sector only through some linear mixing with composite operators. This scenario has two major phenomenological consequences:

- It predicts the existence of exotic spin-1/2 and spin-1 resonance particles, especially colored fermions with masses around the compositeness scale. These are expected to be observed in the various on-going and proposed collider experiments.

- The couplings of the 125 GeV neutral Higgs boson with other SM particles are modified with respect to their corresponding SM values. Increasing luminosity at the subsequent runs of LHC would enable us to probe the Higgs couplings with finer precision to decide the fate of a large class of BSM theories.

In this thesis, we have explored models that enable a relaxation to the parameter space of these colored particles, as well as analyzed the allowed window of new physics in the Higgs couplings in the context of various strongly interacting electroweak symmetry breaking scenarios.

In the minimal composite Higgs setup, the generic expectation is that the light Higgs would require either large fine-tuning or light top-partner resonances, which is in severe tension with the current data. We have investigated in the **Chapter 3**, the next-to-minimal composite Higgs model with SO(6)/SO(5) coset, where pNGB sector is extended by a SM gauge singlet scalar in addition to the usual Higgs doublet. The ensuing doublet-singlet mixing provides a handle to accommodate heavier top-partners for a given value of the compositeness scale in comparison to the minimal case, thereby relaxing the tension with the direct LHC bounds. Major phenomenological consequences of this setup include sizable deviation of the Higgs couplings as well as significant compositeness of the top quark.

We have then systematically studied, in the **Chapter 4**, the modifications of the Higgs couplings in the light of LHC Run 1 and Run 2 data. Employing a model independent phenomenological Lagrangian and using the latest data from the ATLAS and CMS collaborations, we have obtained the allowed window for the BSM physics in the Higgs couplings with other SM particles. We have also provide future prospects of Higgs coupling measurements at the HL-LHC. Our results have shown that the discovery of the $ht\bar{t}$ and $hb\bar{b}$ couplings have major impact in constraining space for new physics. The LHC Run 2 data, in comparison to the Run 1 case, have narrowed down the 2σ window for new physics in the Yukawa couplings from 25% to less than 15% around the SM value. The limits on the hVV couplings from the LHC have become competitive with respect to the electroweak precision data. At the HL-LHC, the limits on hVV and $hf\bar{f}$ couplings would further sharpened to be within 5% of the SM reference point. The model independent bounds on the Higgs couplings are then interpreted in the context of composite Higgs scenario. We have considered cases, where the left- and right-handed third generation quarks are either in the $\mathbf{5}$ or in the symmetric $\mathbf{14}$ representation of SO(5). Going beyond the minimal $\mathbf{5}_L - \mathbf{5}_R$ representation, we have observed that in the *extended* models where either of the left- or right- handed quarks are embedded in the $\mathbf{14}$, more than one opearator may exist in the Lagrangian of the Yukawa sector. In such cases, the Yukawa couplings of the Higgs develop nontrivial modifications, depending on the details of the masses and decay constants of the top-partners. This can be contrasted with the minimal $\mathbf{5}_L - \mathbf{5}_R$ case where the modifications of the Yukawa coupling solely varies with the compositeness scale. The pattern of such modifications have been encoded through a generic phenomenological Lagrangian which may be applied to a wide class of such models. We have shown that the existence of more than one Yukawa operator allows the gauge and Yukawa coupling modifiers to get decorrelated, which leads to a relaxation of the bound on the compositeness scale:

$$f \gtrsim 660 \text{ GeV} \quad (\text{extended models}), \quad f \gtrsim 1.2 \text{ TeV} \quad (\text{MCHM}_{\mathbf{5}_\mathrm{L}-\mathbf{5}_\mathrm{R}}).$$

We have extended the analysis to the next-to-minimal model with coset $\mathrm{SO}(6)/\mathrm{SO}(5)$, for fermion-embeddings up to representations of dimension $\mathbf{20}$.

The search for additional Higgs bosons at the collider experiments, motivated from a large range of BSM scenarios is an important ongoing exercise. In the **Chapter 5**, we have analyzed the effects of including Yukawa-like dimension-five operators in the Georgi-Machacek model where the SM is augmented with triplet scalars. The speciality of this model is that, the Higgs potential preserves tree level custodial symmetry, even if the triplets receive vevs. We have investigated the constraints on the charged Higgs sector of the model, arising from radiative B-meson decays, neutral B-meson mixing and precision measurement of $Zb\bar{b}$ vertex. Our main observation is that the inclusion of the dimension-five operators have caused substantial alteration of the limits on the charged Higgs masses and the vevs of the triplets, derived otherwise using only the dimension-four operators. The allowed range for the couplings of the 125 GeV Higgs is also observed to be significantly dependent on the presence of higher dimensional operators.

Though we have focused mostly on the deviations of the Higgs couplings and the connection between the top-partners and the electroweak symmetry breaking dynamics, several other important questions concerning the composite Higgs scenarios are worthy of serious attention. While the modifications of the Higgs couplings from the SM predictions indicate towards the existence of new physics, tracking non-trivial momentum dependence of these couplings in future colliders, captured through the form factors, would have been a tell-tale signature of composite Higgs models. Besides, the UV completion of the partial compositeness paradigm and explanation of flavor hierarchy in this context pose interesting theoretical challenges, that require more dedicated study.

Apart from the Higgs physics, we have ventured into BSM theories that provide explanation for the existence of dark matter in the universe. In the **Chapter 6**, we specifically focused on the DM production by the freeze-in mechanism, which is motivated from the lack of any signature of the standard WIMP candidates in various ongoing experiments. The DM relic density in freeze-in scenario slowly builds up starting from the reheating era. The sharp distinction between the UV freeze-in scenario where the major amount of DM is produced during the inflaton dominated period, as opposed to more conventional IR freeze-in case, is discussed in details. We have demonstrated that the loop-driven kinetic mixing between visible and dark Abelian gauge bosons can facilitate the DM production by creating a 'dynamic' portal, whose interaction strength is sensitive on the energy of the processes. The required smallness of the interaction strength of the freeze-in portal, can be justified by a suppression arising from the mass of a heavy vector-like fermion along with a loop factor. The strong temperature dependence of the portal is responsible for most of the DM production during the early stages of reheating, leading to the UV freeze-in. A more sophisticated treatment of the UV freeze-in mechanism by including non-perturbative effects during the reheating epoch is worth pursuing. Although the freeze-in mechanism, in the first place, is put forward to account for the absence of any evidence in the direct search of dark matter, a serious attention is, nevertheless, required for the development of possible alternate strategies to probe such scenarios. All in all, continuous lookout for the signature of new physics at experiments in the energy and intensity frontiers together with various astrophysical observations will lead to more deeper understanding of the nature.

Summary

The Standard Model (SM) of particle physics is plagued with various serious limitations from both theoretical and observational perspectives. Several issues like the stability of the weak scale, or the existence of hypercharge Landau pole at some trans-Planckian scale, suggest that the SM has an ultraviolet cut-off. These theoretical issues as well as other observational facts, including the existence of non-zero neutrino mass and dark matter, are the primary motivations for investigating the physics beyond the SM (BSM). However, the continued absence of new physics at collider experiments complemented with lack of any pointers from astrophysical observations have considerably squeezed the window for the BSM physics. In this thesis we primarily address the hierarchy problem, armed with a composite pseudo Goldstone Higgs boson. The composite Higgs framework, where the Higgs originates as a pseudo Nambu-Goldstone boson of a spontaneously broken global symmetry in some strongly interacting sector, provides a consistent framework to shield the weak scale from the gauge hierarchy problem. The major phenomenological consequences of this setup include existence of exotic spin-1/2 and spin-1 particles and finite deviations of the Higgs couplings from their SM reference values. In the precision Higgs era following the discovery of the Higgs boson at 125 GeV and its Yukawa couplings with

the third generation quarks, a set of new constraints from the Higgs physics along with the electroweak precision constraints are imposed on BSM scenarios. We confront the composite Higgs models and associated extensions using the latest experimental results on the Higgs physics. The connection between a light Higgs boson and a light top-partner resonance in such models has been studied in details and, possible avenues departing from such strong correlations have been suggested. Modifications of the Higgs couplings in the various composite Higgs frameworks are systematically studied and constrained using the current data. We have also explored scenarios involving triplet-Higgs boson à la Georgi and Machacek and investigated its phenomenology in the presence of higher dimensional operators. The BSM solutions to the hierarchy problem admit a number of new particles that can possibly explain the presence of significant amount of non-baryonic matter in the total energy budget of the universe. Nevertheless, the most popular models of dark matter with weak scale masses are in severe tension with the dark matter direct search experiments. Motivated by the scarcity of any experimental signature regarding the nature of the dark matter, we explore an alternate scenario where the dark matter is frozen 'in' the early universe by an energy dependent portal interaction with the visible matter.

Chapter 1

Introduction

The discovery of the Higgs boson at the Large Hadron Collider (LHC) [1, 2] marks a new era in the field of particle physics. The Standard Model (SM) of particle physics comes to a completion and the search for the physics beyond the Standard Model (BSM) begins. Several theoretical issues, for example, the stability of the weak scale from any high scale dynamics, or the existence of the hypercharge Landau pole [3] at a super-Planckian scale demanding nontrivial physics at higher scales, indicate that the SM is an effective theory. Besides these theoretical issues, several experimental observations like the confirmation of neutrino oscillation indicating the existence of non-zero neutrino mass [4–7] , the presence of dark matter [8–11], the fact that the universe is dominated with matter in comparison to the anti-matter [12–14], etc., demands an extension of the SM from its current avatar. These and associated phenomenological issues remain the main driving force behind search for the BSM physics over the past decades. In the first part of this thesis, we will primarily focus on the problem related to the stability of the weak scale and address this issue with the assumption that the Higgs boson is a composite object. In the second part, we present a particular model of dark matter (DM), shedding some light on the freeze-in mechanism of DM production in the early universe.

1.1 The hierarchy problem and popular solutions

To begin with, we briefly describe the issue of stability of the weak scale under quantum corrections, which is known as the 'Hierarchy problem'. The only relevant operator containing a mass dimensional parameter in the SM is the quadratic operator associated with the Higgs mass as given by

$$\mathcal{L} = \mu^2 H^\dagger H \,. \tag{1.1}$$

The parameter μ^2, being the only dimensionful parameter sets the electroweak scale and determines the tree level masses of all the massive SM particles. The measurements of the weak gauge boson masses and the Higgs mass in the experiments yield the value of μ^2 *aka* the electroweak scale to be around $(100~\mathrm{GeV})^2$. However, to predict the physical masses of different SM particles and match with their experimentally measured values, one needs to take into account the effects of quantum corrections involving higher order loop diagrams. Loop corrections to the fermion or gauge boson masses in the SM are found to be proportional to their masses themselves as follows:

$$\delta m_f \sim \frac{m_f}{16\pi^2} \ln\left(\frac{\Lambda_{\mathrm{UV}}^2}{m_f^2}\right) , \qquad \delta M_{W,Z}^2 \sim \frac{M_{W,Z}^2}{16\pi^2} \ln\left(\frac{\Lambda_{\mathrm{UV}}^2}{M_{W,Z}^2}\right) , \tag{1.2}$$

where Λ_{UV} denotes the ultra-violet cut-off scale of the SM. The reason for this behavior can be explained in view of the 't Hooft's idea of 'technical naturalness' [15]. According to this idea, a small parameter in a theory is technically natural, if the theory possesses an enhanced symmetry in the limit where the concerned parameter vanishes. The real

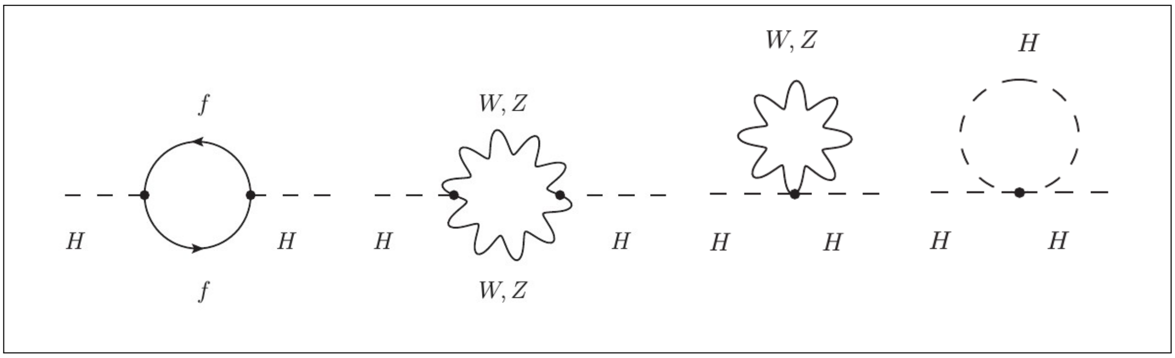

Figure 1.1: *One loop corrections to Higgs mass in the SM. Diagram involving the top quark has the largest contribution to Higgs mass correction due to large Yukawa coupling.*

significance of ‘technical naturalness’ lies in the fact that the smallness of the parameter does not get spoiled by quantum corrections, due to the underlying symmetry protection. In the limit of vanishing fermion (gauge boson) masses, the theories involving them enjoy a chiral (gauge) symmetry. Due to these underlying symmetries, masses of fermions (gauge bosons) are stable under quantum corrections and are technically natural.

On the contrary, situation with the Higgs mass, or for that matter the mass of any elementary scalar field is completely different. For example in the SM, the mass of the Higgs boson receives loop corrections from the Higgs self-interaction and interactions with the weak gauge bosons, quarks, and leptons, as shown in Fig. 1.1. Simple dimension counting shows that the contributions to the Higgs mass coming from these loops are quadratically sensitive to the hard cut-off scale, introduced in order to tame the quadratic divergences. The one loop contributions to the Higgs mass can be expressed as

$$\delta m_H^2 \simeq \frac{\Lambda_{\rm UV}^2}{16\pi^2}(-c_1 y_t^2 + c_2\lambda + c_3 g^2)\ , \tag{1.3}$$

where $c_{1,2,3}$ are positive $\mathcal{O}(1)$ constants coming from the details of the loop integrations. Note that among the three terms, the maximum contribution will come from the top quark loop due to its large Yukawa coupling in comparison to that of the other quarks and leptons, the gauge couplings and the Higgs self-coupling. Clearly this result is fundamentally different from the cases for fermion and gauge bosons, as it depends on a completely new energy scale rather than depending on the Higgs mass itself. For the purpose of illustration we show that with $\Lambda_{\rm UV} \sim 10^{18}$ GeV, the correction is much larger than the observed Higgs mass ($\delta m_H^2 \gg m_H^2 \simeq (125 \text{ GeV})^2$). The basic reason behind this instability is the fact that the Higgs mass parameter is not technically natural, because the symmetry of the underlying theory does not get enhanced in the limit of the vanishing Higgs mass. That explains why the quantum corrections to the Higgs mass is independent of the mass itself. The cut-off scale can be interpreted as the scale where the SM alone stops to work as a valid effective theory and new dynamics beyond the SM kicks in. There are plenty of motivations to assume the existence of such a high energy scale above the scale of electroweak symmetry breaking (EWSB). Obvious examples of such new physics scales constitute Planck scale (M_p) associated with the scale of quantum gravity, trans-Planckian hypercharge Landau pole, mass of the right handed neutrino, etc. Therefore, to reproduce the observed Higgs mass, it is essential to make a tuning between the SM contribution and that coming from the *a priori* unrelated BSM physics above the $\Lambda_{\rm UV}$. Assuming $\Lambda_{\rm UV} \sim M_p$, one can estimate that a fine tuned cancellation of around one part in 10^{32} is required between the SM and BSM contributions. This goes quite contrary to our common intuition that the microscopic details of the physics at smaller length scales can be coarse-grained and has no impact on the physics at larger length scales (*e.g.* atomic physics does not depend on the details of the internal structure of the protons and neutrons). This states the crux of the 'hierarchy' problem.

It is, however, worthy to note a few points regarding this issue. First, in the dimensional regularization scheme both logarithmic and quadratic divergences appear as $1/\epsilon$ pole, in contrast with the cut-off regularization method. Although, a specific choice of regularization scheme seems to be the apparent solution for the hierarchy problem, in reality it does not improve anything. The inherent issue is not with cancellation of the divergence, rather the problem is with the large finite part of the correction that is quadratically sensitive to the scale at which new physics couples to the SM. If for the moment we assume that there exists no other physical energy scales other than the electroweak scale, there would not be any hierarchy problem. The Higgs mass corrections in that case would be proportional to the square of the weak scale itself and only $\mathcal{O}(1)$ cancellation between different parameters of the SM would have been required to reproduce the observed value of m_H. On the other hand existence of any new scale hierarchically larger than the weak scale will destabilize this scenario and introduce large tuning. In order to further clarify the issue let us take a simple example, where the SM particle content is extended with a real scalar field (η) with mass $m_\eta^2 \gg \mu^2$, which is a singlet under the SM gauge group. The Lagrangian for such a singlet scalar with a quartic coupling with the SM Higgs boson can be written as

$$\mathcal{L}_\eta = \frac{1}{2}\partial^\mu \eta \partial_\mu \eta - \frac{1}{2} m_\eta^2 \eta^2 + \lambda_{H\eta} |H|^2 \eta^2 \,. \tag{1.4}$$

The one loop correction to the Higgs mass coming from this additional coupling depends quadratically on the mass of the scalar η as

$$\delta m_H^2 \propto \frac{\lambda_{H\eta} m_\eta^2}{16\pi^2} \gg m_H^2 \,. \tag{1.5}$$

Clearly, the correction to Higgs mass is sensitive to the new mass scale introduced in the model, while the divergence ($1/\epsilon$ pole in the dimensional regularization scheme) can be absorbed by a suitable counterterm. Note that even if new physics does not couple to the

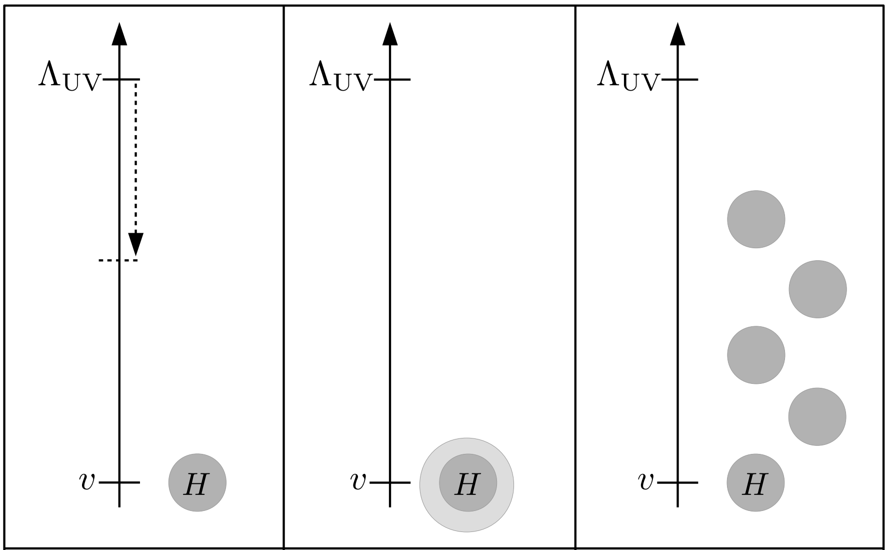

Cut-off lowering	Symmetry protection	Vacuum selection
Technicolor Compositeness	Supersymmetry Shift symmetry Discrete symmetry 5D gauge symmetry	Anthropic selection Relaxion NNaturalness

Figure 1.2: *Categorization of popular solutions to address the hierarchy problem.*

Higgs boson directly but couples to other SM particles, the same quadratic sensitivity will appear through higher order loop diagrams, if not through one loop.

Hierarchy problem provides a guideline to build theories of electroweak symmetry breaking beyond the SM. Are the SM gauge forces fundamental or they originate from some underlying UV dynamics? Is the Higgs boson elementary or a composite object? Even if the Higgs boson is an elementary object, is it the only neutral scalar that Nature offered us? All these questions are intimately linked to the dynamics of EWSB. Plausible avenues addressing the hierarchy issue sheds some light on these questions as well. Possibly, the most natural approach to address this issue is to provide an additional symmetry to protect the Higgs mass. While symmetry principle constitutes the major category of solutions, there exists other approaches to dynamically generate the weak scale in the presence of higher energy scales. Here we divide the well-explored solutions of the hierarchy problem in three major categories (see Fig. 1.2), which we discuss below with example models in each category.

Symmetry protection: This category of solution involves making the Higgs mass parameter technically natural, in analogy to the cases for the fermions and gauge bosons, by adding a symmetry associated with it. The symmetry in question can be continuous or discrete, local or global depending on the model in question. We itemize below different examples for each of these cases.

- Supersymmetry: Supersymmetry is by far the most well discussed solution to the hierarchy issue in the literature [16–21]. It is an extension of the standard Poincaré algebra to include a symmetry transformation between the fermions and the bosons. If we demand that nature is supersymmetry invariant, we expect to have bosonic (fermionic) partners of all the SM fermions (bosons), with same mass and quantum numbers. Therefore, the one loop contributions to the Higgs mass coming from the SM particles will get canceled by the loops containing their corresponding superpartners due to a sign difference coming from integrating fermionic and bosonic loops. Needless to say, this is an artefact of the underlying symmetry of the theory, which is Supersymmetry. More precisely, here the Higgs mass is protected and therefore technically natural due to the chiral symmetry of its fermionic superpartner.

- Global / local symmetries: The global continuous symmetries can also be used to make the Higgs mass technically natural. One of the interesting possibilities, that we will explore in more details in this thesis, is usage of the shift symmetry of the Goldstone bosons [22–28]. Higher dimensional gauge symmetry is also useful in this context, and is explored in the literature quite exhaustively [29–32]. Analogous to the supersymmetry case, the common feature for all of these cases is the presence of colored partners of the SM particles, which, however, is in tension with the latest LHC data.

- Discrete symmetry: Third possibility of symmetry protection using discrete symmetries is rather modern and is motivated by the absence of any signals of new physics at the LHC [33–36]. The basic idea is to invoke a discrete symmetry between the SM particles and their partners (*e.g.* a $\mathbb{Z}_2$ symmetry). As a result, contributions to the Higgs mass coming from SM loops can be canceled by that of their discrete partners. However, the important difference of this class of models from the previous two classes is that the partners, being related to the SM particles by discrete transformations, may not necessarily carry other SM quantum numbers. Therefore, in contrast with the previous two scenarios, the discrete partners of the SM particles can have relatively smaller masses while evading otherwise strong bounds imposed by the LHC data.

Cut-off lowering: As we have discussed earlier, the main point of the hierarchy problem is the quadratic sensitivity of the Higgs mass to the UV cut-off of the theory. Thus lowering the cut-off of the SM as an effective theory and envisaging a more fundamental theory beyond that cut-off constitutes a motivating solution. Major example in this category is the Technicolor models [37–41], which employ a confining theory, analogous to the Quantum Chromodynamics (QCD), giving rise to the electroweak scale by dimensional transmutation. However, this scenario does not predict the existence of any candidate for the observed Higgs-like spin zero boson. Furthermore, vanilla technicolor models got ruled out from the electroweak precision data from the LEP [42], much before the discovery of the Higgs boson. Composite Higgs models, as a modified *avatar* of the old technicolor idea will be our focus of discussion throughout the major part of this thesis.

Vacuum selection: The idea involves selection of electroweak vacuum by scanning over a bunch of vacuua statistically distributed at different scales. Although the old idea of anthropic selection [43] has lost much attention, relatively modern examples involving some dynamics for the selection of the electroweak vacuum are quite interesting. Relaxion models [44–46], NNaturalness model [47], etc. fall in this later category.

In this thesis we will concentrate on the composite pseudo Nambu-Goldstone Higgs to address the hierarchy problem.

1.2 Other BSM motivations: Dark matter and all that

While the hierarchy problem appears to be one of the major motivations from the theoretical point of view to build models beyond the SM, there exists a lot of other incentives for constructing BSM extensions, many of them driven by the experimental observations. We list some of the major motivations to investigate BSM physics in Table 1.1. Note that most of the BSM avenues to address the hierarchy problem add more structures by extending the SM gauge symmetry and particle content. This aspect provides a possibility that the same theories may have the potential to account for other limitations of the SM, thereby serving both purposes at one shot.

Fritz Zwicky, in his seminal 1933 paper [8], concluded that the amount of dark matter present in the Coma cluster is much greater than that of the luminous or visible matter. Loads of indirect confirmations like the Cosmic Microwave Background measurements [11] and astrophysical observations [9, 10] provide enough evidences for the significant

Motivations for BSM physics	
Hierarchy problem	Non-zero neutrino mass
Quantum theory of Gravity	Nature of dark matter
Strong CP problem	Inadequate Baryon-asymmetry
Hypercharge Landau pole	Why three generations?
Unification of forces	Cosmological inflation
...	...

Table 1.1: *Some major limitations of the SM and motivations to search for BSM physics.*

presence of DM in the total energy density of the Universe. However, the nature of the DM is still an open question. The Weakly Interacting Massive Particles (WIMP) constitute the maximally explored genre of DM candidates, primarily because of its simplicity and predictability. The WIMP candidates are prevalent in many well-known BSM theories, which are motivated from other perspectives. For examples, WIMP scenarios arising from supersymmetric candidates to Kaluza-Klein excitations, which justify freeze out of DM from the primordial plasma after a long period of thermal equilibrium [48, 49], are crying out for verification even otherwise. On the contrary, the 'null results' from the DM direct search experiments like XENON100 [50], LUX [51], PandaX-II [52] or more recently XENON1T [53], compel us to look for alternative scenarios, where the DM is assumed to be produced 'in' the process of progressing towards thermal equilibrium [54], rather than being perceived as frozen 'out' from the thermal bath. Among the various possibilities for freeze-in type scenarios of DM production, interesting models should naturally predict why the DM is out of the equilibrium with the primordial plasma. We aim to discuss a freeze-in scenario of DM production, which provides a justification of the above mentioned question within a natural framework.

1.3 Organization of the thesis

A major part of this thesis is devoted to address a theoretical issue of the SM, viz. the hierarchy problem. We explore the composite pseudo Nambu-Goldstone Higgs model as a solution to the hierarchy problem. The rest of the thesis is focused on an observational limitation of the SM, the substantial dark matter abundance in the universe. We discuss in particular, the freeze-in mechanism of dark matter production in the early universe. We have employed novel model building techniques beyond the SM as well as effective field theory frameworks for our purpose.

The plan of the thesis is given below:

- In Chapter 2, a brief review of the basic ideas of composite Higgs framework is given followed by the example of the minimal composite Higgs model. The origin of the Higgs potential and the mechanism of EWSB are also discussed. We explicitly show the relation between the spectrum of the composite particles with the Higgs mass, and the tension therein for this category of models.

- In Chapter 3 we present the next-to-minimal composite Higgs model, where the scalar sector is enhanced by a SM singlet along with the usual Higgs doublet. We then describe how a doublet-singlet mixing can provide a handle to accommodate heavier top-partners, thereby releasing the strong connection between a light Higgs and light top-partners. We also comment on the phenomenological consequences of this model.

- One of the major signature for the composite Higgs scenario is the modification of the neutral Higgs couplings with other SM particles. In Chapter 4, we discuss these modifications in the context of both minimal and next-to-minimal composite Higgs models and provide bounds on them in the light of Run 1 and Run 2 data from the LHC.

- We explore the significance of higher dimensional effective operators in a triplet-Higgs scenario (Georgi-Machacek model), in Chapter 5. Specifically we use flavor and electroweak observables to constrain the charged Higgs sector in the presence of higher dimensional operators.

- Moving on from the Higgs physics, in Chapter 6, we concentrate on explaining the substantial relic abundance of the dark matter in the universe. We explore a novel production mechanism for the DM in the early universe by freeze-in mechanism employing an energy dependent portal between the dark sector and the visible sector.

- In Chapter 7 we draw our conclusions and outline future scopes in these directions.

CHAPTER 2

THE COMPOSITE NAMBU-GOLDSTONE HIGGS: A BRIEF REVIEW

The brief review presented in this chapter is based on the existing literatures on the composite pseudo Nambu-Goldstone Higgs framework.

In the composite Higgs scenario, the Higgs boson originates as a pseudo Nambu-Goldstone boson (pNGB), arising from the spontaneous breaking of a global symmetry associated with the condensation of a strongly interacting sector [22–24, 55–59]. This setup is quite analogous to the familiar case of QCD, where the chiral symmetry of the quarks break spontaneously around the QCD condensation scale ($\Lambda_{\rm QCD}$). The pNGBs that arise in this case can be identified as the usual pions, which are bound states formed by quark anti-quark condensates. Similarly, the pNGB Higgs which is a bound state of some hypothetical strong dynamics is assumed to have a finite geometric size, inverse of which sets the compositeness scale ($l_H^{-1} \sim m_*$) of the strong sector. The composite pNGB Higgs framework has the potential to solve the hierarchy problem in an elegant way, that has been

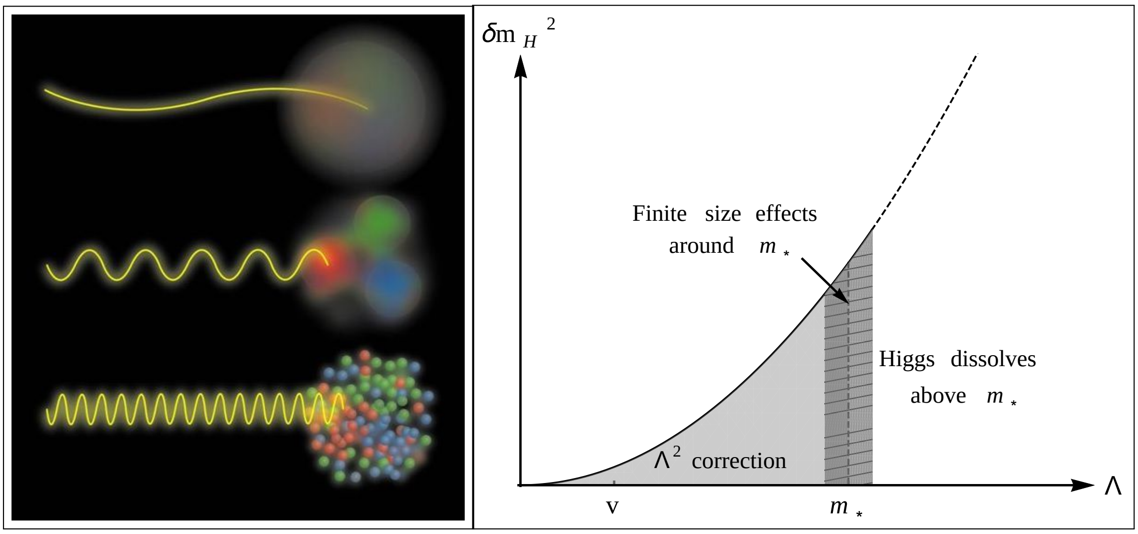

Figure 2.1: *Left panel shows the behaviour of a composite object under a probe particle with different wavelengths. As long as the virtual probe particles have wavelength $\lambda \gg l_H$, the Higgs boson behaves as an elementary particle. If $\lambda \lesssim l_H$, Higgs is resolved into its substructures. The right panel qualitatively shows the quantum corrections to the mass of the composite Higgs as a function of energy scales.*

illustrated qualitatively in the Fig. 2.1 and described below.

Role of compositeness: If the energy of the virtual particles running in the loops, as shown in Fig. 1.1, is much lower than the scale of the compositeness (in other words, if the wavelength of the probe particle is much bigger than the finite geometric dimension of the Higgs), the Higgs boson effectively behaves as an elementary entity and receives corrections to its mass with quadratic UV sensitivity. This region is marked with a grey shade in the right panel of Fig. 2.1. However, if the loop-particles have energies higher than the compositeness scale, they would start probing the microscopic substructure of the Higgs boson. Much above the compositeness scale, Higgs boson would dissolve into its fundamental constituents, consequently the loop processes in question would not contribute to the Higgs mass. Therefore, the UV cut-off of composite Higgs framework is essentially lowered down to the compositeness scale, which is assumed to be around few TeV, thereby solving the 'big hierarchy' problem.

Role of Goldstone nature: Yet, one needs to explain the 'little hierarchy' *i.e.* why the mass of the Higgs boson is much smaller than the condensation scale of the strong sector[1]. Like pions in QCD, the Goldstone nature of the Higgs ensures this relative lightness compared to the order TeV compositeness scale. The approximate shift symmetry of the pNGB Higgs protects the Higgs mass from sensitivity to the compositeness scale. However, we shall see later that simply having the shift symmetry is in general not enough to reproduce the observed Higgs mass. Additional mechanisms, like collective symmetry breaking or imposing some sum rules are required for that purpose.

2.1 From Technicolor to composite Higgs

The predecessor of the modern composite Higgs scenario is 'Technicolor' model which provides an explanation for the generation of the weak scale [37–41]. Original technicolor model is composed of a strong sector sitting near a fixed point at the UV scale $\Lambda_{\rm UV}$. The dimensional transmutation mechanism generates the confinement scale by the slow running of the strong coupling constant towards the IR as

$$m_*^2 \sim \Lambda_{\rm UV}^2 \exp\left(-16\pi^2/g_{\rm UV}^2\right) . \tag{2.1}$$

Clearly, an exponential hierarchy is obtained between the confinement scale and the UV cut-off, similar to the case of QCD. The technicolor sector, which is nothing but a scaled up version of QCD, confines around the weak scale and provides mass to the weak gauge

[1]Natural expectation is that, the bound states originating from a strong sector have masses around the condensation scale. For example, in the familiar case of QCD which confines at around $\Lambda_{\rm QCD} \sim 200$ MeV, the bound states like proton and neutron have masses of the order of a GeV.

bosons. It assumes the existence of some hypothetical quark-like fermions, called techniquarks which are charged under the technicolor gauge group. The condensates formed by this techniquarks and their anti-particles act as the would be Goldstone bosons to give mass to the W and Z bosons.

One of the major issue with the original technicolor scenario is that it does not predict any suitable candidate for the observed spin-0 boson with mass around 125 GeV. However, even before the Higgs discovery at the LHC, this scenario was ruled out by the precision measurements of the electroweak oblique parameters at the LEP. Specifically speaking, technicolor setup induces an unacceptably large contribution to the oblique S-parameter through the exchange of virtual techniquarks. An effective operator depicting this large contribution to the S-parameter can be obtained after integrating out the heavy techniquarks as [60, 61]

$$\mathcal{O} \sim \frac{1}{f^2} H^\dagger W_{\mu\nu} B^{\mu\nu} H \,, \tag{2.2}$$

where f is the decay constant associated with the confinement of the strong sector. Since, the condensation in the technicolor scenario occurs around the weak scale itself, *i.e.* $v \sim f$, the operator in Eq. (2.2) gives very large contribution to the S-parameter, in conflict with the data [42].

The modern avatars of composite Higgs models are built after incorporating the lessons taken from the drawbacks of the technicolor theories. The problem in technicolor theory that strong dynamics *directly* participates in EWSB, is solved by constructing a theory where $v \ll f$. The strong dynamics is only responsible to produce a set of pNGBs by spontaneous breaking of some global symmetry, which in turn may trigger EWSB.

2.2 Anatomy of composite Higgs framework

Here we present the structure of a generic composite pNGB Higgs framework [55, 56, 58]. We will work in four spacetime dimension and assume the existence of a strongly interacting composite sector which confines near the TeV scale. We will also assume the presence of an purely elementary sector containing SM matter content, except the Higgs boson and possibly the right-handed component of the top quark.

2.2.1 Coset structure

Some global symmetry (G) associated with the composite sector is assumed to be spontaneously broken at a scale f when the strong dynamics confine. The vacuum is invariant only under a subgroup $H \subset G$. This leads to the generation of Goldstone bosons in the coset space G/H. The number of such NGBs are given by the number of broken generators as

$$\#\mathrm{NGB} = \dim(G) - \dim(H), \tag{2.3}$$

where $\dim(G)$ denotes the number of generators of the group G. The NGBs ($\pi_{\hat{a}}$) can be conveniently parametrized in terms of the broken generators ($T^{\hat{a}}$) of G in a matrix, known as the Goldstone matrix as follows [62, 63]:

$$U = \exp\left[i\frac{\sqrt{2}}{f}\pi_{\hat{a}}(x)T^{\hat{a}}\right]. \tag{2.4}$$

One can always define a specific vacuum Σ_0, invariant under H, which can be used to parametrize the NGBs in terms of a linear representation as, $\Sigma = U\Sigma_0$[2]. The lowest order

[2]Since $T^a\Sigma_0 = 0$, $T^{\hat{a}}\Sigma_0 \neq 0$, where T^a ($T^{\hat{a}}$) are the unbroken (broken) generators of G, Σ can be expressed solely in terms of the broken generators through the matrix U.

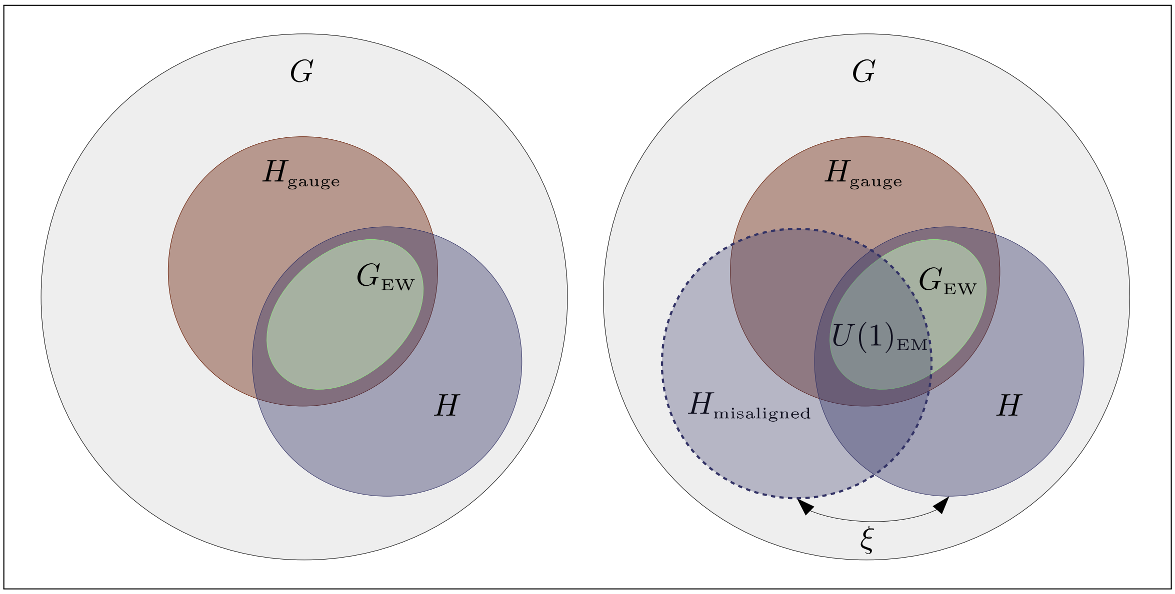

Figure 2.2: *Coset structure of the strong sector is displayed. Left panel shows spontaneous breaking of a global symmetry G to its subgroup H, while only $H_{\text{gauge}} \supset G_{\text{EW}}$ is gauged. Right panel shows misalignment of the vacuum (parametrized by the tuning parameter ξ) due to the explicit G breaking by gauging. The remnant gauge symmetry after vacuum misalignment $H \cap H_{\text{gauge}} \cap H_{\text{misaligned}}$ should contain $\mathrm{U}(1)_{\text{EM}}$ as a subgroup.*

Lagrangian for the NGBs can be written in terms of Σ as

$$\mathcal{L} = \frac{f^2}{2} \left(\partial_\mu \Sigma\right)^\dagger \left(\partial^\mu \Sigma\right) \simeq \frac{1}{2} \left(\partial_\mu \pi_{\hat{a}}\right) \left(\partial^\mu \pi_{\hat{a}}\right) + \ldots \tag{2.5}$$

At this stage, clearly the NGBs enjoy a shift symmetry which demands presence of only the derivative interactions. The shift symmetry also ensures that the vev of the NGBs can be rotated away by a global transformation and therefore has no physically relevant consequences. However, in addition to the spontaneous symmetry breaking, gauging a subgroup H_{gauge} of G can explicitly break the full global symmetry G. The structure of spontaneous and explicit breaking of G is pictorially shown in the left panel of Fig. 2.2. Explicit breaking of G may radiatively induce a potential for the Goldstones by breaking in turn the shift symmetry of the NGBs and converting them to pseudo Nambu-Goldstone bosons. Obviously, the gauging of H_{gauge} introduces $\dim(H_{\text{gauge}})$ number of gauge bosons, out of which $[\dim(H_{\text{gauge}}) - \dim(H_{\text{gauge}} \cap H)]$ number of gauge bosons will be massive by eating up some of the NGBs. The number of left over NGBs is then given by

$$\#\text{NGB} = [\dim(G) - \dim(H)] - [\dim(H_{\text{gauge}}) - \dim(H_{\text{gauge}} \cap H)] \,. \tag{2.6}$$

Now let us take the simple example of QCD. In case of QCD with two quark flavors, the global symmetry G can be identified as the $\text{SU}(2)_L \times \text{SU}(2)_R$, chiral symmetry of quarks which spontaneously breaks down to a diagonal $\text{SU}(2)_V$ around Λ_{QCD}. This yields three NGBs which can be identified with two charged ($\pi^{\pm}$) and one neutral (π^0) pions. The electroweak interactions of the quarks are introduced by identifying H_{gauge} with the electroweak gauge group, which explicitly breaks the chiral symmetry of the quarks. Now, coming back to the composite Higgs scenario, we observe that there are two important requirements for the choice of G as follows:

- SM electroweak group ($G_{\text{EW}} \equiv \text{SU}(2)_L \times \text{U}(1)_Y$) must be embedded as a subgroup of the unbroken $H_{\text{gauge}} \cap H \supset G_{\text{EW}}$.

- There should be at least four NGBs present in the G/H coset which can form a $\text{SU}(2)_L$ Higgs doublet to trigger EWSB at low energies.

- A third requirement, motivated from the electroweak precision data from LEP, is to preserve the global custodial symmetry in the Higgs sector.

The minimal coset structure, compatible with the above three requirements, is given by $\text{SO}(5)/\text{SO}(4)$, which forms the minimal composite Higgs model.

2.2.2 Vacuum misalignment mechanism

The right panel of the Fig. 2.2 illustrates the vacuum misalignment mechanism [22–24], which is crucial for the working of composite Higgs scenario. We have already stated that without any explicit G breaking, the NGBs can not achieve any potential and their vev is completely arbitrary and unobservable. On the other hand, the explicit G breaking by gauging the subgroup $H_{\rm gauge}$ induces radiative potential by Coleman-Weinberg mechanism [64]. The interactions between the composite degrees of freedom with the elementary fermions also break the global symmetry of the strong sector explicitly and contribute to the loop generated potential. The potential thus formed may tilt the vacuum with respect to H. As shown in the right panel of Fig. 2.2, the new vacuum, defined by non-zero vevs of the pNGBs will be invariant under $H_{\rm misaligned}$. This mechanism is called vacuum misalignment and the amount of misalignment is proportional to the vev of the pNGBs. As an example, let us take SO(3)/SO(2) as the coset space, which is pictorially shown by the surface of the sphere in Fig. 2.3. The generators of the SO(3) rotations are given by

$$T^1 = \begin{pmatrix} 0 & 0 & 1 \\ 0 & 0 & 0 \\ -1 & 0 & 0 \end{pmatrix}, \qquad T^2 = \begin{pmatrix} 0 & 0 & 0 \\ 0 & 0 & 1 \\ 0 & -1 & 0 \end{pmatrix}, \qquad T^3 = \begin{pmatrix} 0 & 1 & 0 \\ -1 & 0 & 0 \\ 0 & 0 & 0 \end{pmatrix}. \tag{2.7}$$

We choose the vacuum $\Sigma_0 = (0\,,0\,,f)^T$ along the vertical direction in the Fig. 2.3 such that $T^1\Sigma_0 \neq 0$, $T^2\Sigma_0 \neq 0$, $T^3\Sigma_0 = 0$. Clearly, the unbroken SO(2) is given by the horizontal circular ring, the rotation along which is generated by T^3. The SO(3) is explicitly broken by gauging the subgroup SO(2), as shown by the tilted blue circle in Fig. 2.3. The pNGB vevs $\langle\pi\rangle$, thus achieved by the explicit breaking of the shift symmetry, misaligned the vacuum with respect to its original direction. Note that, since the gauged SO(2) and the

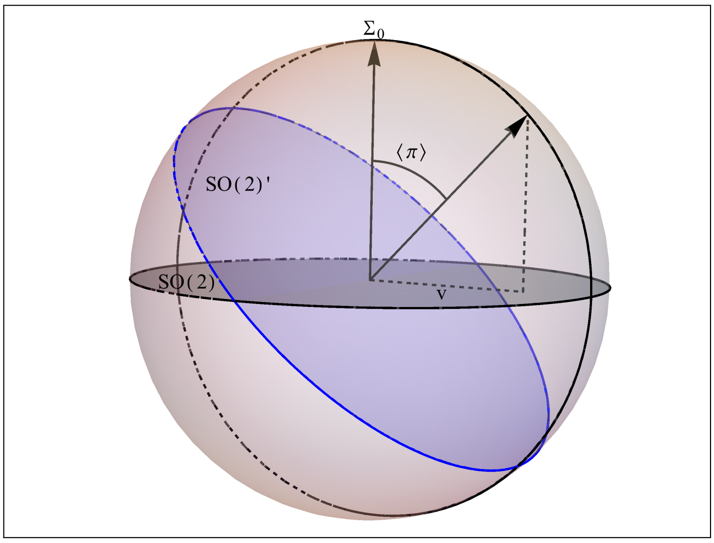

Figure 2.3: *Illustrative figure for the breaking of* $\mathrm{SO}(3) \to \mathrm{SO}(2)$ *is shown. The reference vacuum is chosen along the* T^3 *direction leaving the SO(2), indicated by the horizontal circular ring, invariant. Explicit breaking of SO(3) leads to vacuum misalignment, shown by the tilted circular ring. The vev breaking the gauged SO(2) is given by the projection of the tilted vacuum on the horizontal unbroken global SO(2) direction.*

global SO(2) intersects only at two points, no remnant invariance is present, *i.e.* vacuum misalignment mechanism breaks the gauge symmetry to nothing. The vev that breaks the gauged SO(2) symmetry is given by the projection of the misaligned vacuum on the unbroken global symmetry (on the horizontal circular plane) as

$$v = f \sin \frac{\langle\pi\rangle}{f}\,. \tag{2.8}$$

In the context of a realistic composite Higgs scenario, on the other hand, the gauged symmetry would be the electroweak symmetry group G_{EW}. The vev of the pNGB Higgs will break G_{EW} to the $\mathrm{U}(1)_{\mathrm{EM}}$, which must be a subgroup of both the unbroken global symmetry and the gauge symmetry. The electroweak scale v will be determined by the projection of the misaligned vacuum on the electroweak plane, which makes it different from the strong sector scale f by an amount given by the pNGB vevs as,

$$\xi \equiv \frac{v^2}{f^2} = \sin^2 \frac{\langle \pi \rangle}{f} \, . \tag{2.9}$$

Two special limits of the tuning parameter ξ, parametrizing the hierarchy between v and f are worth noting. The limit $\xi \to 0$ implies $f \to \infty$, which means we get back the SM scenario where the strong sector is completely decoupled. The other important case $\xi \to 1$, which means $v \sim f$, corresponds to the technicolor limit.

2.3 Partial compositeness paradigm

We now discuss how the quarks and leptons interact with the composite sector and receive masses. We have already mentioned that the fermions are assumed to be elementary, and are external to the strong sector. Let us first recall that, in technicolor scenario 4-fermion interactions involving the quarks and techniquarks are postulated as [37–41, 65–69]

$$\mathcal{L} \sim \frac{1}{\Lambda_{\mathrm{UV}}^2} \left(\bar{q} q\right) \left(\bar{\psi}_{\mathrm{TC}} \psi_{\mathrm{TC}}\right) \, , \tag{2.10}$$

where Λ_{UV} denotes the UV cut-off scale of the operator. Such interactions can be induced by a bi-linear mixing between the quarks and some bosonic operator belonging to the strong sector, given by

$$\mathcal{L} \sim \frac{\lambda}{\Lambda_{\mathrm{UV}}^{d-1}} \left(\bar{q} q\right) \mathcal{O}_d \, , \tag{2.11}$$

with d as the operator dimension of $\mathcal{O}_d$. Mapping $\mathcal{O}_d \equiv \bar{\psi}_{\mathrm{TC}} \psi_{\mathrm{TC}}$, we observe that below the scale of technicolor condensation (which is around the weak scale v), this operator can interpolate a Higgs field and contributes to the quark mass. In such case, the quark mass is estimated as

$$m_q \sim \frac{1}{\Lambda_{UV}^2}\langle\bar{\psi}_{\rm TC}\psi_{\rm TC}\rangle \sim v\lambda[v]\left(\frac{v}{\Lambda_{\rm UV}}\right)^{d-1}. \tag{2.12}$$

Note that the renormalization group evolution above the condensation scale may lead to a large anomalous dimension of $\mathcal{O}_d$ which in turn can play an essential role in the generation of the fermion mass hierarchies. However, the major challenge in this scenario is to reproduce the observed hierarchy of the SM quark sector without introducing either large contributions to the flavor changing neutral current processes or a considerable fine tuning through the new operator $\mathcal{O}_d$ with large negative anomalous dimensions [55, 56].

To mitigate these issues in the modern composite Higgs model, a linear mixing in lieu of a bi-linear one, between the SM fermions and the operators of the composite sector is proposed [70, 71]. This new mechanism of transmitting the effect of electroweak breaking to the matter sector through a linear mixing is known as the *partial compositeness* paradigm. While we only consider the interactions of the SM fermions in this section, we want to mention that analogous arguments also work for the gauge sector as well. A schematic diagram of the linear mixing in the partial compositeness scenario is shown in Fig. 2.4. The linear mixing terms between the quarks and the composite operators are given by

$$\mathcal{L}_{\rm mix} \simeq \frac{\lambda_L}{\Lambda_{\rm UV}^{d_L-5/2}}\bar{q}_L\mathcal{O}_R + \frac{\lambda_R}{\Lambda_{\rm UV}^{d_R-5/2}}\bar{u}_R\mathcal{O}_L + \text{h.c.} \tag{2.13}$$

The operators $\mathcal{O}_{L,R}$ are fermionic in nature, in contrast to the technicolor scenario, and possess the same quantum numbers as the quarks under the SM gauge group. This has significant phenomenological implications because, below the compositeness scale these operators can excite composite massive fermions with identical electroweak and color quantum numbers as the SM fermions, and thus can in principle be detectable in the collider experiments. It constitutes one of the major signature of composite Higgs scenarios. The

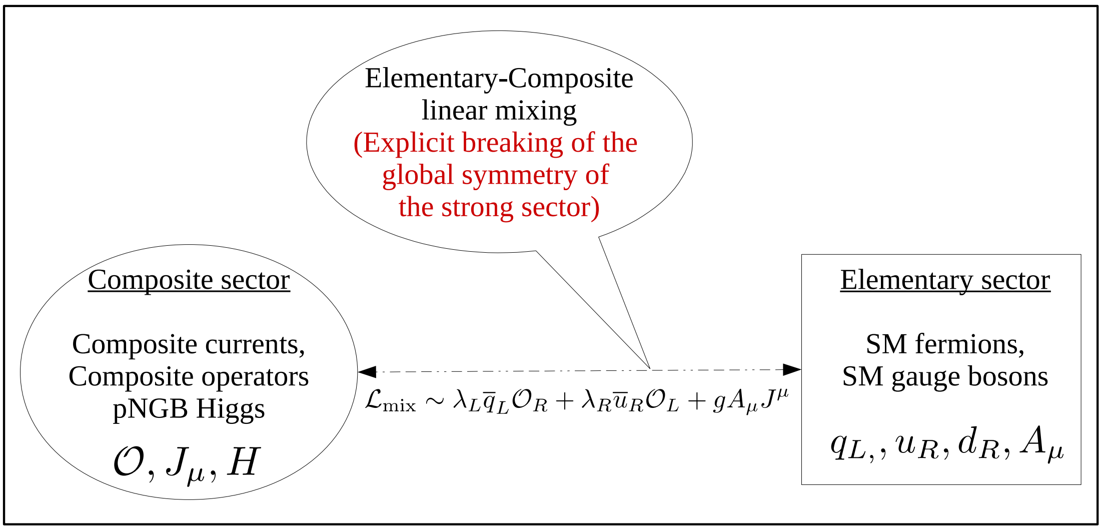

Figure 2.4: *Schematic diagram demonstrating the partial compositeness scenario. The SM gauge and matter sector are assumed to be elementary. They mix linearly with vector currents and fermionic operators of the composite sector, respectively. The linear mixing communicates the explicit breaking of the strong sector to generate a potential for the pNGB Higgs bosons.*

operators mixing with left- and right- chiral quarks are in general different and may have different operator dimensions. The elementary fermions mix linearly with their composite counterparts, which we call as the resonances or composite partners of the elementary fermions. Thus the physical degrees of freedom constitute a linear combinations of elementary and composite degrees of freedom. Note that the linear mixing terms by definition, explicitly break the symmetry of the composite sector, inducing a Higgs potential whose vev may trigger vacuum misalignment. Unlike the bi-linear mixing, here the Higgs field is interpolated at the low energy by the operator pair $\bar{\mathcal{O}}_L \mathcal{O}_R$. The mass of the quarks can be estimated as

$$m_q \sim m_* \lambda_L[m_*] \lambda_R[m_*] \left(\frac{m_*}{\Lambda_{\rm UV}}\right)^{d_L+d_R-5} , \tag{2.14}$$

where $\lambda_{L,R}[m_*]$ denote the strength of mixing evaluated near the compositeness scale. The anomalous dimensions of the operators $\mathcal{O}_{L,R}$ can be such that $d_L + d_R - 5 \gtrsim 0$, without reintroducing any additional UV divergence issue. The fermion mass hierarchy can be generated depending on the anomalous dimension of the operators, which in turn determines the degree of compositeness of the SM fermions [72, 73]. Moreover, the UV stability also ensures that $\Lambda_{\rm UV}$ can be arbitrarily large, thus taming the problems related to the large flavor changing neutral current processes [73–77]. These are the primary advantages of the partially composite scenario over the bi-linear mixing.

We illustrate the low energy behaviour of the formal picture depicted above with a toy example. We consider the following Lagrangian involving a single generation of elementary quarks and some composite vector-like resonances (Q and U):

$$\mathcal{L} = -m_* \bar{Q} Q - m_* \bar{U} U + \Delta_L \bar{q}_L Q_R + \Delta_R \bar{u}_R U_L + \text{h.c.}\,, \tag{2.15}$$

where strengths of the mixing terms are given by $\Delta_L \equiv \langle 0|\mathcal{O}_L|Q\rangle$, $\Delta_R \equiv \langle 0|\mathcal{O}_R|U\rangle$. Note that the generic mass of the resonances are taken, as expected, to be around the scale of condensation (m_*). We assume, for simplicity, all the parameters in the above Lagrangian are real, implying that the composite sector preserves CP. The mass matrix can be diagonalized by the following unitary transformations

$$\begin{pmatrix} q_L \\ Q_L \end{pmatrix} \to \begin{pmatrix} c_{\phi_L} & s_{\phi_L} \\ -s_{\phi_L} & c_{\phi_L} \end{pmatrix} \begin{pmatrix} q_L \\ Q_L \end{pmatrix}, \quad \begin{pmatrix} u_R \\ U_R \end{pmatrix} \to \begin{pmatrix} c_{\phi_R} & s_{\phi_R} \\ -s_{\phi_R} & c_{\phi_R} \end{pmatrix} \begin{pmatrix} u_R \\ U_R \end{pmatrix}, \tag{2.16}$$

where $s_{\phi_{L,R}}(c_{\phi_{L,R}}) \equiv \sin\phi_{L,R}(\cos\phi_{L,R})$ and the fraction of compositeness of the left- and right- handed quarks are given by $\tan\phi_{L,R} = \Delta_{L,R}/m_*$. Two zero modes can be identified with SM chiral degrees of freedom, which would acquire mass after the EWSB. However, the crucial point is that, now the SM degrees of freedom have substantial overlap with the resonances and thus are partially composite in nature. On the other hand, the masses of

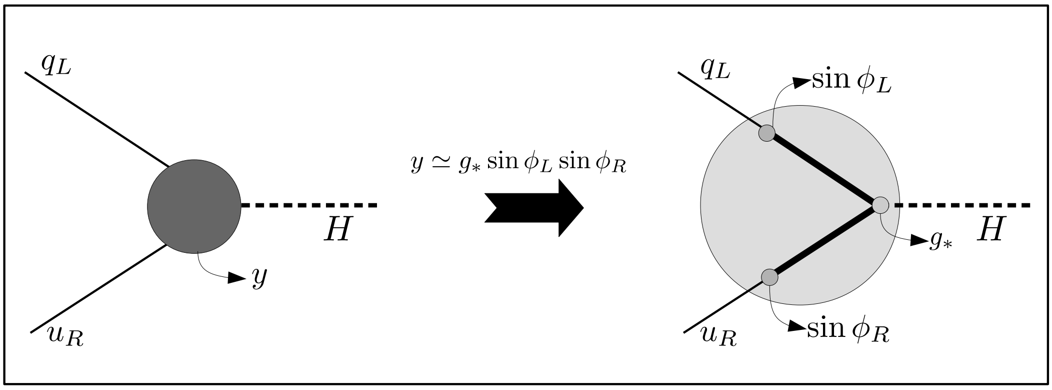

Figure 2.5: *Microscopic origin of Yukawa coupling in the partial compositeness scenario. The SM fermions mix linearly with composite resonances which in turn couples to the pNGB Higgs to generate Yukawa couplings.*

the resonances are given by $\sqrt{m_*^2 + \Delta_{L,R}^2}$, showing a mass splitting proportional to the amount of mixing.

We can also make a naïve estimate of the Yukawa couplings of the SM fermions with the Higgs boson (see Fig. 2.5). As mentioned earlier the operator pair $\bar{\mathcal{O}}_L \mathcal{O}_R$ can interpolate the Higgs field at low energy. Assuming the the coupling between the Higgs and the composite resonances are given by g_*, we find the Yukawa couplings of the SM fermions as

$$y \simeq g_* \sin\phi_L \sin\phi_R \,. \tag{2.17}$$

Clearly, the Yukawa couplings and in turn the masses of the SM fermions depend on the degree of compositeness. Thus, while the light fermions such as leptons, first and second generation quarks are mostly elementary with a very small compositeness fraction, the third generation quarks are relatively more composite in nature. Here, we mention in passing that the top quark can in principle belong entirely to the composite sector, unlike other SM fermions. However, in our discussion we will not consider this particular possibility.

2.4 Multifaceted frameworks: Confinement / Holography / Deconstruction

Composite Higgs framework encompasses a wide class of apparently disparate models. However, the underlying links among these models prove to be a very powerful tool to portray the full picture [78]. Primarily, a composite Higgs scenario possesses two essential features: a pNGB Higgs and a strong confining dynamics. The former can easily be described by the well-known non-linear sigma model framework, while building a predictive model for the non-perturbative strong dynamics is more challenging. Here, comes the help from different class of interlinked models within the larger framework of composite Higgs. Below we outline three such distinct avenues and their relations with each other:

- First, we consider a 4D confining sector, quite analogous to the standard QCD. The strongly interacting sector, endowed with a global symmetry is assumed to be sitting *near* a conformal fixed point in the UV. The low energy non-perturbative behaviour can be captured in terms of momentum dependent form factors, while the pNGB Higgs sector can be described using a non-linear sigma model [55, 58, 79].

- The $\mathrm{AdS/CFT}$ correspondence [80] enables us to relate this 4D strongly coupled theory to a theory in a slice of AdS_5. In this AdS picture the theory is weakly coupled and explicit calculations can be performed. The global symmetry of the 4D CFT is realized as a bulk gauge symmetry in the 5D picture. The Higgs boson from the 4D perspective may originate from the fifth component of a 5D gauge field leading to gauge-Higgs unification [30, 32, 81–85]. The radiatively generated mass of the 'holographic' Higgs boson [71, 86–88] is protected by the 5D gauge symmetry.

- Discretizing the fifth dimension produces a deconstructed theory having multiple sites with different symmetry breaking scales [89, 90]. The site with the lowest energy scale can be identified with the weak scale while the highest scale might be the Planck scale. These kind of deconstructed models with multiple sites exhibit a mechanism called collective symmetry breaking to protect the weak scale [91, 92]. The multi-site models [93, 94] can also be mapped to the QCD-like confining theories described by the non-linear sigma model.

A detailed discussion of all three avenues are beyond the scope of this thesis. *We will primarily focus on the first approach where we will model the momentum-dependent form factors and apply several sum rules, motivated from both 5D pictures as well as the well-known QCD scenario.*

2.5 Minimal composite Higgs model

In this section we illustrate the framework of composite Higgs with an explicit example. We consider the global group of the strong sector as $G = \mathrm{SO}(5) \times \mathrm{U}(1)_X$ whereas the vacuum is only invariant under the $H = \mathrm{SO}(4) \times \mathrm{U}(1)_X$ subgroup of G. Thus $\mathrm{SO}(5)$ breaks down spontaneously into $\mathrm{SO}(4)$ (keeping $\mathrm{U}(1)_X$ unbroken), resulting in four NGBs which can form a SM Higgs doublet. It forms the minimal coset that protects the custodial symmetry [79, 87, 88, 94–106]. A schematic diagram showing the coset structure and vacuum misalignment mechanism in the minimal model is displayed in Fig. 2.6.

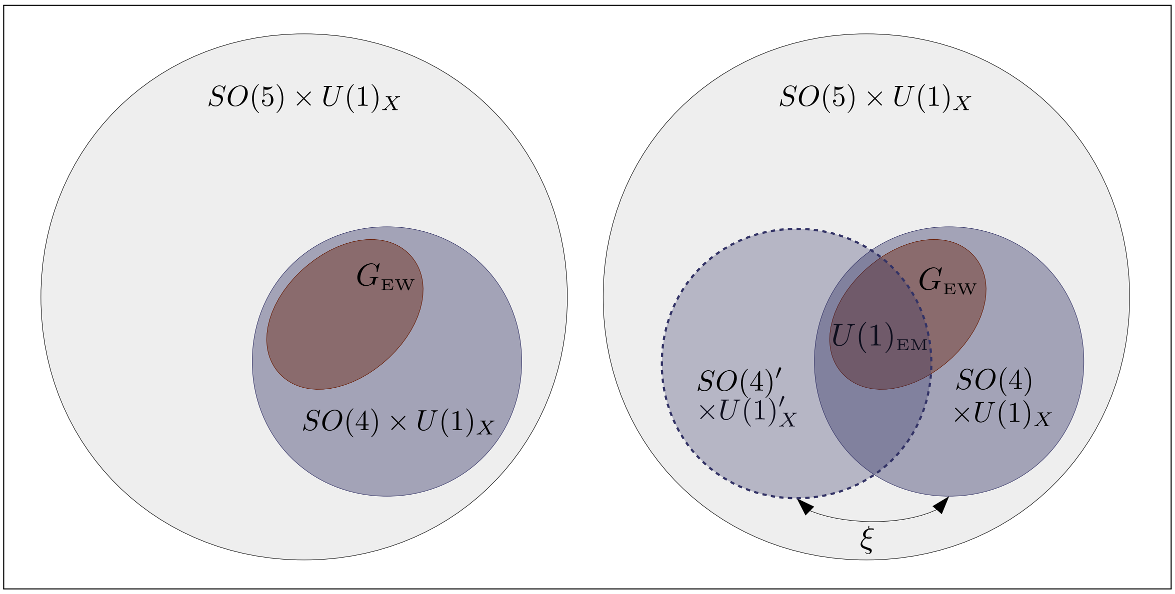

Figure 2.6: *Coset structure, explicit breaking and vacuum misalignment in the minimal composite Higgs model. Global $SO(5)\times U(1)_X$ symmetry is spontaneously broken to $SO(4)\times U(1)_X \simeq SU(2)_L\times SU(2)_R\times U(1)_X$. The electroweak gauge group, identified with a subgroup of the unbroken part, explicitly breaks the global SO(5) symmetry and induces EWSB. The misaligned vacua remains invariant under the electromagnetic $U(1)_{EM}$.*

2.5.1 Symmetry breaking pattern

The four ensuing NGBs can be parametrized by choosing a reference vacuum as $\Sigma_0 = (0,0,0,0,1)^T$. Using this, we can write the Goldstones in terms of a linear field as

$$\Sigma = U\Sigma_0 = \exp\left[i\frac{\sqrt{2}}{f}\pi_{\hat{a}}(x)T^{\hat{a}}\right]\Sigma_0 = \frac{1}{\pi}\sin\frac{\pi}{f}\left(\pi_1,\ \pi_2,\ \pi_3,\ \pi_4,\ \pi\cot\frac{\pi}{f}\right)^T , \qquad (2.18)$$

where $\pi = \sqrt{\sum_{\hat{a}}\pi_{\hat{a}}^2}$ and $T^{\hat{a}}$'s denote the broken generators, whose expressions are given in the Appendix A. Now we describe the transformations of the NGBs under different SO(5) rotations. We divide the SO(5) rotations in two categories:

- Rotation along the unbroken SO(4) directions: under these rotations the NGBs transform linearly in the so called $\mathbf{r}_\pi$ representation as

$$\pi_{\hat{a}} \to [\exp\left(i\alpha_a t_\pi^a\right)]_{\hat{a}}^{\hat{b}}\, \pi_{\hat{b}}\,, \tag{2.19}$$

where the generators t_π^a in the $\mathbf{r}_\pi$ representation, spanning the SO(4) subgroup, can be expressed in terms of the generators of SO(5) as

$$e^{i\alpha_a T^a} T^{\hat{a}} e^{-i\alpha_a T^a} = T^{\hat{b}} \left[e^{i\alpha_a t_\pi^a}\right]_{\hat{b}}^{\hat{a}}\ . \tag{2.20}$$

For the particular coset in consideration, $\mathbf{r}_\pi$ can be identified as the fundamental representation of SO(4). Thus, the rotations along the unbroken directions transform the NGBs as fundamental 4 of SO(4).

- Rotation along the broken directions: the actions of the broken generators on the NGBs induce the 'shift symmetry' of the Goldstone bosons as

$$\pi_{\hat{a}} \to \pi_{\hat{a}} + \frac{f}{\sqrt{2}}\alpha_{\hat{a}} + \mathcal{O}\left(\frac{\pi^2}{f^2}\right)\ . \tag{2.21}$$

  Therefore, the non-derivative interactions of the NGBs, in absence of any source of explicit SO(5) breaking, are prevented by the rotations along the broken generators.

2.5.2 Gauge sector

To describe the SM gauge interactions, we must embed the electroweak gauge group within the unbroken SO(4) part. Note that the Lie algebra of SO(4) is isomorphic to $\mathrm{SU(2)_L} \times \mathrm{SU(2)_R}$. The $\mathrm{SU(2)_L}$ is identified as a part of the electroweak gauge group, while the hypercharge is taken as $Y = T_R^3 + X$. Here T_R^3 and X represent respectively, the generators of the $\mathrm{U}(1)$ subgroup of $\mathrm{SU}(2)_{\mathrm{R}}$ and that of unbroken $\mathrm{U}(1)_{\mathrm{X}}$. The $\mathrm{SU}(2)_{\mathrm{L}}$ Higgs doublet can be constructed from the four NGBs as follows

$$H = \frac{1}{\sqrt{2}} \begin{pmatrix} \pi_2 + i\pi_1 \\ \pi_4 - i\pi_3 \end{pmatrix} . \tag{2.22}$$

The action of $\mathrm{SU}(2)_{\mathrm{L}} \times \mathrm{SU}(2)_{\mathrm{R}}$ on the scalar bosons becomes apparent once we construct a bi-doublet $(\mathbf{2}, \mathbf{2})$ as

$$\mathcal{H} = (H^c,\ H) = \frac{1}{\sqrt{2}} \begin{pmatrix} \pi_4 + i\pi_3 & \pi_2 + i\pi_1 \\ -\pi_2 + i\pi_1 & \pi_4 - i\pi_3 \end{pmatrix} , \tag{2.23}$$

where $H^c = i\sigma_2 H^*$. While the $\mathrm{SU}(2)_{\mathrm{L}}$ rotations act columnwise on $\mathcal{H}$, the $\mathrm{SU}(2)_{\mathrm{R}}$ rotations mix H with H^c along the rows. Note that the presence of unbroken SO(4) is essential to preserve custodial symmetry at tree-level after the EWSB. The explicit SO(5) breaking due to the incomplete gauging of a subgroup breaks the shift symmetry of the NGBs, thereby triggering the EWSB. Without loss of any generality, we will work in the unitary gauge after the EWSB through a SO(4) rotation, *i.e.* we will take $\pi_1 = \pi_2 = \pi_3 = 0$ and $\pi_4 = \langle h \rangle + h$. In this gauge, Σ can be written as [55, 79]

$$\Sigma = \left(0,\ 0,\ 0,\ \sin\frac{\langle h \rangle + h}{f},\ \cos\frac{\langle h \rangle + h}{f} \right)^T . \tag{2.24}$$

The pure kinetic term of the NGBs, in the unitary gauge is given by

$$\mathcal{L}_{\mathrm{kin}} = \frac{f^2}{2} \left(\partial_\mu \Sigma \right) \left(\partial^\mu \Sigma \right) = \frac{1}{2} \left(\partial_\mu h \right) \left(\partial^\mu h \right) . \tag{2.25}$$

We recall that in the partial compositeness paradigm, the gauge bosons are not part of the composite sector, rather they are elementary. To introduce the gauge interactions of the pNGBs, we introduce spurionic fields so that the gauge bosons transform in the adjoint representations of $\mathrm{SO}(5) \times \mathrm{U}(1)_X$. Assuming Σ as a background field[3], the formally $\mathrm{SO}(5) \times \mathrm{U}(1)_X$ invariant Lagrangian in the momentum space involving the gauge bosons can be written as [55, 79]

$$\mathcal{L} = \frac{1}{2} P_T^{\mu\nu} \left[\Pi_0(p^2) \mathrm{Tr}(\mathrm{A}_\mu \mathrm{A}_\nu) + \Pi_1(\mathrm{p}^2) \Sigma^{\mathrm{T}} \mathrm{A}_\mu \mathrm{A}_\nu \Sigma + \Pi_0^{\mathrm{X}}(\mathrm{p}^2) \mathrm{X}_\mu \mathrm{X}_\nu \right] . \tag{2.26}$$

Here $P_T^{\mu\nu} = (\eta^{\mu\nu} - p^\mu p^\nu / p^2)$ is the standard transverse projector, while $A_\mu = A_\mu^a T^a + A_\mu^{\hat{a}} T^{\hat{a}}$ and X_μ denote the gauge bosons corresponding to SO(5) and $\mathrm{U}(1)_X$ respectively. In the physical limit, the spurions can be turned off and we will set $A_\mu^a = W_\mu^\alpha T_L^\alpha + B_\mu T_R^3$ and $X_\mu = B_\mu$. The form factors in Eq. (2.26), capture the strong sector dynamics, and can be written in terms of form factors associated with the conserved currents along broken ($\Pi_{\hat{a}} \sim \langle J_{\hat{a}} J_{\hat{a}} \rangle$) and unbroken ($\Pi_a \sim \langle J_a J_a \rangle$) generators. To do that we rewrite the Lagrangian in Eq. (2.26) by replacing $\Sigma = \Sigma_0$ as

$$\mathcal{L} = \frac{1}{2} P_T^{\mu\nu} \left[\Pi_0^X(p^2) X_\mu X_\nu + \Pi_a(p^2) A_\mu^a A_\nu^a + \Pi_{\hat{a}}(p^2) A_\mu^{\hat{a}} A_\nu^{\hat{a}} \right] . \tag{2.27}$$

In principle, the form factors depend on the details of the confining sector and only be determined using a non-perturbative approach. However, in the 'Large N' limit in the strong sector [107], Π_a and $\Pi_{\hat{a}}$ can be parametrized in terms of a tower of spin-1 resonances with increasing masses (m_{ρ_n, a_n}) and decay constants (f_{ρ_n, a_n}) as follows:

[3]Since we are only interested in the non-derivative interactions of the pNGBs with the gauge bosons, we may assume Σ as a classical background.

$$\Pi_a = \Pi_0 = p^2 \sum_n \frac{f_{\rho_n}^2}{p^2 - m_{\rho_n}^2}\,, \quad \Pi_{\hat{a}} = \Pi_0 + \frac{\Pi_1}{2} = p^2 \left[\sum_n \frac{f_{a_n}^2}{p^2 - m_{a_n}^2} + \frac{f^2}{2p^2} \right]\,. \tag{2.28}$$

Note that in case of $\Pi_{\hat{a}}$, the second term proportional to f^2 can excite pNGBs with proper quantum numbers from vacuum with the decay constant f. These resonances are expected to be light ($m_{\rho_n, a_n} \lesssim 4\pi f$) to account for the perturbative unitarity of the theory [108]. In the physical limit we turn off the spurions and using the definition of Σ at the electroweak vacuum we obtain

$$\mathcal{L} \supset \frac{P_T^{\mu\nu}}{2} \left[\Pi_0^X B_\mu B_\nu + \left(\Pi_0 + \Pi_1 \frac{\langle s_h \rangle^2}{4} \right) \left(W_\mu^a W_\nu^a + B_\mu B_\nu \right) - \Pi_1 \frac{\langle s_h \rangle^2}{2} W_\mu^3 B_\nu \right]\,, \tag{2.29}$$

where $\langle s_h \rangle \equiv \sin\langle h \rangle / f$. The standard $\mathrm{SU}(2)_L$ and $\mathrm{U}(1)_Y$ gauge couplings, g and g' respectively, can be identified by Taylor expanding the form factors and extracting the coefficients of $\mathcal{O}(p^2)$ as

$$\frac{1}{g^2} = -\Pi_0'(0) + \frac{1}{g_0^2}\,, \qquad \frac{1}{g'^2} = -\left(\Pi_0'(0) + \Pi_0'^X(0) \right) + \frac{1}{g_0'^2}\,. \tag{2.30}$$

Here g_0 and g_0' denote the bare gauge couplings corresponding to the kinetic terms of the elementary gauge bosons. The electroweak vev can be defined by the usual vacuum misalignment relation

$$\xi = \frac{v^2}{f^2} = \sin^2 \frac{\langle h \rangle}{f}\,. \tag{2.31}$$

The low energy interactions of the Higgs boson with the weak gauge bosons can be calculated by expanding s_h^2 around $\langle h \rangle / f \to 0$ as

$$\mathcal{L}_V = \frac{g^2 v^2}{4}\left(W^+_\mu W^{-\mu} + \frac{1}{2\cos^2\theta_w} Z_\mu Z^\mu\right)\left[2\sqrt{1-\xi}\frac{h}{v} + (1-2\xi)\frac{h^2}{v^2} + ...\right]. \quad (2.32)$$

Clearly, both hVV and $hhVV$ interactions are modified due to the presence of higher dimensional operators. The strengths of these interactions are reduced as compared to their SM values by a universal factor controlled by the parameter ξ as

$$\frac{g_{hVV}}{g^{SM}_{hVV}} = \sqrt{1-\xi}\,, \qquad \frac{g_{hhVV}}{g^{SM}_{hhVV}} = 1 - 2\xi\,. \quad (2.33)$$

Note that, in the limit $\xi \to 0$ or equivalently $f \to \infty$ the strong sector decouples and SM couplings get restored. A major constraint on the composite Higgs models come from the precision measurement of the electroweak 'S'-parameter at the LEP. In minimal composite Higgs model, the correction to the 'S'-parameter depends on the form factors as follows:

$$\Delta S \simeq \frac{16\pi^2}{g^2}\frac{\langle s_h\rangle^2}{4}\Pi'_1(0)\,. \quad (2.34)$$

Evidently the electroweak precision constraint demands $\xi = \langle s_h\rangle^2 \ll 1$. On the contrary, in the technicolor models as we have discussed earlier, $\xi \to 1$, which implies that 'S'-parameter alone can rule out such models.

2.5.3 Fermion sector

Now we describe the fermion sector of the minimal model. To implement the partial compositeness paradigm, the SM fermions are embedded in different incomplete SO(5) multiplets. Unlike the gauge sector, the Yukawa couplings of the SM fermions with the

SO(5)		$\mathrm{SO(4)} \simeq \mathrm{SU(2)_L} \times \mathrm{SU(2)_R}$
$\mathbf{4}$	$\rightarrow$	$(\mathbf{2},\mathbf{1})+(\mathbf{1},\mathbf{2})$
$\mathbf{5}$	$\rightarrow$	$(\mathbf{2},\mathbf{2})+(\mathbf{1},\mathbf{1})$
$\mathbf{10}$	$\rightarrow$	$(\mathbf{2},\mathbf{2})+(\mathbf{3},\mathbf{1})+(\mathbf{1},\mathbf{3})$
$\mathbf{14}$	$\rightarrow$	$(\mathbf{1},\mathbf{1})+(\mathbf{2},\mathbf{2})+(\mathbf{3},\mathbf{3})$

Table 2.1: *List of $SO(5)$ representations and their decomposition under $SU(2)_L \times SU(2)_R$, upto dimension $\mathbf{14}$.*

Higgs boson depends on the specific SO(5) representation in which the former are embedded. A list of irreducible representations of SO(5) and their decomposition under $\mathrm{SO}(4) \simeq \mathrm{SU}(2)_L \times \mathrm{SU}(2)_R$ are displayed in Table 2.1. Here we will confine ourselves to the cases where the third generation quarks are embedded in the fundamental $\mathbf{5}$ of SO(5) only. This is the minimal representation that ensures a custodial protection of the $Zb_L\bar{b}_L$ coupling [109]. The cases with higher representations will be discussed in details in Chapter 4. To reproduce the correct hypercharge to the SM fermions, assigning specific $\mathrm{U}(1)_X$ charge is essential. For example, we embed both chiralities of the top quark in $\mathbf{5}_{2/3}$, while the bottom quark is embedded in the $\mathbf{5}_{-1/3}$ of $\mathrm{SO}(5) \times \mathrm{U}(1)_X$, where the subscript denotes $\mathrm{U}(1)_X$ charge. Decomposition of $\mathbf{5}_{2/3}$ under the SM gauge group is shown below:

$$\mathbf{5}_{2/3} \rightarrow \mathbf{2}_{7/6} + \mathbf{2}_{1/6} + \mathbf{1}_{2/3}\,. \tag{2.35}$$

Clearly, t_L and t_R would be embedded in $\mathbf{2}_{1/6}$ and $\mathbf{1}_{2/3}$, respectively. The explicit expressions for the embeddings of the top quark are given by

$$Q_L = \frac{1}{\sqrt{2}}(-ib_L,\ -b_L,\ -it_L,\ t_L,\ 0)^T\,, \tag{2.36}$$

$$T_R = (0,\ 0,\ 0,\ 0,\ t_R)^T\,. \tag{2.37}$$

Following the same trick as shown in the gauge sector, formally SO(5) invariant effective Lagrangian for the top quark in terms of Q_L, T_R and Σ can be written as

$$\begin{aligned}\mathcal{L} &= \Pi_0^L(p)\bar{t}_L\not{p}t_L + \Pi_1^L(p)(\overline{Q}_L\Sigma)\not{p}(\Sigma^T Q_L) + \Pi_0^R(p)\bar{t}_R\not{p}t_R + \Pi_1^R(p)(\overline{T}_R\Sigma)\not{p}(\Sigma^T T_R) \\ &+\Pi_1^{LR}(p)(\overline{Q}_L\Sigma)(\Sigma^T T_R) + \text{h.c.}\end{aligned} \tag{2.38}$$

In analogy to the gauge sector, the form factors which depend on the details of the top-partners, encapsulate the dynamics of the strong sector. Implementing the physical limit where Q_L and T_R contains only SM degrees of freedom, the Lagrangian becomes [79]

$$\mathcal{L} = \bar{t}_L\not{p}\left[\Pi_0^L + \frac{\Pi_1^L}{2}s_h^2\right]t_L + \bar{t}_R\not{p}\left[\Pi_0^R + \Pi_1^R c_h^2\right]t_R + \bar{t}_L\left[\frac{\Pi_1^{LR}}{\sqrt{2}}s_h c_h\right]t_R + \text{h.c.} \tag{2.39}$$

Mass of the top quark is obtained as

$$m_t \simeq \frac{\left|\Pi_1^{LR}(0)\right|}{\sqrt{2\Pi_0^L(0)\Pi_0^R(0)}}\langle s_h c_h\rangle\,, \tag{2.40}$$

where we have assumed $\Pi_1^{L,R} \ll \Pi_0^{L,R}$. The Yukawa coupling of the top quark after EWSB can be calculated by expanding the sines and cosines. The low energy interactions involving the top quark and the Higgs boson are given by

$$\mathcal{L}_t = -m_t\bar{t}\left[1 + \frac{1-2\xi}{\sqrt{1-\xi}}\frac{h}{v} - 2\xi\frac{h^2}{v^2} + ...\right]t\,. \tag{2.41}$$

2.6 Radiative Higgs potential and Higgs mass

In this section we briefly review the generation of Coleman-Weinberg scalar potential [64] and spell out the correlation between the light top-partners and the Higgs mass within the minimal setup. The main contribution to the Higgs potential driving EWSB comes from the top quarks, which is assumed to be embedded in fundamental **5** of SO(5). The generic structure of the one loop potential is given by [56, 98]

$$V_{\text{eff}} = -\alpha s_h^2 + \beta s_h^4 \, . \tag{2.42}$$

Minimization of the potential in Eq. (2.42) yields

$$\xi \equiv \langle s_h \rangle^2 = \frac{\alpha}{2\beta} \, . \tag{2.43}$$

The Higgs mass can be calculated as a function of β and ξ as

$$m_h^2 = \frac{8}{f^2} \xi (1-\xi) \beta \, . \tag{2.44}$$

Note that the mass dimensionful parameters α and β receive contributions from both gauge sector and the top quark sector. Now we calculate these parameters in terms of the microscopic details of the model given by the form factors. The Feynman diagrams corresponding to the one loop gauge and top quark contributions to the C-W potential are displayed in Fig. 2.7. Using the standard technique [55, 79], we calculate the gauge contribution to the scalar potential as

$$V_{\text{gauge}}(h) = \frac{9}{2} \int \frac{d^4 q_E}{(2\pi)^4} \log \left[1 + \frac{\Pi_1(-q_E^2)}{4\Pi_0(-q_E^2)} s_h^2 \right] \simeq \frac{9}{2} \int \frac{d^4 q_E}{(2\pi)^4} \left[\frac{\Pi_1}{4\Pi_0} s_h^2 - \frac{\Pi_1^2}{32\Pi_0^2} s_h^4 \right] . \tag{2.45}$$

Here q_E denotes momentum in Euclidean space. In the second equality, the logarithm is expanded assuming $\Pi_1 s_h^2 \ll 4\Pi_0$. In order to calculate the integrals we utilize Weinberg sum rules, in analogy to QCD [110], for modeling the form factors. Clearly, convergence

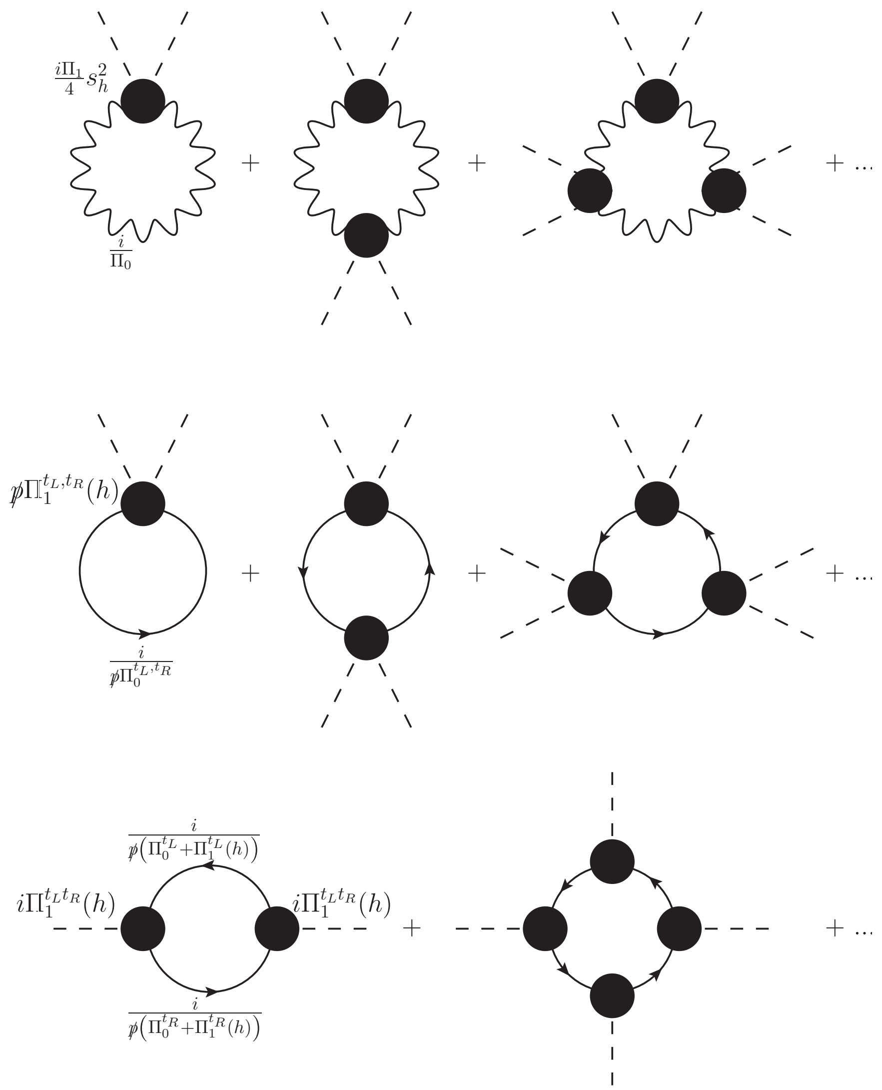

Figure 2.7: *Feynman diagrams for gauge and fermionic contributions to the one loop Coleman-Weinberg potential. The top row displays the gauge contribution while the middle and bottom rows show the top quark contributions to the potential. The black blobs captures the strong sector dynamics through the momentum dependent form factors. The form factors used in the bosonic loops are defined in Eqs.* (2.28) *and* (2.30)*. We use the the following notations for the form factors displayed in the fermionic loop contributions:* $\Pi_0^{t_L,t_R} \equiv \Pi_0^{L,R}$, $\Pi_1^{t_L} \equiv \Pi_1^L s_h^2/2$, $\Pi_1^{t_R} \equiv \Pi_1^R c_h^2$ *and* $\Pi_1^{t_Lt_R} \equiv \Pi_1^{LR} s_h c_h/\sqrt{2}$.

of the integrals in Eq. (2.45) requires $\Pi_1(q_E^2)$ to fall as $\mathcal{O}(1/q_E^4)$ or faster, which leads to the following two conditions on the UV behaviour of Π_1 [79, 98]:

$$\lim_{q_E^2\to\infty} \Pi_1(q_E^2) = 0, \qquad \lim_{q_E^2\to\infty} q_E^2\Pi_1(q_E^2) = 0\,. \tag{2.46}$$

Utilizing the definition of the form factors in Eq. (2.28) and the conditions given in Eq. 2.46, we find the Weinberg's sum rules as

$$\sum_n \left({f_{\rho_n}}^2 - {f_{a_n}}^2\right) = \frac{f^2}{2}, \qquad \sum_n \left({f_{\rho_n}}^2 m_{\rho_n}^2 - {f_{a_n}}^2 m_{a_n}^2\right) = 0\,. \tag{2.47}$$

Note that the Weinberg's sum rules, and thus the conditions in Eq. (2.46) can be saturated using only two resonances ρ and a in the summation in Eq. (2.47). We find the explicit expression for Π_1, satisfying the sum rules, as

$$\Pi_1(q_E^2) \simeq \frac{f^2 m_\rho^2 m_a^2}{(q_E^2+m_\rho^2)(q_E^2+m_a^2)}\,. \tag{2.48}$$

Finally we show the gauge contribution to the parameters α and β by explicitly calculating the integrals over the form factors as

$$\alpha_g = -\frac{9}{2}\int \frac{d^4q_E}{(2\pi)^4}\frac{\Pi_1(-q_E^2)}{4\Pi_0(-q_E^2)} = -\frac{9g^2f^2m_\rho^2m_a^2}{128\pi^2(m_a^2-m_\rho^2)}\log\left(\frac{m_a^2}{m_\rho^2}\right), \tag{2.49}$$

$$\begin{aligned}\beta_g = {} & -\frac{9}{2}\int \frac{d^4q_E}{(2\pi)^4}\frac{\Pi_1(-q_E^2)^2}{32\Pi_0(-q_E^2)^2} = -\frac{9g^4f^4}{1024\pi^2}\left[\log\left(\frac{m_a m_\rho}{M_W^2}\right) - \frac{(m_a^4+m_\rho^4)}{(m_a^2-m_\rho^2)^2}\right.\\ & \left. -\frac{(m_a^2+m_\rho^2)(m_a^4-4m_a^2m_\rho^2+m_\rho^4)}{2(m_a^2-m_\rho^2)^3}\log\left(\frac{m_a^2}{m_\rho^2}\right)\right].\end{aligned} \tag{2.50}$$

It is crucial to note that, the sign of the s_h^2 term from the gauge contribution alone is always positive and can not, thus, trigger EWSB. It is therefore necessary to include the fermion contributions (especially the top quark contribution) to correctly reproduce the weak vev. The top quark contribution to the C-W potential can be calculated using the Lagrangian in Eq. (2.39) as

$$V_{\text{top}}(h) = -\,2N_c \int \frac{d^4q_E}{(2\pi)^4} \log\left[-q_E^2\left(\Pi_0^L + \frac{\Pi_1^L}{2}s_h^2\right)\left(\Pi_0^R + \Pi_1^R c_h^2\right) - \frac{|\Pi_1^{LR}|^2}{2}s_h^2 c_h^2\right]\,, \tag{2.51}$$

where N_c denotes number of QCD color of the top quark. Similar to the gauge sector, we use the Weinberg's sum rules to model the form factors and introduce minimal set of resonances required to saturate the integrals and make them finite. Following conditions on each of the form factors, leading to the Weinberg's sum rules, are employed:

$$\lim_{q_E^2\to\infty} q_E^n \frac{\Pi_1^{L,R}}{\Pi_0^{L,R}} = 0\,,\ \text{with}\ (n=0,2) \quad \text{and,} \quad \lim_{q_E^2\to\infty}\left(\frac{\Pi_1^L}{2\Pi_0^L} - \frac{\Pi_1^R}{\Pi_0^R}\right) = 0\,. \tag{2.52}$$

We employ two strong sector resonances (one singlet and a quadruplet under the unbroken $\mathrm{SO}(4)$) with masses m_{Q_1} and m_{Q_4} to saturate the integrals. Detailed expressions for the form factors are given in Appendix B. The first condition in Eq. (2.52) yields $\left|F_1^{L,R}\right| = \left|F_4^{L,R}\right| = \left|F^{L,R}\right|$, using which the expression for $\Pi_1^{L,R}$ is given by

$$\Pi_1^{L,R} = \frac{\left|F^{L,R}\right|^2 (m_{Q_4}^2 - m_{Q_1}^2)}{(q_E^2 + m_{Q_1}^2)(q_E^2 + m_{Q_4}^2)}\,. \tag{2.53}$$

For the purpose of calculating Π_1^{LR}, on the other hand, we further assume that $F_1^{L,R}$s are real and $F_4^L F_4^{R*} \simeq \left|F^L\right|\left|F^R\right| e^{i\theta_{\text{phase}}}$. This implies

$$\Pi_1^{LR} = \frac{\left|F^L\right|\left|F^R\right|}{(q_E^2 + m_{Q_1}^2)(q_E^2 + m_{Q_4}^2)}\left[(m_{Q_1} - m_{Q_4}e^{i\theta_{\text{phase}}})q_E^2 \right.$$
$$\left. + \, m_{Q_1}m_{Q_4}(m_{Q_4} - m_{Q_1}e^{i\theta_{\text{phase}}})\right]\,. \tag{2.54}$$

The top quark contribution to the parameters of the potential can now be calculated as

$$\begin{aligned}\alpha_t = \beta_t &= 2N_c \int \frac{d^4 q_E}{(2\pi)^4} \left[\frac{1}{8} \left(\frac{\Pi_1^L}{\Pi_0^L} \right)^2 + \frac{1}{2} \left(\frac{\Pi_1^R}{\Pi_0^R} \right)^2 + \frac{|\Pi_1^{LR}|^2}{2 q_E^2 \Pi_0^L \Pi_0^R} \right] , \\ &= \frac{N_c}{8\pi^2} \frac{m_t^2 m_{Q_1}^2 m_{Q_4}^2}{m_{Q_1}^2 - m_{Q_4}^2} \log \left(\frac{m_{Q_1}^2}{m_{Q_4}^2} \right) \frac{1}{\xi(1-\xi)} . \end{aligned} \tag{2.55}$$

It follows from Eq. (2.55) that, the top-quark contribution can trigger EWSB and alone gives $\xi = 0.5$. The gauge contribution, on the other hand, enables a cancellation with the fermion contribution to effectively reduce ξ. Clearly, to drive EWSB, $\alpha_g < \alpha_t$ is a requirement. The numerical impact of β_g, on the contrary, is small compared to β_t.

2.6.1 Light Higgs and light top-partner

We now explain the relation between a light Higgs boson and light top-partners. Within the partial compositeness framework, generic scaling of the Higgs mass is expected to be [79]

$$m_h^2 \sim \frac{N_c}{\pi^2} \frac{m_t^2 m_Q^2}{f^2} \sim \frac{N_c}{\pi^2} y_t^2 \frac{m_Q^2}{\Delta} , \tag{2.56}$$

where m_Q is the mass of a strong sector resonance that can mix with the top quark. The ratio $\Delta \equiv \xi^{-1} \equiv f^2/v^2$ is a measure of tuning required to obtain the electroweak vev compared to the compositeness scale[4]. It is clear from Eq. (2.56) that the relative lightness of

[4]In general, the vev-tuning in this class of models is expected to be greater than Δ, and in most cases it can be estimated as $\sim \Delta/\kappa$, where $\kappa (\lesssim 1)$ is a model dependent parameter [99, 111–114]. This is known as 'double-tuning' [97, 99]. It emerges when the coefficients of the quadratic and quartic terms in the potential do not arise in the same order of the elementary-composite mixing parameter. However, Δ quantifies as the *minimal* tuning in the Higgs vev. The situation changes when the fermions are embedded in other representations, see for example [115]. The issue of double-tuning eases in cases when multiple invariants in the Yukawa structure exist. A complementary method based on statistical approach to estimate the fine-tuning can be found in [114]. In case of MCHM_5, κ can be naïvely parametrized as $\kappa \sim (|F_Q|/m_Q)^2$. For illustration, a typical estimate shows $\kappa \sim 0.3$ with the resonance mass $m_Q \leq 1.5$ TeV and $\Delta = 10$ [99].

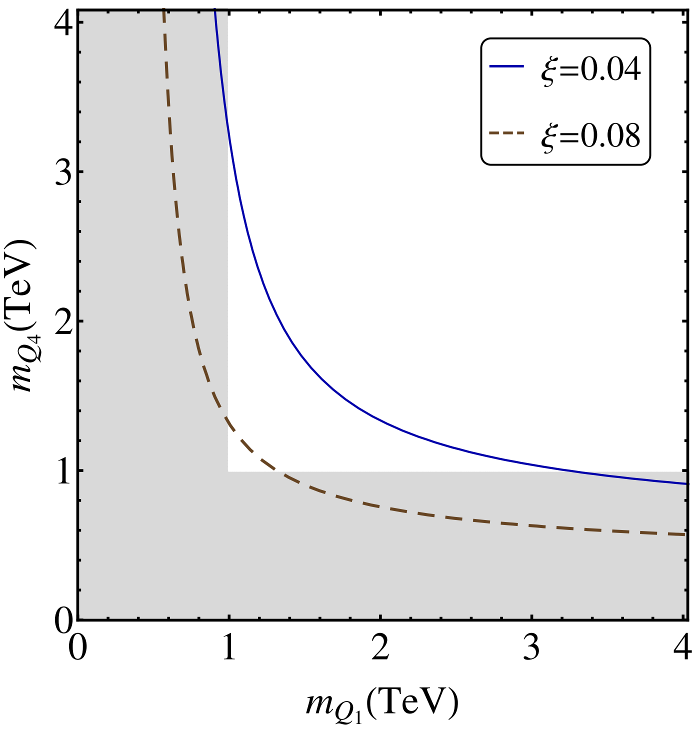

Figure 2.8: *The 125 GeV Higgs mass contour in $m_{Q_1} - m_{Q_4}$ plane is shown for two different choices $\xi = 0.04$ (blue solid line), and $\xi = 0.08$ (brown dashed line). The gray area is excluded by the direct search limits from LHC Run 1.*

the Higgs boson requires either a relatively light colored top-partner or a large fine-tuning. The non-observation of any exotic colored particle at the LHC [116] pushes to larger values of Δ implying more fine-tuned scenarios. This is nothing but a restatement of the more generic observation that the measured Higgs boson mass of ~ 125 GeV is somewhat on the lower side for the otherwise well-motivated composite Higgs framework. It may be contrasted with the supersymmetric extension of the SM where the observed Higgs mass is perceived to be on the heavier side [117, 118]. The connection of light resonances with composite Higgs mass has been studied extensively in the context of minimal model applying the QCD-like Weinberg sum rules [79, 87, 96, 97, 99], effective two-site models [99] or from explicit calculations with the 5D duals of these theories [88, 119]. In the specific scenario we are discussing, the explicit expression for the Higgs mass can be calculated using Eqs. (2.44) and (2.55) as

$$m_h^2 = \frac{N_c}{\pi^2}\frac{m_t^2}{f^2}\frac{m_{Q_1}^2 m_{Q_4}^2}{m_{Q_1}^2 - m_{Q_4}^2}\log\left(\frac{m_{Q_1}^2}{m_{Q_4}^2}\right) . \tag{2.57}$$

In Fig. 2.8 we plot the contours of $m_h = 125$ GeV in the $m_{Q_1} - m_{Q_4}$ plane for $\xi = 0.08$ and 0.04. The figure suggests that the LHC Run 1 constraints on the top-partners exclude the region below $(m_{Q_1},\ m_{Q_4}) \sim 1$ TeV [116]. It has been shown that two-loop contributions to the C-W potential from the colored vector resonances of the strong sector can relax this by $5 - 10\%$ [120]. Implications of the lepton (τ) resonances on fine-tuning have also been considered in the literature [102, 121]. Discrete parities can also be employed to gain more breathing space for the top-partners, as shown in [113, 122, 123]. In Section 3, we demonstrate a novel avenue to disentangle the connection between light Higgs boson and light top-partners by going beyond the minimal setup.

2.7 Summary

We present in this chapter, a short review of existing literature on the composite pNGB Higgs models. We have focused on the basic framework of the composite scenario that will be relevant for discussions in the subsequent chapters. The modern incarnation of the technicolor models, consisting a strongly interacting sector endowed with a global symmetry, can yield pNGB Higgs boson in the low energy spectrum. The SM matter sector, however, communicates via linear mixing with the operators of the composite sector. The explicit breaking of the global symmetry induces the generation of the radiative Higgs potential by Coleman-Weinberg mechanism, that in turn triggers EWSB. The composite scenarios exhibit two major phenomenological consequences:

- existence of exotic spin-1/2 and spin-1 resonances, in particular the presence of colored fermions,
- and, modification of the Higgs couplings with other SM particles.

These are testable in the collider experiments and put severe constraints on the microscopic model parameter space. In the context of the minimal composite Higgs scenario, we observe that the pNGB Higgs mass is on the heavier side to account for the observed 125 GeV Higgs boson, unless a large fine-tuning or a light top-partner is advocated. In the next few chapters we will discuss:

- how to accommodate heavier top-partners without affecting the minimal tuning by going to the next-to-minimal composite Higgs setup,
- and, how to test the modified Higgs couplings to discriminate various BSM scenarios at the present and future runs of the LHC.

Chapter 3

Next-to-minimal composite Higgs model

This chapter is based on the work published in the following paper:

A. Banerjee, G. Bhattacharyya and T. S. Ray, *Improving Fine-tuning in Composite Higgs Models*, *Phys. Rev.* D96 (2017) 035040, [1703.08011].

The $\mathrm{SO}(5)/\mathrm{SO}(4)$ coset, although provides a minimal realization of the composite pNGB Higgs framework, suffers from two important limitations. First, as we have seen in the last chapter, in the absence of severe tuning the Higgs mass naturally comes out to be too heavy to serve as a candidate for the observed 125 GeV Higgs boson. Second, the minimal coset does not allow for a 4D ultraviolet completion. Both of these issues can be addressed to some extent by an enlargement of the coset space. Many such non-minimal composite Higgs frameworks have been discussed in the literature [124–131]. In this chapter, we will confine ourselves to the next-to-minimal composite Higgs model with a coset $\mathrm{SO}(6)/\mathrm{SO}(5)$, that represents the minimal extension beyond MCHM, as it introduces an extra SM gauge-singlet scalar along with the four components of the usual Higgs doublet [124, 132–142]. Several aspects of this model has been discussed in the literature, e.g. in the context of dark matter [143–146] and electroweak baryogenesis [147]. Incidentally this also represents the minimal coset that allows for a 4D ultraviolet completion [148–153]. After laying out the fundamentals of the next-to-minimal model we explore the possibility of increasing the mass gap between the top-partner resonances and the Higgs boson for a given ξ by employing a possible tree-level doublet-singlet mixing in the pNGB scalar sector [154].

3.1 $\mathbf{SO(6)/SO(5)}$ coset structure

The next-to-minimal model is comprised of the $\mathrm{SO}(6)/\mathrm{SO}(5)$ coset [124, 133, 151, 155], which is homomorphic to $\mathrm{SU}(4)/\mathrm{Sp}(4)$. In comparison to the minimal coset, this one includes an additional CP-odd SM singlet along with the usual pNGB Higgs doublet.

3.1.1 Parametrization of pNGB degrees of freedom

Among the five pNGBs arising from the spontaneous breaking of the global $\mathrm{SO}(6) \to \mathrm{SO}(5)$, four pNGBs transform as $(\mathbf{2}, \mathbf{2})$ under $\mathrm{SO}(4) \simeq \mathrm{SU}(2)_{\mathrm{L}} \times \mathrm{SU}(2)_{\mathrm{R}}$, and the other is a singlet of $\mathrm{SO}(4)$ transforming as $(\mathbf{1}, \mathbf{1})$. The parametrization of the pNGB degrees of freedom is given as

$$\Sigma = e^{i\frac{\sqrt{2}}{f}\pi_{\hat{\alpha}}T^{\hat{\alpha}}}\Sigma_0 = \frac{1}{\pi}\sin\frac{\pi}{f}\left(\pi_1,\ \pi_2,\ \pi_3,\ \pi_4,\ \pi_5,\ \pi\cot\frac{\pi}{f}\right)^T, \tag{3.1}$$

where the broken generators denoted by $T^{\hat{\alpha}}$ are given in Appendix A, and Σ_0 represents the vacuum $(0, 0, 0, 0, 0, 1)^T$. In unitary gauge, Σ is given in terms of a CP-even field,

$h/f \equiv (\pi_4/\pi)\sin(\pi/f)$, and a CP-odd field, $\eta/f \equiv (\pi_5/\pi)\sin(\pi/f)$, as [143]

$$\Sigma = \left(0,\ 0,\ 0,\ \frac{h}{f},\ \frac{\eta}{f},\ \sqrt{1-\frac{h^2}{f^2}-\frac{\eta^2}{f^2}}\right)^T . \tag{3.2}$$

3.1.2 Gauge sector and kinetic mixing

The kinetic term for the pNGBs can be written as

$$\mathcal{L}_{\text{kin}} = \frac{f^2}{2}(\partial_\mu\Sigma)^T(\partial^\mu\Sigma) = \frac{1}{2}\left[(\partial_\mu h)^2 + (\partial_\mu \eta)^2 + \frac{(h\partial_\mu h + \eta\partial_\mu\eta)^2}{f^2-h^2-\eta^2}\right] . \tag{3.3}$$

If both h and η receive vevs, a kinetic mixing between h and η is obtained. This becomes apparent once we express the quadratic part of the above Lagrangian in terms of the shifted fields (*i.e.* $h \to h + \langle h\rangle$ and $\eta \to \eta + \langle\eta\rangle$)

$$\begin{aligned}\mathcal{L}_{\text{kin}} \ \supset\ & \frac{1}{2}\left[\left(1+\frac{\langle h\rangle^2}{f^2-\langle h\rangle^2-\langle\eta\rangle^2}\right)(\partial_\mu h)^2 + \left(1+\frac{\langle \eta\rangle^2}{f^2-\langle h\rangle^2-\langle\eta\rangle^2}\right)(\partial_\mu \eta)^2\right. \\ & \left. + \left(\frac{2\langle h\rangle\langle\eta\rangle}{f^2-\langle h\rangle^2-\langle\eta\rangle^2}\right)(\partial_\mu h)(\partial_\mu\eta)\right] . \end{aligned} \tag{3.4}$$

The canonical normalization of the kinetic term is possible by a non-unitary rotation of h and η, as is routinely employed in Radion-Higgs scenarios [156–158] or in the case of kinetic mixing in Abelian gauge extensions of the SM [159]. The general non-unitary rotation from $(h,\eta) \to (h_n, \eta_n)$ basis can be written in the form

$$h = a h_n + d\eta_n\ , \qquad \eta = b h_n + c\eta_n\ . \tag{3.5}$$

SO(6)		$\mathrm{SU(2)_L \times SU(2)_R \times U(1)_\eta}$
$\mathbf{4}$	$\to$	$(\mathbf{2},\mathbf{1})_1 + (\mathbf{1},\mathbf{2})_{-1}$
$\mathbf{6}$	$\to$	$(\mathbf{2},\mathbf{2})_0 + (\mathbf{1},\mathbf{1})_2 + (\mathbf{1},\mathbf{1})_{-2}$
$\mathbf{10}$	$\to$	$(\mathbf{2},\mathbf{2})_0 + (\mathbf{3},\mathbf{1})_2 + (\mathbf{1},\mathbf{3})_{-2}$
$\mathbf{15}$	$\to$	$(\mathbf{1},\mathbf{1})_0 + (\mathbf{2},\mathbf{2})_2 + (\mathbf{2},\mathbf{2})_{-2} + (\mathbf{3},\mathbf{1})_0 + (\mathbf{1},\mathbf{3})_0$
$\mathbf{20}$	$\to$	$(\mathbf{2},\mathbf{1})_1 + (\mathbf{2},\mathbf{1})_{-3} + (\mathbf{1},\mathbf{2})_3 + (\mathbf{1},\mathbf{2})_{-1} + (\mathbf{3},\mathbf{2})_{-1} + (\mathbf{2},\mathbf{3})_1$
$\mathbf{20'}$	$\to$	$(\mathbf{1},\mathbf{1})_0 + (\mathbf{1},\mathbf{1})_4 + (\mathbf{1},\mathbf{1})_{-4} + (\mathbf{2},\mathbf{2})_2 + (\mathbf{2},\mathbf{2})_{-2} + (\mathbf{3},\mathbf{3})_0$
$\mathbf{20''}$	$\to$	$(\mathbf{3},\mathbf{2})_{-1} + (\mathbf{2},\mathbf{3})_1 + (\mathbf{4},\mathbf{1})_{-3} + (\mathbf{1},\mathbf{4})_3$

Table 3.1: *List of $SO(6)$ representations and their decomposition under $SU(2)_L \times SU(2)_R \times U(1)_\eta$, upto dimension 20. The subscripts denote the $U(1)_\eta$ charges.*

To calculate the coefficients, we need to put the above transformations back in Eq. (3.4) and demand that, coefficients of $(\partial_\mu h_n)^2$ and $(\partial_\mu \eta_n)^2$ would be $1/2$, while that of $(\partial_\mu h_n)(\partial_\mu \eta_n)$ would be zero. Evidently, three constraint equations, thus obtained, can not be used to uniquely determine the four variables a, b, c, d. We, therefore, take a special choice $d = 0$ for our analysis. The solutions obtained for a, b and c are given by

$$a = \frac{1}{f}\sqrt{f^2 - \langle h\rangle^2}, \qquad b = -\frac{1}{f}\frac{\langle h\rangle\langle\eta\rangle}{\sqrt{f^2 - \langle h\rangle^2}}, \qquad c = \frac{\sqrt{f^2 - \langle h\rangle^2 - \langle\eta\rangle^2}}{\sqrt{f^2 - \langle h\rangle^2}}\ . \tag{3.6}$$

We have checked that the phenomenology of the ensuing theory is independent of this particular choice. With our parametrization given in Eq. (3.2), we obtain the $h_n WW$ and $h_n ZZ$ couplings scale in the same way as in the MCHM case. On the contrary, η, being a SM gauge singlet, does not couple to the gauge bosons at the lowest order.

3.1.3 Fermion sector

The one loop scalar potential receives contributions from both the gauge and fermion sectors. Gauge interactions can generate a potential only for the doublet state h, while the potential for η is protected by a global $\mathrm{U}(1)_\eta$ symmetry, which is isomorphic to a $\mathrm{SO}(2)$ rotation in the 5-6 direction of Eq. (3.2) [124, 143]. This particular symmetry manifests as the shift symmetry of η. The explicit breaking of the $\mathrm{U}(1)_\eta$ by the SM Yukawa couplings can generate a potential for η. This implies that some SM fermions, embedded in an incomplete multiplet of $\mathrm{SO}(6)$, should be charged under $\mathrm{U}(1)_\eta$. In Table 3.1, we present the representations of $\mathrm{SO}(6)$ upto dimension $\mathbf{20}$ and their decomposition under $\mathrm{SU}(2)_\mathrm{L} \times \mathrm{SU}(2)_\mathrm{R} \times \mathrm{U}(1)_\eta$. For the present purpose, we embed the SM fermions in the fundamental **6** of SO(6). Note that the two singlets $(\mathbf{1},\mathbf{1})_{\pm 2}$ in the decomposition of **6** are charged under $U(1)_\eta$ and hence are capable of breaking the symmetry protecting η. The left-handed top quark is embedded into the $(\mathbf{2},\mathbf{2})$ protecting the $Zb_L\bar{b}_L$ coupling [109], while the right-handed top quark is embedded as a linear combination in both $(\mathbf{1},\mathbf{1})$. We assume that the $\mathrm{U}(1)_\mathrm{X}$ charge of **6** is given by $X = 2/3$, which is essential to reproduce the correct SM hypercharges. The explicit embeddings for the top quark is given as

$$Q_L = \frac{1}{\sqrt{2}}(-ib_L,\ -b_L,\ -it_L,\ t_L,\ 0,\ 0)^T, \tag{3.7}$$

$$T_R = (0,\ 0,\ 0,\ 0,\ e^{i\delta}c_\theta t_R,\ s_\theta t_R)^T, \tag{3.8}$$

where $c_\theta(s_\theta)$ denote the cosine (sine) of an angle θ which is taken as a free parameter [132]. In the limit, $\theta = \pi/4$ and $\delta = \pi/2$, the $\mathrm{U}(1)_\eta$ symmetry is restored in the sense that potential for η vanishes, making it an electroweak axion which is severely constrained from charged kaon decay [160]. We assume $\delta = \pi/2$, which considerably simplifies the derived potential without losing any key feature required for the present discussion. The effective Lagrangian for the top-Higgs sector can be written in terms of formally $\mathrm{SO}(6)$ invariant objects as

$$\begin{aligned}\mathcal{L} &= \Pi_0^L(p)\bar{t}_L \not{p} t_L + \Pi_1^L(p)(\overline{Q}_L\Sigma)\not{p}(\Sigma^T Q_L) + \Pi_0^R(p)\bar{t}_R\not{p} t_R + \Pi_1^R(p)(\overline{T}_R\Sigma)\not{p}(\Sigma^T T_R) \\ &\quad + \Pi_1^{LR}(p)(\overline{Q}_L\Sigma)(\Sigma^T T_R) + \text{h.c.}\,. \end{aligned} \tag{3.9}$$

The momentum dependent form factors capture the details of the dynamics of composite resonances, whose detailed expressions in terms of the masses and decay constants of the top-partners are given in Appendix C. Substituting explicit forms of $Q_L,\ T_R$ and Σ, using Eqs. (3.7), (3.8) and (3.2) respectively, the effective Lagrangian can be rewritten as

$$\begin{aligned}\mathcal{L} &= \bar{t}_L\not{p}\left[\Pi_0^L + \frac{\Pi_1^L}{2}\frac{h^2}{f^2}\right] t_L + \bar{t}_R\not{p}\left[\Pi_0^R + \Pi_1^R\left(c_{2\theta}\frac{\eta^2}{f^2} + s_\theta^2\left(1 - \frac{h^2}{f^2}\right)\right)\right] t_R \\ &\quad + \bar{t}_L\left[\frac{\Pi_1^{LR}}{\sqrt{2}}\frac{h}{f}\left(ic_\theta\eta + s_\theta\sqrt{1 - \frac{h^2}{f^2} - \frac{\eta^2}{f^2}}\right)\right] t_R + \text{h.c.} \end{aligned} \tag{3.10}$$

Note that, due to the non-trivial η-charge of t_R, the couplings to η appears through t_R alone.

3.2 One loop scalar potential

The generic radiatively generated potential for h and η in this setup, originated by integrating out top quark and SM gauge boson loops, can be parametrized simply as

$$V_{\text{eff}}(h,\eta) = -\frac{\mu_1^2}{2}\frac{h^2}{f^2} + \frac{\lambda_1}{4}\frac{h^4}{f^4} - \frac{\mu_2^2}{2}\frac{\eta^2}{f^2} + \frac{\lambda_2}{4}\frac{\eta^4}{f^4} - \frac{\lambda_m}{2}\frac{h^2}{f^2}\frac{\eta^2}{f^2}\,, \tag{3.11}$$

where the coefficients can be calculated in terms of microscopic parameters of the composite sector using Coleman-Weinberg prescription. Before explicitly calculating the coefficients, we first discuss the minimization of the potential and present the expressions for the scalar masses. Note that, gauge interactions contribute only to the Higgs quadratic and quartic terms in addition to the top contributions, and can be absorbed inside the parameters μ_1^2 and λ_1. A generic minimization of the potential is, thus, expected to yield a non-zero vev for η arising from the negative contribution of the top sector to the η quadratic. On contrary, for the doublet case a cancellation between the top and gauge sectors is required to reproduce the electroweak vev. The minimum of the potential corresponds to

$$\xi \equiv \frac{\langle h\rangle^2}{f^2} = \frac{\lambda_2\mu_1^2 + \lambda_m\mu_2^2}{\lambda_1\lambda_2 - \lambda_m^2}\,, \qquad \chi \equiv \frac{\langle \eta\rangle^2}{f^2} = \frac{\lambda_1\mu_2^2 + \lambda_m\mu_1^2}{\lambda_1\lambda_2 - \lambda_m^2}\,. \tag{3.12}$$

Recall that, $\xi \equiv v^2/f^2$, with $v = 246$ GeV. The conditions for both h and η to develop vevs imply $\mu_1^2, \mu_2^2 > 0$. The stability of the potential can be ensured by the conditions $\lambda_1,\ \lambda_2 > 0$ and $\lambda_1\lambda_2 - \lambda_m^2 > 0$. Also, Eq. (3.2) guarantees that $\xi + \chi \leq 1$. The mass matrix of the canonically normalized fields (h_n, η_n) can be obtained by double differentiating the potential at the minima, after expressing it in terms of the shifted fields as

$$M^2(h_n, \eta_n) = \begin{pmatrix} m^2_{h_n h_n} & m^2_{h_n \eta_n} \\ m^2_{\eta_n h_n} & m^2_{\eta_n \eta_n} \end{pmatrix}\,. \tag{3.13}$$

The entries of the mass matrix are related to the parameters of the potential and the dimensionless vevs ξ and χ as follows:

$$m^2_{h_n h_n} = 2\lambda_1 a^2 \xi + 2\lambda_2 b^2 \chi - 4\lambda_m ab\sqrt{\xi\chi}\,, \tag{3.14}$$

$$m^2_{\eta_n \eta_n} = 2\lambda_2 c^2 \chi\,, \tag{3.15}$$

$$m^2_{h_n \eta_n} = m^2_{\eta_n h_n} = 2\lambda_2 bc\chi - 2\lambda_m ac\sqrt{\xi\chi}\,. \tag{3.16}$$

In order to avoid tachyonic eigenvalues, we impose the conditions $m^2_{h_n h_n}, m^2_{\eta_n \eta_n} > 0$ and $\det[M^2] > 0$. Clearly, a non-zero value of $m^2_{h_n \eta_n}$ yields a mass-mixing between the doublet and singlet. The mass eigenvalues can be calculated as [161]

$$m_{\hat{\eta}} = \sqrt{m^2_{\eta_n \eta_n} + m^2_{h_n \eta_n} \tan\theta_{\text{mix}}}\,, \tag{3.17}$$

$$m_{\hat{h}} = \sqrt{m^2_{h_n h_n} - m^2_{h_n \eta_n} \tan\theta_{\text{mix}}}\,, \tag{3.18}$$

with the corresponding eigenvectors given by

$$\begin{aligned} \hat{\eta} &= \cos\theta_{\text{mix}}\eta_n + \sin\theta_{\text{mix}} h_n\,, \\ \hat{h} &= -\sin\theta_{\text{mix}}\eta_n + \cos\theta_{\text{mix}} h_n\,. \end{aligned} \tag{3.19}$$

The doublet-singlet mixing angle θ_{mix} can be expressed in terms of the entries of the mass matrix as

$$\tan 2\theta_{\text{mix}} = \frac{2m^2_{h_n \eta_n}}{m^2_{\eta_n \eta_n} - m^2_{h_n h_n}}\,. \tag{3.20}$$

Now we calculate the coefficients of the potential in terms of parameters of the composite sector. The potential given in Eq. (3.11) can in fact be calculated by the Coleman-Weinberg prescription using the Lagrangian in Eq. (3.10) as

$$\begin{aligned} V_{\text{eff}}(h,\eta) = -2N_c \int \frac{d^4 q_E}{(2\pi)^4} \Bigg[\log\left(1 + \frac{\Pi_1^L}{2\Pi_0^L}\frac{h^2}{f^2}\right) + \log\Bigg(1 + \frac{\Pi_1^R}{\Pi_0^R}\Bigg\{ c_{2\theta}\frac{\eta^2}{f^2} \\ + s^2_\theta\left(1 - \frac{h^2}{f^2}\right)\Bigg\}\Bigg) + \log\left(1 + \frac{|\Pi_1^{LR}|^2}{2q_E^2 \Pi_0^L \Pi_0^R}\frac{h^2}{f^2}\left\{c_{2\theta}\frac{\eta^2}{f^2} + s^2_\theta\left(1 - \frac{h^2}{f^2}\right)\right\}\right)\Bigg]\,. \end{aligned} \tag{3.21}$$

After expanding all the logarithms one gets back the potential given in Eq. (3.11). The parameters $\mu_1, \lambda_1, \mu_2, \lambda_2$ and λ_m can be read off as

$$\begin{aligned} &\mu_1^2 = 2\alpha_L - 4s_\theta^2\alpha_R + 4s_\theta^4\beta_R + 2s_\theta^2\epsilon, \qquad\qquad \mu_2^2 = 4c_{2\theta}\alpha_R - 4s_\theta^2 c_{2\theta}\beta_R, \\ &\lambda_1 = \beta_L + 4s_\theta^4\beta_R + 4s_\theta^2\epsilon, \qquad \lambda_2 = 4c_{2\theta}^2\beta_R, \qquad \lambda_m = 4s_\theta^2 c_{2\theta}\beta_R + 2c_{2\theta}\epsilon\,, \end{aligned} \tag{3.22}$$

where $\alpha_{L,R}$, $\beta_{L,R}$ and ϵ encode the integrals over the momentum dependent form factors given below:

$$\alpha_{L,R} = N_c \int \frac{d^4q_E}{(2\pi)^4}\frac{\Pi_1^{L,R}}{\Pi_0^{L,R}}, \;\; \beta_{L,R} = N_c \int \frac{d^4q_E}{(2\pi)^4}\left(\frac{\Pi_1^{L,R}}{\Pi_0^{L,R}}\right)^2, \;\; \epsilon = N_c \int \frac{d^4q_E}{(2\pi)^4}\frac{|\Pi_1^{LR}|^2}{q_E^2\Pi_0^L\Pi_0^R}\,. \tag{3.23}$$

In order to calculate the integrals we will impose Weinberg sum rules on the form factors, just as in the case of minimal model. Assuming $\Pi_0^{L,R} \sim 1$ at the leading order, observe that $\beta_{L,R}$ and ϵ would converge if $\Pi_1^{L,R} \sim \mathcal{O}(1/q_E^4)$, which can be achieved with two resonances only. On the other hand, $\alpha_{L,R}$ would converge only if $\Pi_1^{L,R}$ fall faster than $\mathcal{O}(1/q_E^4)$. To achieve the latter, minimum three resonances are required. Note that, $\alpha_{L,R}$ are present only in the expressions for μ_1 and μ_2. Thus, finiteness of μ_1 and μ_2 requires introduction of at least three top-partner resonances, while for the calculability of λ_1, λ_2 and λ_m only two resonances would suffice. Since the scalar mass matrix involves only the λ's (see Eqs. (3.14)-(3.16)), employing only two resonances we can calculate the scalar masses for fixed values of ξ and χ. We will treat ξ and χ as free parameters in our analysis. Then the incalculable coefficients μ_1^2 and μ_2^2 can be expressed in terms of ξ, χ and the λs:

$$\mu_1^2 = \lambda_1\xi - \lambda_m\chi\,, \qquad \mu_2^2 = \lambda_2\chi - \lambda_m\xi\,. \tag{3.24}$$

The Weinberg sum rules arising from the condition, $\lim\limits_{q_E^2\to\infty} q_E^n \Pi_1^{L,R} = 0$, with $(n = 0, 2)$ lead to the following condition on the decay constants $F_{1,5}^{L,R}$ of the vector-like fermionic resonances:

$$\left|F_1^{L,R}\right| = \left|F_5^{L,R}\right| \equiv \left|F^{L,R}\right| \, . \tag{3.25}$$

Using this condition and the expressions for the form factors given in Appendix C, we found

$$\Pi_1^{L,R} = \frac{\left|F^{L,R}\right|^2 (m_{Q_5}^2 - m_{Q_1}^2)}{(q_E^2 + m_{Q_1}^2)(q_E^2 + m_{Q_5}^2)} \, , \tag{3.26}$$

where m_{Q_1} and m_{Q_5} denote the masses of the two lightest resonances (one singlet and another a five-plet of $\mathrm{SO}(5)$). On the other hand, to calculate Π_1^{LR}, we further assume that $F_1^{L,R}$ are real, and

$$F_5^L F_5^{R*} \simeq \left|F^L\right| \left|F^R\right| e^{i\theta_{\text{phase}}} \, . \tag{3.27}$$

With the above assumption Π_1^{LR} is found to be

$$\begin{aligned}\Pi_1^{LR} = \frac{\left|F^L\right| \left|F^R\right|}{(q_E^2 + m_{Q_1}^2)(q_E^2 + m_{Q_5}^2)} &\left[(m_{Q_1} - m_{Q_5} e^{i\theta_{\text{phase}}}) q_E^2\right. \\ &\left.+ m_{Q_1} m_{Q_5} (m_{Q_5} - m_{Q_1} e^{i\theta_{\text{phase}}})\right] \, .\end{aligned} \tag{3.28}$$

The expression for the physical top quark mass can be used to determine the product of $\left|F^L\right| \left|F^R\right|$, as shown below

$$\begin{aligned} m_t^2 &= \frac{\left|\Pi_1^{LR}(0)\right|^2}{2} \xi \left(\chi c_{2\theta} + (1-\xi) s_\theta^2\right) \\ &= \frac{\left|F^L\right|^2 \left|F^R\right|^2}{2 m_{Q_1}^2 m_{Q_5}^2} \left[m_{Q_1}^2 + m_{Q_5}^2 - 2 m_{Q_1} m_{Q_5} \cos\theta_{\text{phase}}\right] \xi \left(\chi c_{2\theta} + (1-\xi) s_\theta^2\right) \, , \end{aligned} \tag{3.29}$$

while we parametrize the ratio of the decay constants by $\left|F^L\right| \equiv r \left|F^R\right|$. It is worthwhile to mention that $F^{L,R}$ give the measures of compositeness fraction of the left- and right-handed top quarks as [98]

$$\sin\phi_L \equiv \frac{\left|F^L\right|}{\sqrt{m_{Q_5}^2 + |F^L|^2}}\,, \qquad \sin\phi_R \equiv \frac{\left|F^R\right|}{\sqrt{m_{Q_1}^2 + |F^R|^2}}\,. \tag{3.30}$$

The degree of compositeness of t_L is expected to be smaller than t_R from the precision measurements of $Zb\bar{b}$ [162], i.e. $r < 1$. Also the expression for top mass shows that for smaller values of θ_{phase} the top quark has to be more composite in order to generate $m_t \simeq 173$ GeV. Finally, after introducing all of the above relations, the free parameters in the theory now reduce to $\theta, \xi, \chi, r, \theta_{\text{phase}}$ and the top-partner resonance masses m_{Q_1}, m_{Q_5}. Employing all these relations, the integrals $\beta_{L,R}$ and ϵ can be evaluated exactly as

$$\beta_{L,R} = \frac{N_c}{8\pi^2}\left|F^{L,R}\right|^4 \left[\frac{m_{Q_1}^2 + m_{Q_5}^2}{2(m_{Q_1}^2 - m_{Q_5}^2)}\log\left(\frac{m_{Q_1}^2}{m_{Q_5}^2}\right) - 1\right]\,, \tag{3.31}$$

and

$$\epsilon = \frac{N_c}{8\pi^2}\left|F^L\right|^2\left|F^R\right|^2\left[1 - \cos\theta_{\text{phase}}\frac{m_{Q_1}m_{Q_5}}{m_{Q_1}^2 - m_{Q_5}^2}\log\left(\frac{m_{Q_1}^2}{m_{Q_5}^2}\right)\right]\,. \tag{3.32}$$

3.3 Level-splitting mechanism

We have already seen that the generic parametrization of the Higgs mass in the composite pNGB Higgs scenarios follow the pattern

$$m_h^2 \sim \frac{N_c}{\pi^2}\frac{m_t^2 m_Q^2}{f^2} \sim \frac{N_c}{\pi^2}y_t^2\frac{m_Q^2}{\Delta}\,, \tag{3.33}$$

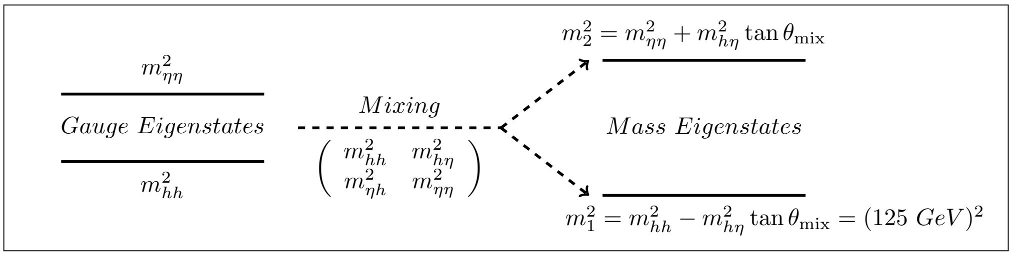

Figure 3.1: *Schematic diagram describing level-repulsion.*

leading to a strong connection between a light resonance and the light composite Higgs. However, the existence of relatively light colored top-partners is severely challenged at the LHC [116] implying larger values of Δ and hence more fine-tuned scenario. In this section we study the improvement in this tension between a light Higgs mass and the top-partner masses for a given Δ in the context of $\mathrm{SO}(6)/\mathrm{SO}(5)$ coset. We focus on the region of parameter space where a *level-splitting* mechanism, operative when both h and η develop vevs, is used to release this tension. The main idea is, if the singlet state is heavier than the doublet, the mixing between them can lead to the level-repulsion pushing the dominantly doublet eigenstate down to match the observed Higgs mass at 125 GeV. The masses of both the states before mixing are conceivably larger and hence natural from the perspective of composite Higgs scenario. The setup is depicted schematically in Fig. 3.1. To achieve our objective using the level-splitting mechanism, a few conditions are essential as follows:

1. $m^2_{\eta_n\eta_n} > m^2_{h_n h_n}$.

2. $m^2_{h_n\eta_n} \neq 0$.

3. The predominantly doublet state $(\hat{h})$ should have a mass ~ 125 GeV.

Guided by the above conditions, we choose the free parameters to zoom into the region where the relaxation of the top-partner masses is most pronounced. The condition for

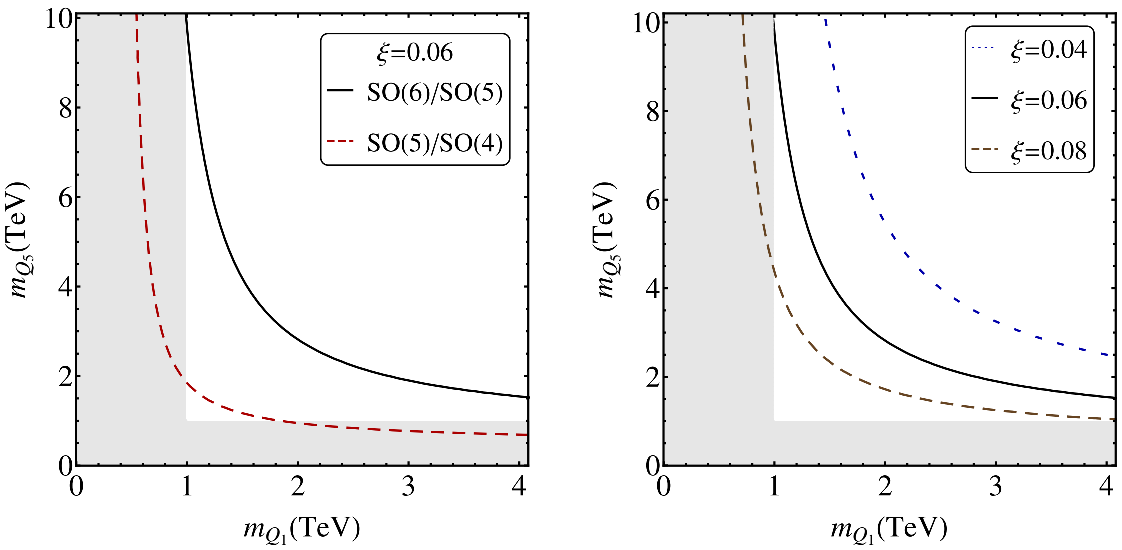

Figure 3.2: *In the left panel, we demonstrate how level-splitting enables relaxation in the parameter space of masses of the top-partners for the same value of ξ (fixed at $\xi = 0.06$, i.e. $\Delta \simeq 17$). The red dashed line shows the minimal model $m_{\hat{h}}$ =125 GeV contour. Gray areas are already excluded from the LHC Run 1 searches. The black contour refers to the next-to-minimal model. We have fixed $\theta = \pi/2,\ \chi = 0.84,\ r = 0.52$. In the right panel, three different contours are drawn for different values of ξ in the SO(6)/SO(5) coset, keeping θ, χ and r same as in the left panel. For all cases, the doublet-singlet mixing is kept within $\theta_{\rm mix} < 0.16$.*

nonzero vevs for both the doublet and the singlet requires θ to be close to $\pi/2$ and we choose $\theta_{\rm phase}$ to be near zero to keep the doublet-like state lighter. The vev of η is taken to be close to its natural value $\xi \ll \chi \lesssim 1$, a choice that does not considerably worsen the vev-tuning. Thus Δ still notionally represents the minimal vev-tuning in this model. Further the choice of r is constrained by the measurements of the Higgs couplings at the LHC, as well as meeting the condition $\Pi_0^{L,R} \simeq 1$. The latter constraints prefer the region where $m_{Q_1} < m_{Q_5}$, which will be our region of attention. Choosing these parameters admittedly results in additional tuning in the model. In any case, we obtain a considerable relaxation in the top-partner masses for a given f, as we will discuss below.

In the left panel of Fig. 3.2 we demonstrate the quantitative impact of level-splitting

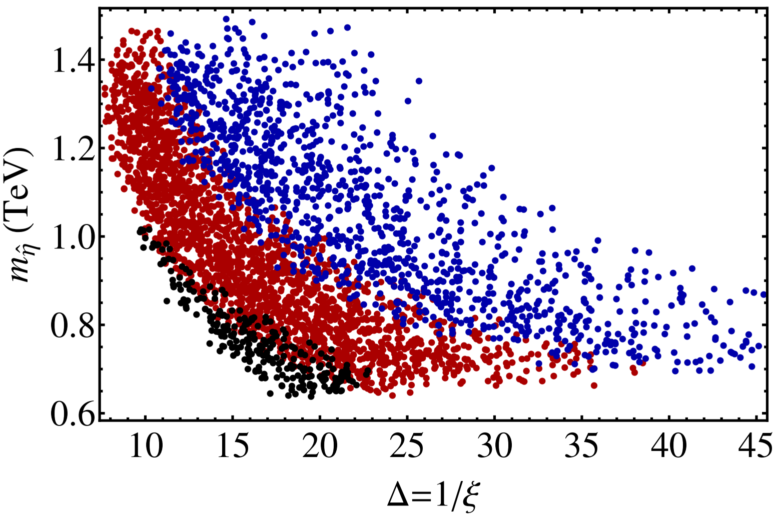

Figure 3.3: *The mass of the heavier singlet-like eigenstate ($m_{\hat{\eta}}$) is plotted as a function of Δ. Blue points correspond to $\theta_{\rm mix} < 0.15$, red to $0.15 < \theta_{\rm mix} < 0.2$ and black points to $0.2 < \theta_{\rm mix} < 0.3$. We have fixed the model parameters in the following ranges: m_{Q_1} =[1.0-1.2] TeV, m_{Q_5} =[5.5-6.0] TeV, χ =[0.75-0.90] and r =[0.45-0.90].*

in the $m_{Q_5} - m_{Q_1}$ space. The red dashed line is the contour on which the Higgs mass is 125 GeV for the minimal model for $\xi = 0.06$. Here we have mapped $m_{Q_5} \to m_{Q_4}$ while comparing the contours for the minimal and non-minimal cosets. For the same ξ, we find that the contour shifts to heavier resonance masses away from the LHC direct search limits, due to the level-repulsion mechanism. The magnitude of this shift depends on the amount of mass mixing. The right panel of Fig. 3.2 shows the Higgs mass contours in the next-to-minimal coset for different choices of ξ. The enhanced breathing space for the two lightest top-partners can be simply understood by looking at the modified expression of the Higgs mass in the next-to-minimal coset as

$$m_{\hat{h}}^2 \sim \frac{N_c}{\pi^2} y_t^2 \frac{m_Q^2}{\Delta} - m_{h_n\eta_n}^2 \tan\theta_{\rm mix} \, , \tag{3.34}$$

where the second term in the right-hand side is necessarily positive. Eq. (3.34) thus allows for a larger value of m_Q compared to what is admissible by Eq. (3.33) for the same choice of Δ. In Fig. 3.3, we plot the mass of the dominantly singlet state with Δ. It is evident from Fig. 3.3 that a smaller Δ can be obtained at the expense of increasing $m_{\hat{\eta}}$. Also, for the same Δ larger mixing results in smaller $m_{\hat{\eta}}$, as evident from Eq. (3.20).

3.4 Phenomenological consequences

In this section we discuss some major phenomenological consequences of the next-to-minimal setup. We have already mentioned that the modification of the $h_n VV$ couplings show a similar pattern of suppression as in the minimal case, quantified by $\sqrt{1-\xi}$ with respect to the SM value. However, on top of that, doublet-singlet mixing induces an additional suppression by a factor of $\theta_{\rm mix}$, to finally yield the modification of the physical Higgs couplings with the weak gauge bosons as

$$k_V = \frac{g_{\hat{h}VV}}{g^{SM}_{\hat{h}VV}} = \cos\theta_{\rm mix}\sqrt{1-\xi}\,. \tag{3.35}$$

Within the minimal model, a lower bound $f \gtrsim 700$ GeV was obtained from the Higgs physics in [163]. This is a somewhat conservative estimate compared to the limit [164] obtained from electroweak precision tests involving uncertainties arising from some incalculable UV dynamics. In the next-to-minimal scenario, the extra suppression in general strengthens the above limit on f. In fact, we have estimated that with $\theta_{\rm mix} = 0.2$, the lower bound $f \gtrsim 700$ GeV increases to $f \gtrsim 850$ GeV. For all the parameter choices that have gone into Fig. 3.2, we always keep the doublet-singlet mixing below $\theta_{\rm mix} = 0.16$, and $f > 850$ GeV (i.e. $\xi < 0.084$). In Fig. 3.4 we present the deviation of the Higgs couplings to massive gauge bosons, defined in Eq. (3.35), with the parameter Δ. The

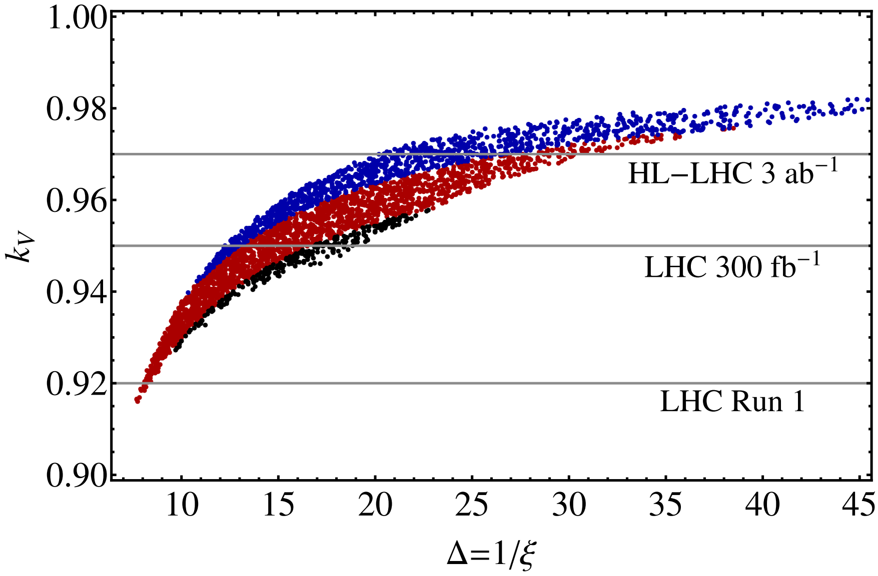

Figure 3.4: *The variation of k_V with the parameter Δ is shown. The horizontal gray lines represent the 1σ present [165] and anticipated [166, 167] LHC limits with different luminosities. For the colour codes and the values of model parameters, see caption of Fig. 3.3 (essentially $\theta_{\rm mix}$ decreases as we go up).*

plot shows that even a moderate $\Delta = 10$ is well within the LHC Run 1 tolerance limit [165]. However, future Higgs branching ratio measurements with higher luminosities at the LHC would challenge such tolerance [166, 167]. Moreover, mixing between CP-even and CP-odd states would also have consequences testable in future measurements. It is worth noting that unlike the physical Higgs couplings with the gauge bosons, the coupling of the physical Higgs to the top quark is not necessarily suppressed, leading to interesting phenomenological consequences. In the next chapter we will present a systematic study of the bounds on the Higgs couplings using the Higgs signal strength measurement data from the Run 1 and Run 2 of LHC.

In the region of parameter space of our interest (*viz.* $m^2_{\eta_n\eta_n} > m^2_{h_nh_n}$), the top quark (mainly the right-handed component) turns out to be substantially composite. In Fig. 3.5, we show the compositeness fraction of t_L (left panel) and t_R (right panel), defined in

Eq. (3.30), in the space of the top-partner masses. Note that t_L turns out to be relatively elementary [162][1], while t_R is mostly composite in a large portion of viable parameter space. Suggested studies to probe the compositeness of t_R [168, 169] would provide another handle to constrain and explore this mechanism.

Finally, we briefly comment on the phenomenology of the additional singlet-like state $\hat{\eta}$, whose detailed collider phenomenology has been studied in [136, 137]. The decay signatures of the singlet-like state $\hat{\eta}$ would leave tangible imprint in colliders. The small doublet component present in $\hat{\eta}$ is responsible for a nontrivial coupling to the weak gauge bosons. It also has a nontrivial coupling to the third generation quarks. Provided the mass of $\hat{\eta}$ is within the LHC range, it can be produced in an analogous way as the 125 GeV Higgs has been produced with the maximum contribution coming from the gluon fusion process. For large $\hat{\eta}$ mass the production will be suppressed even for sizable mixing. For $m_{\hat{\eta}} > 2m_{\hat{h}}$ and $m_{\hat{\eta}} > 2m_t$, novel decay channels like $\hat{\eta} \to \hat{h}\hat{h}$ and $\hat{\eta} \to t\bar{t}$ would open up. As shown in [137], for the choice of $m_{\hat{\eta}} = 1$ TeV, the production cross section of $\hat{\eta}$ times its branching ratio into $\hat{h}\hat{h}$ channel in LHC (13 TeV) lies in the range $(0.01 - 0.1)$ pb, and the same for $t\bar{t}$ channel is two orders of magnitude smaller. While the CMS and ATLAS exclusion limits on the same quantity for the $\hat{h}\hat{h}$ final states hovers around the predicted upper limit, the experimental exclusion limits for the $t\bar{t}$ channel currently lie substantially above the predicted numbers. As regards the production cross section times the branching ratio in the diphoton channel, the theory prediction for $m_{\hat{\eta}} = 1$ TeV is in the range $(10^{-5} - 10^{-4})$ pb, while the CMS and ATLAS sensitivities lie two orders above.

[1] However, in the region where $m_{Q_1} \sim m_{Q_5}$, t_L appears to be composite. This is a calculational artifact of forcing $r = |F^L|/|F^R|$ to fixed values for simplified presentation in the plot and simultaneously determining m_t from Eq. (3.29) using $\theta_{\rm phase} = 0$. In fact, t_L can be consistently kept mostly elementary by choosing appropriate values of r.

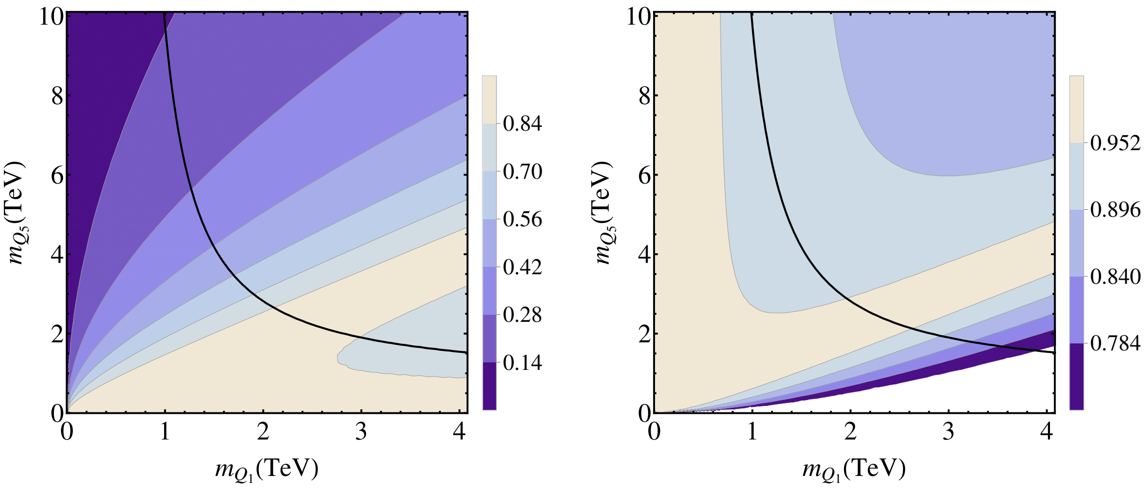

Figure 3.5: *The background shades represent the compositeness fraction of t_L (t_R), defined in Eq. (3.30), are shown in the left (right) panels, respectively, keeping $\xi = 0.06$. The black line refers to $m_{\hat{h}}$ =125 GeV, as in the left panel of Fig. 3.2.*

3.5 Summary

In this chapter we have explored the scalar sector of the next-to-minimal composite Higgs model, having a coset $\mathrm{SO}(6)/\mathrm{SO}(5)$. The set of pNGB states arising in this model contains an additional SM singlet compared to the minimal $\mathrm{SO}(5)/\mathrm{SO}(4)$ model. We demonstrate that a relaxation in the top-partner mass for a fixed value of the compositeness scale and the measured Higgs mass can be achieved in the next-to-minimal setup employing the *level-splitting* mechanism. This is operative in a generic vacuum where both the doublet and the singlet pNGBs receive non-zero vevs leading to non-trivial doublet-singlet mixing. As a result, the relatively lighter doublet-like state becomes even more lighter, to be identified with the observed 125 GeV Higgs boson, while the singlet-like state becomes further heavier.

We have discussed the main phenomenological consequences of this setup as follows:

- There would be a larger deviation in the Higgs couplings to the weak gauge bosons compared to the minimal case, which are still within the LHC limit but would start getting constrained with more precise measurements of the Higgs branching ratios. The Higgs coupling to the top quark would also be modified.

- The pronounced compositeness of the t_R that dominates the parameter space of our interest can be searched in collider and may provide a tool to probe such a mechanism.

- The phenomenology of the singlet-like scalar $\hat{\eta}$ would be similar to that of the observed Higgs boson *modulo* a significant suppression in its couplings.

CHAPTER 4

MODIFIED HIGGS COUPLINGS IN THE LIGHT OF LHC DATA

This chapter is based on the work published in the following papers:

A. Banerjee, G. Bhattacharyya, N. Kumar and T. S. Ray, ***Constraining Composite Higgs Models using LHC data*****,** ***JHEP*** **1803, 062 (2018), [1712.07494],**

A. Banerjee and G. Bhattacharyya, ***Probing the Higgs boson thorugh Yuakwa force*****, [2006.01164].**

One of the major testable signatures of composite Higgs models are deviations of the Higgs couplings from their corresponding SM predictions. As a consequence of compositeness the couplings are replaced by momentum dependent form factors, however, tracking this momentum dependence at the LHC at present is very difficult. Nevertheless, the non-linearity of the pNGB dynamics provides a finite and measurable shift in the low energy Higgs couplings at the LHC. In this chapter we systematically study the pattern and constraints on such modifications that arise in a general class of composite Higgs models. We survey various possibilities in the context of both the minimal and the next-to-minimal cosets, by varying the representations in which the elementary fermions are embedded [170]. Model independent constraints are imposed on the allowed range of the Higgs couplings using the Run 1 and Run 2 data from the ATLAS and CMS collaborations[171]. For this purpose we use an effective phenomenological Lagrangian, whose parameters can capture the coupling modifications of a general class of models. To show the future prospects, we also give the projections of the Higgs coupling measurements at the high luminosity runs of the LHC (HL-LHC). Finally we translate the limits on the generic coupling modification factors to constrain the microscopic model parameters.

4.1 Modification of Yukawa Couplings

In this section we consider different representations for the top quark in $\mathrm{SO}(5)/\mathrm{SO}(4)$ and $\mathrm{SO}(6)/\mathrm{SO}(5)$ cosets and calculate the modifications in the Yukawa coupling in a systematic manner. We categorize the cases considered under three major heads:

- *Minimal model*: Coset $\mathrm{SO}(5)/\mathrm{SO}(4)$, where both left- and right-handed fermions embedded in the fundamental **5** of $\mathrm{SO}(5)$, denoted in literature as $\mathrm{MCHM}_{5_L-5_R}$ [79, 88, 94, 97, 98, 100].

- *Extended models*: Coset $\mathrm{SO}(5)/\mathrm{SO}(4)$, where at least one of the left- or right-handed fermions embedded in the symmetric **14** of $\mathrm{SO}(5)$. They are represented in literature as $\mathrm{MCHM}_{14_L-14_R}$, $\mathrm{MCHM}_{14_L-5_R}$, and $\mathrm{MCHM}_{5_L-14_R}$ [99–102, 104–106].

- *Next-to-minimal models*: Coset $\mathrm{SO}(6)/\mathrm{SO}(5)$, denoted as NMCHM, where different choices of representation up to dimension **20** are considered [124, 132–137, 172].

In the partial compositeness paradigm, the Yukawa couplings are generated through a linear mixing between the elementary fermions and the operators of the strong sector. Once the strong sector is integrated out the effective interaction term between the Higgs boson and the fermions becomes [59, 173]

$$\mathcal{L}_{\text{eff}} \propto \bar{f}_L H f_R \mathcal{F}\left(\frac{H^\dagger H}{f^2}\right) . \tag{4.1}$$

Here $\mathcal{F}(H^\dagger H/f^2)$ is a function of the $\mathrm{SU}(2)_L$ doublet Higgs field which captures the contributions from higher dimensional operators with independent coefficients, in addition to the SM dimension-4 Yukawa term. This gives rise to a modification in the couplings of the Higgs boson with the fermions ($hf\bar{f}$), see also [174, 175] in a different context. In case of minimal model, the SM fermions can couple to only one operator of the strong sector. As a result, the modification of the Yukawa coupling, similar to the hVV couplings, depend only on the parameter ξ. The strong correlation between the $hf\bar{f}$ and hVV couplings results in stringent constraints on f [163, 176] from the increasingly precise measurements of Higgs signal strengths at the LHC. In the extended models the presence of more than one operator in the Yukawa sector with different coefficients weakens this correlation. This may result in a possible relaxation of the bound on f, because an enhancement in $hf\bar{f}$ vertex can partially offset the suppression in hVV coupling[1].

[1] Additionally, the extended models, carrying more than one invariant in the Yukawa sector, have the distinct advantage of being free from 'double tuning' [99].

4.1.1 $\mathrm{SO}(5)/\mathrm{SO}(4)$ Coset

As mentioned earlier, the modification in hVV coupling is solely determined by ξ, as

$$k_V = \frac{g_{hVV}}{g_{hVV}^{\mathrm{SM}}} = \sqrt{1-\xi} \simeq 1 - \frac{1}{2}\xi\,. \tag{4.2}$$

The number of Yukawa operators, on the contrary, depend on the SO(5) representations in which t_L and t_R are embedded. The relevant invariants can be written using the pNGB representation Σ in the unitary gauge as

- t_L and t_R in **5** ($\mathrm{MCHM}_{5_\mathrm{L}-5_\mathrm{R}}$): $(\overline{Q}_L^5.\Sigma)(\Sigma^T.T_R^5)$,
- t_L and t_R in **14** ($\mathrm{MCHM}_{14_\mathrm{L}-14_\mathrm{R}}$): $\Sigma^T.\overline{Q}_L^{14}.T_R^{14}.\Sigma$, $(\Sigma^T.\overline{Q}_L^{14}.\Sigma)(\Sigma^T.T_R^{14}.\Sigma)$,
- t_L in **14**, t_R in **5** ($\mathrm{MCHM}_{14_\mathrm{L}-5_\mathrm{R}}$): $\Sigma^T.\overline{Q}_L^{14}.T_R^5$, $(\Sigma^T.\overline{Q}_L^{14}.\Sigma)(\Sigma^T.T_R^5)$,
- t_L in **5**, t_R in **14** ($\mathrm{MCHM}_{5_\mathrm{L}-14_\mathrm{R}}$): $\overline{Q}_L^5.T_R^{14}.\Sigma$, $(\overline{Q}_L^5.\Sigma)(\Sigma^T.T_R^{14}.\Sigma)$.

The detailed expressions of the incomplete SO(5) multiplets Q_L and T_R are given in Appendix B. A generic Lagrangian involving the top quark is given by

$$\mathcal{L} = \bar{t}_L \not{q}\, \Pi_{t_L}(q,h) t_L + \bar{t}_R \not{q}\, \Pi_{t_R}(q,h) t_R + \bar{t}_L \Pi_{t_L t_R}(q,h) t_R + \mathrm{h.c.} \tag{4.3}$$

The details of the strong sector dynamics are encoded inside the momentum dependent Π-functions. In Table 4.1, we display the explicit forms of those functions for various representations in terms of the Higgs field with coefficients $\Pi_{0,1,2}^{L,R,LR}(q)$. The expressions for the latter in terms of the masses (m_{Q_i}) and decay constants ($F_i^{L,R}$) of the composite resonances are given in the Appendix C. The mass of the top quark and the modification of

Models	$\Pi_{t_L}(q,h)$	$\Pi_{t_R}(q,h)$	$\Pi_{t_Lt_R}(q,h)$
$\mathrm{MCHM}_{5_{\mathrm{L}}-5_{\mathrm{R}}}$	$\Pi_0^L+\Pi_1^L\frac{h^2}{f^2}$	$\Pi_0^R+\Pi_1^R\frac{h^2}{f^2}$	$\Pi_1^{LR}\frac{h}{f}\sqrt{1-\frac{h^2}{f^2}}$
$\mathrm{MCHM}_{14_{\mathrm{L}}-14_{\mathrm{R}}}$	$\Pi_0^L+\Pi_1^L\frac{h^2}{f^2}+\Pi_2^L\frac{h^4}{f^4}$	$\Pi_0^R+\Pi_1^R\frac{h^2}{f^2}+\Pi_2^R\frac{h^4}{f^4}$	$\frac{h}{f}\sqrt{1-\frac{h^2}{f^2}}\left(\Pi_1^{LR}+\Pi_2^{LR}\frac{h^2}{f^2}\right)$
$\mathrm{MCHM}_{14_{\mathrm{L}}-5_{\mathrm{R}}}$	$\Pi_0^L+\Pi_1^L\frac{h^2}{f^2}+\Pi_2^L\frac{h^4}{f^4}$	$\Pi_0^R+\Pi_1^R\frac{h^2}{f^2}$	$\frac{h}{f}\left(\Pi_1^{LR}+\Pi_2^{LR}\frac{h^2}{f^2}\right)$
$\mathrm{MCHM}_{5_{\mathrm{L}}-14_{\mathrm{R}}}$	$\Pi_0^L+\Pi_1^L\frac{h^2}{f^2}$	$\Pi_0^R+\Pi_1^R\frac{h^2}{f^2}+\Pi_2^R\frac{h^4}{f^4}$	$\frac{h}{f}\left(\Pi_1^{LR}+\Pi_2^{LR}\frac{h^2}{f^2}\right)$

Table 4.1: *List of Π-functions, defined in Eq. (4.3) for different representations.*

the Yukawa coupling can be calculated from Eq. (4.3) as

$$m_t = \left.\frac{|\Pi_{t_Lt_R}(q,h)|}{\sqrt{\Pi_{t_L}(q,h)\Pi_{t_R}(q,h)}}\right|_{q\to0,\ h\to v}, \qquad k_t = \frac{y_{ht\bar{t}}}{y_{ht\bar{t}}^{\mathrm{SM}}} = \frac{1}{y_{ht\bar{t}}^{\mathrm{SM}}}\left(1-\frac{1}{2}\xi\right)\frac{\partial m_t}{\partial v}\,. \tag{4.4}$$

The factor $\left(1-\frac{1}{2}\xi\right)$, in the second equality of Eq. (4.4), arises due to the canonical normalization of the Higgs field. The one loop contribution of the top quark to the effective Higgs-gluon-gluon (hgg) vertex in composite Higgs models is independent of the wave function renormalization effects of the top quark due to a cancellation with the loops of the colored top-partners [96, 101, 177]. The top quark contribution to the modification of the effective hgg vertex can be calculated as

$$k_{gg}^{(t)} = \frac{c_{gg}}{c_{gg}^{\mathrm{SM}}} = \frac{1}{c_{gg}^{\mathrm{SM}}}\left(1-\frac{1}{2}\xi\right)\left.\frac{\partial \log|\Pi_{t_Lt_R}(q,h)|}{\partial h}\right|_{q\to0,\ h\to v}. \tag{4.5}$$

To identify viable regions of parameter space for each of the models listed above, we construct one loop C-W potential as shown in Eq. (2.42), and reproduce the top mass, Higgs mass and the electroweak vev. The top-induced contributions to α and β in the scalar potential are calculated using certain parametrization of the form factors based on scaling arguments. The decay constants and the top-partner masses are parametrized as $F_i^{L,R} = \lambda_i^{L,R} f$ and $m_{Q_i} = g_i f$, respectively where the dimensionless constants $\lambda_i^{L,R}$ are assumed to be smaller than the strong sector couplings g_i. We keep g_i well within the perturbative limits, *i.e.* $1 < g_i < 2\pi$. Instead of using Weinberg's sum rules, the integrals over the form factors are estimated on the dimensional grounds, by incorporating sufficient number of resonances to saturate the form factors, rendering the integrals finite. For example, we display one of the integrals involved in the Higgs potential, as parametrized in [55, 178, 179]

$$\int \frac{d^4q}{(2\pi)^4} \left(\frac{\Pi_{1,2}^{L,R}(q)}{\Pi_0^{L,R}(q)} \right)^n \simeq c_{1,2}^{(n)} \frac{1}{16\pi^2} \left(\frac{\Pi_{1,2}^{L,R}(0)}{\Pi_0^{L,R}(0)} \right)^n g_i^4 f^4 \,, \quad n = 1, 2, \tag{4.6}$$

where $c_{1,2}^{(n)}$ are $\mathcal{O}(1)$ numbers and the forms factors are shown in Appendix C. The following phenomenological constraints are used to generate the allowed parameter space:

$$\begin{aligned} 169 \text{ GeV} < m_t < 176 \text{ GeV}, \;\; v = 246 \text{ GeV}, \\ 123 \text{ GeV} < m_h < 127 \text{ GeV}, \;\; 1 \text{ TeV} < m_{Q_i} = g_i f < 2\pi f \,. \end{aligned} \tag{4.7}$$

The results of our numerical analysis is presented in Fig. 4.1. The variation of k_t with ξ depends on the embedding of the top quark. For $\mathrm{MCHM}_{14_\mathrm{L}-14_\mathrm{R}}$ and $\mathrm{MCHM}_{14_\mathrm{L}-5_\mathrm{R}}$ there exist a possibility of enhancement in the top Yukawa coupling compared to its SM value ($k_t > 1$), for a large number of model points, while for $\mathrm{MCHM}_{5_\mathrm{L}-14_\mathrm{R}}$ we find k_t is always less than one. This can be attributed to the relative sign between the coefficients of the two Yukawa invariants. In Fig. 4.1 (right panel) we present the variation of $k_{gg}^{(t)}$ with k_t, and one observes that the two quantities are almost equal for all viable parameter space. This signifies that the numerical impact of the wave function renormalization of the top quark is

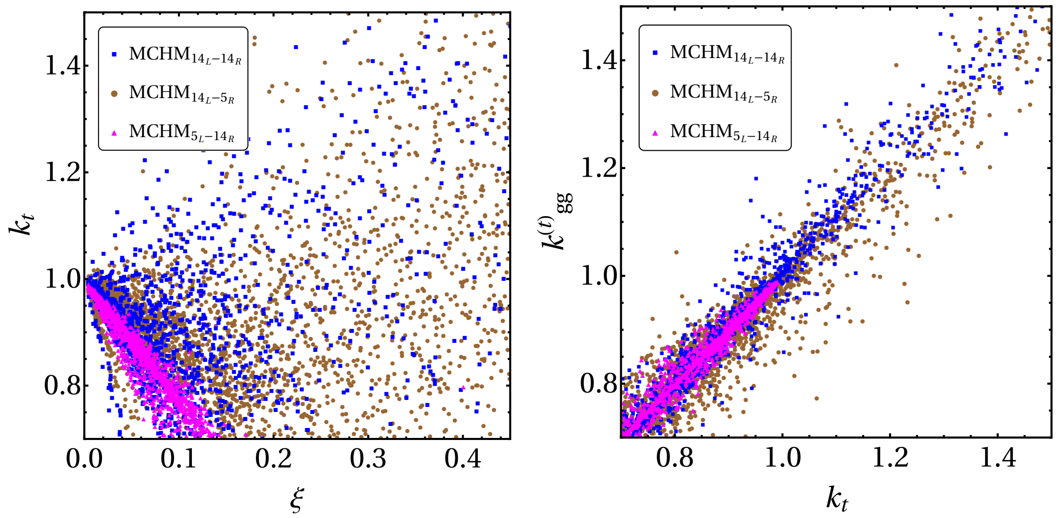

Figure 4.1: *Results from the numerical analysis for* $\mathrm{MCHM}_{14_\mathrm{L}-14_\mathrm{R}}$ *(blue),* $\mathrm{MCHM}_{14_\mathrm{L}-5_\mathrm{R}}$ *(brown) and* $\mathrm{MCHM}_{5_\mathrm{L}-14_\mathrm{R}}$ *(magenta) are shown. While generating the model points we vary the strong couplings* g_i *and* g_ρ *in the range* $[1, 2\pi]$ *and* $\lambda_i^{L,R}/g_i$ *within* $[-1, 1]$*. All the points shown in the plots satisfy the constraints given in Eqs.* (4.7).

negligible.

4.1.2 $\mathbf{SO(6)/SO(5)}$ Coset

The pNGB content of the next-to-minimal model with $\mathrm{SO}(6)/\mathrm{SO}(5)$ coset, includes a real singlet scalar (η) along with the usual Higgs doublet. Depending on whether η acquires a vev [137, 154, 172] or not [143–146], quite a few interesting features may arise in this model. Here we discuss the effect of the η-vev and consequently the doublet-singlet scalar mixing on the couplings of the Higgs boson. The structure of the generic Lagrangian involving the top quark is similar to that of the SO(5)/SO(4) coset, as shown in Eq. (4.3), however, the Π-functions now depend on both h and η (see Table D.1 of Appendix D for detailed expressions for different representations). As for the embedding of t_L and t_R in different $\mathrm{SO}(6)$ multiplets, we stick to the choices shown in the Appendix B.2 only. After the EWSB, the Lagrangian is given in terms of the canonically normalized quantum fields

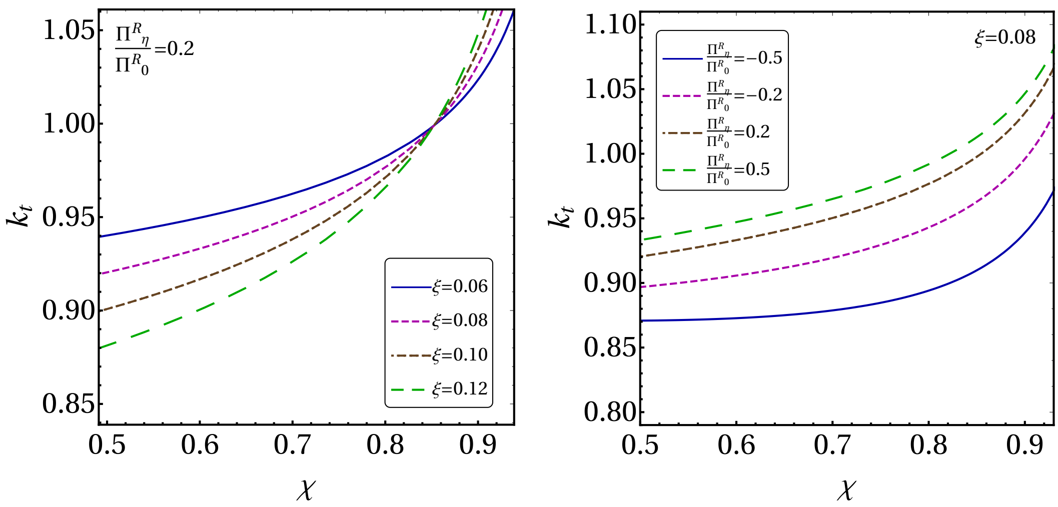

Figure 4.2: *The variation of k_t with $\chi = \langle\eta\rangle^2/f^2$ is shown. In the left panel, we fix $\Pi^R_\eta/\Pi^R_0 = 0.2$ (see Appendix D), while in the right panel we fix $\xi = 0.08$. We also assume that $\Pi^{L,R}_1 \ll \Pi^{L,R}_0$ and the mixing angle $\theta_{\rm mix} < 0.25$ is respected.*

(h_n, η_n) as

$$\mathcal{L} \supset m_t\bar{t}t + k_{t\bar{t}h_n}\left(\frac{m_t}{v}\right)h_n\bar{t}t + k_{t\bar{t}\eta_n}\left(\frac{m_t}{v}\right)\eta_n\bar{t}t\,. \tag{4.8}$$

The expression for the Yukawa coupling modifier involving the physical Higgs boson, as defined in Eq. (3.19), can be written as

$$k_t = \cos\theta_{\rm mix}k_{t\bar{t}h_n} - \sin\theta_{\rm mix}k_{t\bar{t}\eta_n}\,, \tag{4.9}$$

where $\theta_{\rm mix}$ denotes the doublet-singlet scalar mixing. In case where both $m_\eta \gg m_h$ and $\langle\eta\rangle \gg \langle h\rangle$, the mixing angle can be simply parametrized as [172]

$$\theta_{\rm mix} \sim \frac{\langle h\rangle\langle\eta\rangle}{m_\eta^2} \ll 1\,. \tag{4.10}$$

We have also observed that

$$k_{t\bar{t}\eta_n} \propto -\sqrt{\frac{\xi\chi}{1-\chi}}\,, \tag{4.11}$$

where $\chi = \langle\eta\rangle^2/f^2$. The χ dependence appears due to the spontaneous breaking of a $\mathbb{Z}_2$ symmetry associated with our choice of embedding. The appearance of ξ, on the other hand, is the consequence of constructing $\mathrm{SU}(2)$ invariant Yukawa-like term involving the η field. In Fig. 4.2 we show the variation of k_t with χ for $\mathrm{NMCHM}_{6_\mathrm{L}-6_\mathrm{R}}$. Extra model dependence would obviously appear in the case of symmetric **20**, where more than one Yukawa operator can be constructed.

4.2 Effective Phenomenological Lagrangian

The modifications of the Higgs couplings as demonstrated in the previous section have two generic features: (*i*) the hVV coupling modifier which arises from the non-linearity of the pNGBs, is universal (modulo the mixing with other states), while (*ii*) modification of the Yukawa couplings depend on the choice of representations in which the elementary fermions are embedded. Here we take a different approach to study these features of the Higgs couplings. In the absence of any definite hint of BSM physics at the collider experiments, the use of effective field theoretic descriptions have gained considerable attention [175, 180–192]. In an effective theory, the new physics contributions can be captured through the presence of higher dimensional operators. While there exists several basis for the set of independent higher dimensional operators, the strongly interacting light Higgs basis stands as the most suitable one in context of the theories of strongly interacting electroweak symmetry breaking [59, 173, 193, 194]. We use this basis to construct the following dimension-6 operators:

$$\Delta\mathcal{L} \sim \frac{1}{2f^2}\partial_\mu(H^\dagger H)\partial^\mu(H^\dagger H) - \sum_u \hat{\Delta}_u y_u \frac{H^\dagger H}{f^2}\overline{q}_L H^c u_R - \sum_d \hat{\Delta}_d y_d \frac{H^\dagger H}{f^2}\overline{q}_L H d_R + \mathrm{h.c.} \tag{4.12}$$

Below the electroweak symmetry breaking scale, these operators together with the relevant dimension-4 operators from the SM Lagrangian dictate the interactions of the physical Higgs boson with the weak gauge bosons and the quarks and leptons as [163, 195, 196]

$$\mathcal{L} = \frac{h}{v}\left[k_V\left(2M_W^2 W_\mu^\dagger W^\mu + M_Z^2 Z_\mu Z^\mu\right) - k_f \sum_f m_f \bar{f} f\right], \tag{4.13}$$

where the hVV and Yukawa coupling modifiers are given by

$$k_V = 1 - \frac{1}{2}\xi, \qquad k_f = 1 + \left(\hat{\Delta}_f - \frac{1}{2}\right)\xi \equiv 1 + \Delta_f \xi. \tag{4.14}$$

In case of k_f, the factor of $-1/2$ arises due to the canonical normalization of the Higgs field. The loop induced hgg and $h\gamma\gamma$ vertices, on the other hand arise from the following gauge invariant dimension-6 operators:

$$\mathcal{O}_{gg} \sim \frac{H^\dagger H}{v^2} G^a_{\mu\nu} G^{a\mu\nu}, \qquad \mathcal{O}_{\gamma\gamma} \sim \frac{H^\dagger H}{v^2} F_{\mu\nu} F^{\mu\nu}. \tag{4.15}$$

The above vertices may receive contributions from BSM particles along with the SM ones. Among the SM fermions the contribution from the top quark is significantly larger than the rest due to its large mass, while the weak gauge bosons substantially contribute to the $h\gamma\gamma$ vertex. In the composite Higgs scenario, however, contributions from the wave function renormalization of the top quark cancel against the resonance loop contributions [96, 101], yielding the net contribution from the top sector to the coupling modifier as

$$k^{(t)}_{gg/\gamma\gamma} = 1 + \left(\tilde{\Delta}_t - \frac{1}{2}\right)\xi \equiv 1 + \Delta'_t \xi. \tag{4.16}$$

Modifiers	Parameter dependence
k_V	$1-\frac{1}{2}\xi$
k_t	$1+\Delta_t\xi$
$k^{(t)}_{gg/\gamma\gamma}$	$1+\Delta'_t\xi$
k_b	$1+\Delta_b\xi$

Models	Δ'_t	$\Delta_t-\Delta'_t$
$\mathrm{MCHM}_{5_\mathrm{L}-5_\mathrm{R}}$	$-\frac{3}{2}$	$-\left(\frac{\Pi^L_1}{\Pi^L_0}+\frac{\Pi^R_1}{\Pi^R_0}\right)$
$\mathrm{MCHM}_{14_\mathrm{L}-14_\mathrm{R}}$	$2\frac{\Pi^{LR}_2}{\Pi^{LR}_1}-\frac{3}{2}$	$-\left(\frac{\Pi^L_1}{\Pi^L_0}+\frac{\Pi^R_1}{\Pi^R_0}\right)$
$\mathrm{MCHM}_{14_\mathrm{L}-5_\mathrm{R}}$	$2\frac{\Pi^{LR}_2}{\Pi^{LR}_1}-\frac{1}{2}$	$-\left(\frac{\Pi^L_1}{\Pi^L_0}+\frac{\Pi^R_1}{\Pi^R_0}\right)$
$\mathrm{MCHM}_{5_\mathrm{L}-14_\mathrm{R}}$	$2\frac{\Pi^{LR}_2}{\Pi^{LR}_1}-\frac{1}{2}$	$-\left(\frac{\Pi^L_1}{\Pi^L_0}+\frac{\Pi^R_1}{\Pi^R_0}\right)$

Table 4.2: *Scaling of the Higgs effective couplings for $SO(5)/SO(4)$ coset, and the expressions of Δ_t and Δ'_t for different representations of SO(5) in which top quark is embedded are displayed.*

The difference $(\Delta_t-\Delta'_t)$ contributes to the anomalous dimension of the top quark, reflecting the partial composite nature of the top in these theories. Note that, in scenarios containing only one Yukawa invariant Δ_f is a numerical constant (e.g. in $\mathrm{MCHM}_{5_\mathrm{L}-5_\mathrm{R}}$, $\Delta_f\simeq -3/2$), while in the extended models with several invariants it may deviate depending on the details of the resonances of the strong sector. A list of all the coupling modifiers within the $\mathrm{SO}(5)/\mathrm{SO}(4)$ coset is given in the left panel of Table 4.2, while the expressions for Δ_t and Δ'_t, in terms of the form factors, are displayed in the right panel.

The main feature that gets added in the next-to-minimal coset is the presence of an additional scalar singlet and its mixing with the Higgs doublet. An effective field theoretic description in terms of the strongly interacting light Higgs basis in the presence of a SM singlet is discussed in [194]. Motivated from the scenarios presented earlier, we add the following dimension-6 piece involving η to Eqs. (4.12),

$$\Delta\mathcal{L}_\eta \sim \frac{1}{2}\partial_\mu\eta\partial^\mu\eta-\sum_u y_u(\Delta^\eta_u)'\frac{\eta^2}{f^2}\bar{q}_L H^c u_R-\sum_d y_d(\Delta^\eta_d)'\frac{\eta^2}{f^2}\bar{q}_L H d_R\,. \tag{4.17}$$

We have omitted the dimension-5 operators involving a single η field due to the presence of a $\mathbb{Z}_2$ symmetry, as discussed in previous section. The resulting doublet-singlet scalar mixing ensures that the Yukawa coupling modifier of the observed Higgs boson ($\hat{h}$) assumes the following form

$$k_f = \cos\theta_{\rm mix}\,(1+\Delta_f\xi) + \sin\theta_{\rm mix}\Delta_f^\eta\sqrt{\xi}\,, \tag{4.18}$$

where Δ_f^η is a function of $(\Delta_f^\eta)'$ and the η-vev. The expressions for Δ_t^η for different representations are given in Table D.2 of Appendix D. The $\hat{h}VV$ coupling modifier is suppressed by the additional factor of $\cos\theta_{\rm mix}$ compared to the minimal coset

$$k_V = \cos\theta_{\rm mix}\sqrt{1-\xi}\,. \tag{4.19}$$

4.3 Constraints from LHC data

The signal strength (μ) of a specific process $i \to h \to f$ is usually defined as

$$\mu_i^f = \frac{\sigma_i}{\sigma_i^{\rm SM}}\frac{B_f}{B_f^{\rm SM}} = \frac{\sigma_i}{\sigma_i^{\rm SM}}\frac{\Gamma_f}{\Gamma_f^{\rm SM}}\frac{\Gamma_h^{\rm SM}}{\Gamma_h}\,, \tag{4.20}$$

where σ_i, Γ_f and B_f denote respectively, the cross-section of the $i^{\rm th}$ production mode of the Higgs boson, partial decay width of the Higgs into a final state f and the corresponding branching ratio. The total width (Γ_h) is calculated assuming that the Higgs boson can decay only to the SM particles. In terms of the conventional 'κ-framework' [197, 198], the cross-sections and decay widths normalized to their SM values are expressed as

$$\frac{\sigma_i}{\sigma_i^{\rm SM}} = \kappa_i^2, \qquad \frac{\Gamma_f}{\Gamma_f^{\rm SM}} = \kappa_f^2\,. \tag{4.21}$$

The mapping between the κ-framework and the coefficients k_i are adopted from [199]. To put constraints on k_i's, we employ a χ^2-function using the individual signal strengths. We use the ATLAS Run 2 data with $80\ fb^{-1}$ luminosity [200] and the CMS Run 2 data with $137\ fb^{-1}$ luminosity [201]. We also show the results obtained from the combined ATLAS and CMS Run 1 data [165]. In case of the HL-LHC (with luminosity $3000\ fb^{-1}$) projections, the central values are taken to be same as the SM and the uncertainties are obtained from [196]. Few crucial observations regarding the present data are in order now. First, at the Run 2, processes involving $t\bar{t}h$ production mode have been measured with unprecedented precision. Also, the errors for the $hb\bar{b}$ decay channel have improved significantly, in particular for the Higgs production associated with the weak gauge bosons. Apart from these, $gg \to h \to \gamma\gamma$ and $gg \to h \to ZZ^*$ processes that were already measured with less than 30% errors in the Run 1 have been improved to around 15% in the Run 2.

In addition to the conventional approach, we define new variables by normalizing all the signal strengths by that of the $gg \to h \to ZZ^*$ process, which is measured with the highest precision. The dependency on the total width of the Higgs is factored out and canceled in the ratios which eliminates the uncertainties that may arise from our assumption that the invisible branching ratio of the Higgs is zero. The other advantage of using the ratios is that, if we assume only SM particles run inside the loop for processes like $gg \to h$ and $h \to \gamma\gamma$, all the ratios can be expressed solely in terms of two variables, *viz.* k_t/k_V, and k_b/k_V. Thus the constraints from the Higgs signal strength measurements can be easily presented by drawing 2D confidence ellipses in the $k_b/k_V - k_t/k_V$ plane. Admittedly, while the Γ_h dependence is eliminated, the errors and correlations among the ratios slightly increase in comparison to the individual signal strengths.

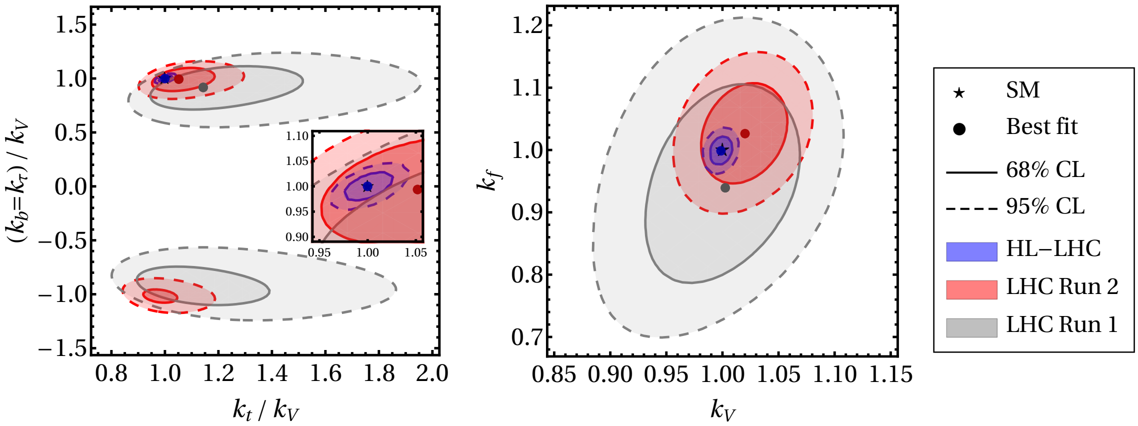

Figure 4.3: *In the left panel, joint confidence intervals on the combinations k_t/k_V and k_b/k_V are shown at 68% CL (area inside the solid lines) and 95% CL (area inside the dashed lines). We use the ratios of signal strengths given by ATLAS and CMS data from Run 1 (grey), Run2 (red) and the HL-LHC projections (blue) to put the limits. The HL-LHC projection is magnified and shown in the inset. In the right panel we use individual signal strengths and put limits on $k_t = k_b = k_\tau = k_f$ and k_V.*

4.3.1 Model independent constraints

It has been shown in [163, 202, 203] that the LEP data [42] allows around $10\% - 20\%$ deviation in k_V from its SM value at 95% CL, strongly suggesting that the observed spin-zero particle is most likely the Higgs boson responsible for the EWSB. Here we show that the present Higgs signal strength data provides competitive, if not better, limits on the Higgs couplings with respect to the electroweak precision data.

Note that, among the Higgs signal strengths, the major constraints on k_t arise from the gluon fusion and $t\bar{t}h$ production modes as well as diphoton decay channel. On the other hand, constraints on k_b arises from the $h \to b\bar{b}$ decay channel (with 58% branching ratio). Moreover, we assume $k_b = k_\tau$ in our analysis, so that data from the $h \to \tau^+\tau^-$ decay channels also contribute to the limits on k_b. The left panel of Fig. 4.3, displays the joint confidence limits on the $k_b/k_V - k_t/k_V$ plane, obtained using the ratios of the

Figure	Quantity	Run 1	Run 2	HL-LHC
Fig. 4.3 left panel	k_b/k_V	[0.55 – 1.24]	[0.81 – 1.16]	[0.95 – 1.05]
	k_t/k_V	[0.86 – 1.96]	[0.90 – 1.30]	[0.96 – 1.05]
Fig. 4.3 right panel	k_f	[0.70 – 1.21]	[0.90 – 1.16]	[0.96 – 1.04]
	k_V	[0.88 – 1.11]	[0.96 – 1.08]	[0.98 – 1.02]

Table 4.3: *The range of allowed values for different coupling modification parameters at 95% CL, extracted from the Fig. 4.3, are tabulated. Though there are two disjoint sets of limits on k_b, one on positive and the other on negative side, as evident from the left panel of Fig. 4.3, for brevity we display in this Table the positive side range only. Assuming $k_b = k_t = k_f$, the allowed 95% CL ranges of k_f/k_V is obtained using the ratios of signal strengths as: Run 1: [0.86 – 1.22], Run 2: [0.92 – 1.14], HL-LHC: [0.97 – 1.03].*

signal strengths. The clear improvement in both the quantities from Run 1 to Run 2 are direct result of more precise measurements of the Yukawa forces after the discovery of $ht\bar{t}$ [204, 205] and $hb\bar{b}$ [206, 207] couplings.

In the right panel of Fig. 4.3, we use individual signal strengths to provide the limits. Here we assume $k_t = k_b = k_\tau = k_f$ to present the joint confidence intervals in the $k_f - k_V$ plane. We extract the allowed range of values for the relevant quantities at 95% CL from the figures for different Runs of LHC and display them in Table 4.3. Two major points are worth noting in context of the right panel of Fig. 4.3. First, the limits on k_V from the Run 2 data are competitive to that obtained from the electroweak precision observables, which signals the beginning of precision Higgs era. It happens primarily due to the reduced errors in the $gg \to h \to ZZ^*$ and $gg \to h \to WW^*$ processes. Second, in addition to the hVV couplings, the window for new physics in the Yukawa couplings also narrowed down significantly. From the present data we observe only around $10\% - 15\%$ deviation is allowed from the SM value. This spectacular development in the Yukawa sector, triggered by the discovery of the Yukawa couplings at the LHC will be crucial to distinguish between various BSM scenarios. We note that the combined Run 1 + Run 2 data improve the limits

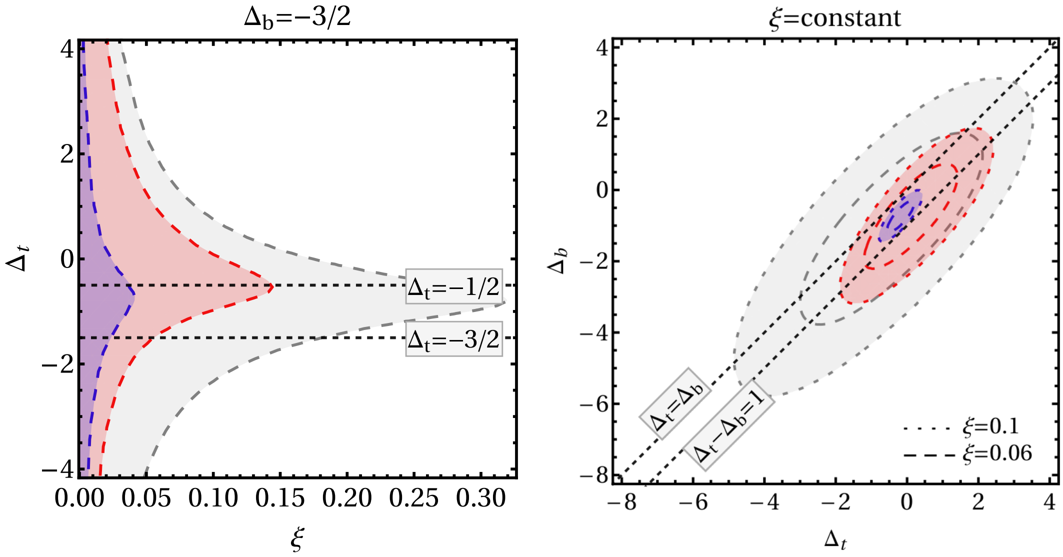

Figure 4.4: *The regions allowed at 95% CL for the minimal composite Higgs models are shown. In left panel, keeping $\Delta_b = -3/2$, joint confidence interval in the $\Delta_t - \xi$ plane is plotted, while in the right panel, the same is shown in the $\Delta_b - \Delta_t$ plane by fixing $\xi = 0.1$ (dotted) and $\xi = 0.06$ (dashed). The horizontal black dashed lines in the left panel corresponds to $\Delta_t = -1/2, -3/2$. In the right panel similar lines represent the contours of $\Delta_t - \Delta_b = 0, 1$. Color codes are same as Fig. 4.3.*

obtained from Run 2 data alone by at most 2% – 3%.

4.3.2 Constraints on composite Higgs models

First we discuss three specific cases in the context of the minimal SO(5)/SO(4) coset as follows:

- $\Delta_t = \Delta_b = \Delta_\tau = -3/2$: It corresponds to the minimal model MCHM$_{5_L-5_R}$, where the χ^2- function depends on a single parameter ξ. The lower bound on the compositeness scale f, derived from ξ, is found to be $f \gtrsim 1.2$ TeV at 95% CL after the inclusion of Run 2 data, while the projection for the same at HL-LHC is $f \gtrsim 1.8$ TeV.

- $\Delta_b = \Delta_\tau = -3/2$: In the extended models where either of the left- or right-handed top quark is embedded in **14** of SO(5), we keep Δ_t as a free parameter. The joint confidence limits at 95% CL in the $\Delta_t - \xi$ plane is shown in the left panel of Fig. 4.4. For the extended models, we obtain a lower bound $f \gtrsim 450$ GeV at 95% CL from Run 1 data only which becomes more stringent, $f \gtrsim 660$ GeV after the inclusion of Run 2 data. The clear relaxation of the bounds on f for the extended models follows from the reduced correlation between k_t and k_V, compared to the tight correlation in $\mathrm{MCHM}_{5_{\mathrm{L}}-5_{\mathrm{R}}}$. We find that projected HL-LHC bound is $f \gtrsim 1.3$ TeV at 95% CL for the extended models.

- $\xi = \mathrm{constant}$: Here we fix two representative values $\xi = 0.1$ and $\xi = 0.06$, to put simultaneous limits in $\Delta_t - \Delta_b$ plane as shown in the right panel of Fig. 4.4. We observe that future measurements at HL-LHC would have better statistical significance to distinguish between between the choices of representations in which the top and bottom quarks are embedded.

In the left panel of Fig. 4.5, the experimentally preferred regions for the Yukawa coupling modifier of the top quark is shown 95% CL in the (k_t–ξ) plane. The model points are observed to span over a large range of the preferred regions. For our analysis, we have neglected the contribution from the wave function renormalization of the top quark in k_t. In the right panel of Fig. 4.5, however, we show the effect of the wave function renormalization in the ($k_{gg}^{(t)}$–k_t) plane. We observe that present experimental precision is not sensitive to the value of $\Delta_t - \Delta_t'$. Future colliders may have sufficient precision to sense the different modifications in the top Yukawa coupling and the effective hgg coupling.

Moving to the next-to-minimal $\mathrm{SO}(6)/\mathrm{SO}(5)$ coset, we deal with a new feature that the Higgs doublet can mix with a real singlet scalar. The doublet-single mixing results

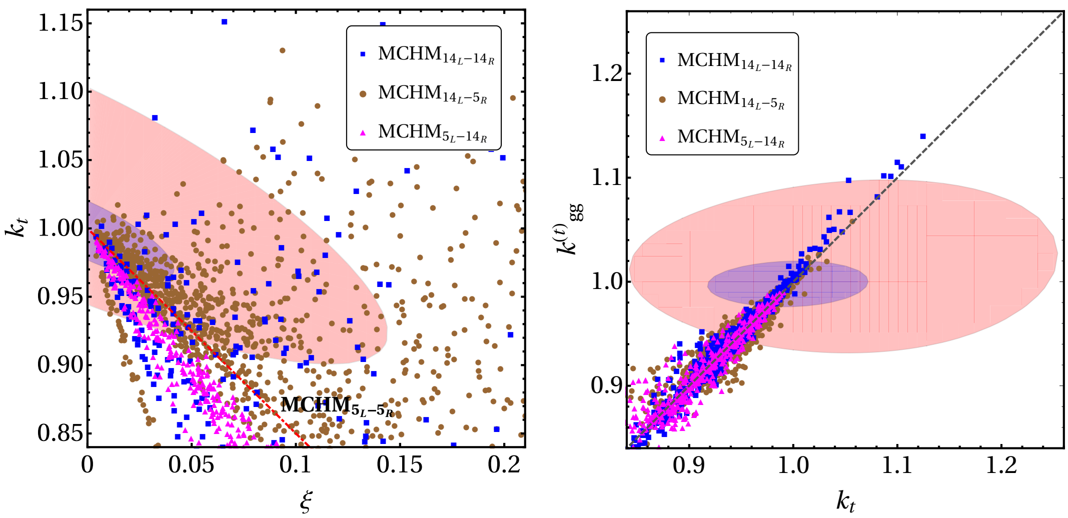

Figure 4.5: *We display the regions in the $k_t - \xi$ and $k_{gg}^{(t)} - k_t$ planes allowed at 95% CL using Run 2 data (red) and the HL-LHC projections (blue). In the left panel the red line corresponds to* $\mathrm{MCHM}_{5_L-5_R}$. *On the right panel, the grey dashed line corresponds to $\Delta_t = \Delta_t'$. Valid 'extended model' points are observed to lie within the allowed regions.*

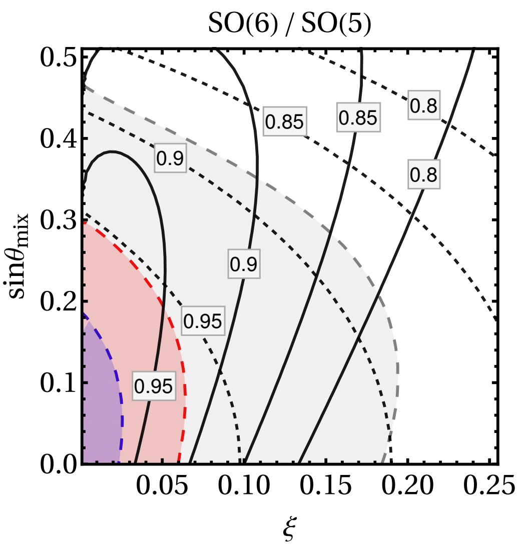

Figure 4.6: *For the next-to-minimal coset, the allowed regions in the* $\sin\theta_{\rm mix} - \xi$ *plane at 95% CL are shown using Run 1 (grey), Run 2 (red) data and the HL-LHC projections (blue). The black solid (dashed) lines represent the contours of fixed k_t (k_V).*

in an additional suppression of the hVV couplings. The Yukawa couplings are modified too because of the presence of a singlet as given in Eq. (4.18). We perform a similar χ^2 analysis, using $\Delta_t^\eta \sim \mathcal{O}(1)$ and $\Delta_b = \Delta_\tau = -3/2$ to impose a conservative upper bound on the amount of mixing. In Fig. 4.6, we present that the maximum amount of mixing allowed so far at 95% CL is $\theta_{\rm mix} \lesssim 0.3$, while the future HL-LHC data would constrain it even further [154].

4.4 Summary

Non-linearity of pNGB dynamics is responsible for modifying the Higgs boson couplings with the weak gauge bosons as well as with the quarks and leptons compared to their SM predictions. This constitutes one of the prime signature of the composite Higgs framework. The ratio ξ, parametrizing the hierarchy between the weak scale and the compositeness scale, is the major factor controlling this deformation.

- We have in fact constructed a simple phenomenological Lagrangian which captures the effects of a vast array of models on the Higgs couplings and constrained the parameters of this model-independent Lagrangian using LHC data.

- In this context we mention that the breakthrough in discovering the Yukawa force for the first time by the ATLAS and CMS collaborations play an important role. The Run 2 data is particularly instrumental in squeezing the 2σ BSM space around the SM reference point from 25% to 15% when compared to the performance of the Run 1 data. HL-LHC would bring it down to within 5%. The limits on hVV $(V = W, Z)$ couplings from the LHC are now competitive with those obtained from electroweak precision tests.

- In $\mathrm{MCHM}_{5_\mathrm{L}-5_\mathrm{R}}$, the Yukawa sector contains a single invariant. As a result the modifications of both hVV and $hf\bar{f}$ couplings are controlled by the single parameter ξ, leading to a rather strong lower limit $f \gtrsim 1.2$ TeV after including the LHC Run 2 data. In the extended models, $\mathrm{MCHM}_{14_\mathrm{L}-14_\mathrm{R}}$, $\mathrm{MCHM}_{14_\mathrm{L}-5_\mathrm{R}}$ and $\mathrm{MCHM}_{5_\mathrm{L}-14_\mathrm{R}}$, on the contrary, owing to the presence of more than one invariants in the Yukawa sector, the $hf\bar{f}$ coupling depends on additional microscopic details of the strong sector together with ξ. In such cases a new lower limit $f \gtrsim 660$ GeV, which is much relaxed compared to the limit in $\mathrm{MCHM}_{5_\mathrm{L}-5_\mathrm{R}}$, is obtained using the Run 2 data. An important feature of these models is the emergence of a parametric difference in the top Yukawa and the effective gluon-gluon-Higgs vertices, due to a cancellation between the loops of top-partners with the wave function renormalization of the top quark. However, the present data is insensitive to smell this difference.

- We have extended our analysis to the next-to-minimal coset where the appearance of a real singlet scalar adds new twists to phenomenology. Interestingly, the scalar singlet contributes to the top Yukawa through an effective higher dimensional operator.

Our analysis shows that higher precision, likely to be achieved in future colliders, would possibly discriminate between individual models, and the proposition that the Higgs boson may have a spatial extension would be challenged with more ammunition.

CHAPTER 5

EXPLORING A MODEL WITH HIGGS TRIPLETS (GEORGI-MACHACEK)

This chapter is based on the work published in the following paper:

A. Banerjee, G. Bhattacharyya and N. Kumar, *Impact of Yukawa-like dimension-five operators on the Georgi-Machacek model*, *Phys. Rev.* D99 (2019) 035028, [1901.01725].

The existence of additional scalars (e.g. $\mathrm{SU}(2)$ singlet/ doublet/ triplet) is postulated by many of the motivated BSM scenarios. Exploration of these exotic scalars through direct searches at the colliders or through their indirect contributions in various precision observables is a major exercise in progress. The absence of any signatures of new physics at the LHC so far, triggers more use of an effective field theory approach with higher dimensional operators [59, 180–182, 187], in place of detailed model building. Construction of effective theories in the singlet and two Higgs doublet extended scenarios has already received appreciable attention [194, 208–212]. Here, following a bottom-up approach we analyze the triplet-extended Higgs models using an effective field theoretic framework, keeping Yukawa-type operators up to dimension-5 [213]. Specifically, we choose a particular Higgs triplet scenario, known as the Georgi-Machacek (GM) model, which protects custodial symmetry at tree level [214–233]. In addition to the renormalizable dimension-4 Yukawa terms involving the SM Higgs doublet, we investigate the impact of including dimension-5 operators in the quark sector (especially, the third generation) employing both the doublet and triplet scalars as well.

5.1 The setup and the relevant operators

Here we present some salient features of the Georgi-Machacek model, discuss how custodial symmetry is protected at the tree level and construct the dimension-5 operators relevant for our discussions.

5.1.1 Scalar potential and custodial invariance

The GM model constitutes two Higgs triplets ξ and χ, respectively, with hypercharge $Y = 0$ and $Y = 1$, on top of the SM Higgs doublet ϕ with $Y = 1/2$. The scalar potential in this model, as we show, is invariant under a global $\mathrm{SU}(2)_\mathrm{L} \times \mathrm{SU}(2)_\mathrm{R}$ symmetry, which after the EWSB preserves a custodial $\mathrm{SU}(2)_\mathrm{V}$ symmetry at tree level without keeping the triplet scalars necessarily inert. Invariance of the scalar potential under $\mathrm{SU}(2)_\mathrm{L} \times \mathrm{SU}(2)_\mathrm{R}$ becomes evident if the Higgs doublet and the triplets are embedded in the following bi-doublet $(\mathbf{2}, \mathbf{2})$ and bi-triplet $(\mathbf{3}, \mathbf{3})$ representations under $\mathrm{SU}(2)_\mathrm{L} \times \mathrm{SU}(2)_\mathrm{R}$, respectively, as

$$\Phi = \begin{pmatrix} \phi^{0*} & \phi^{+} \\ -\phi^{-} & \phi^{0} \end{pmatrix}, \quad \Delta = \begin{pmatrix} \chi^{0*} & \xi^{+} & \chi^{++} \\ -\chi^{-} & \xi^{0} & \chi^{+} \\ \chi^{--} & -\xi^{-} & \chi^{0} \end{pmatrix}. \tag{5.1}$$

Note that, while the $\mathrm{SU}(2)_\mathrm{L}$ acts columnwise on Φ and Δ, the action of $\mathrm{SU}(2)_\mathrm{R}$ mixes elements along the rows. Now we write the most general $\mathrm{SU}(2)_\mathrm{L} \times \mathrm{SU}(2)_\mathrm{R}$ invariant scalar potential involving Φ and Δ as [219, 234]

$$\begin{aligned} V(\Phi,\Delta) \quad &= -m_1^2 \mathrm{Tr}[\Phi^\dagger\Phi] + m_2^2 \mathrm{Tr}[\Delta^\dagger\Delta] + \lambda_1(\mathrm{Tr}[\Phi^\dagger\Phi])^2 + \lambda_2(\mathrm{Tr}[\Delta^\dagger\Delta])^2 \\ &+\lambda_3 \mathrm{Tr}[(\Delta^\dagger\Delta)^2] + \lambda_4 \mathrm{Tr}[\Phi^\dagger\Phi]\mathrm{Tr}[\Delta^\dagger\Delta] + \lambda_5 \mathrm{Tr}\left[\Phi^\dagger\frac{\tau^a}{2}\Phi\frac{\tau^b}{2}\right]\mathrm{Tr}\left[\Delta^\dagger t^a \Delta t^b\right] \\ &+\mu_1 \mathrm{Tr}\left[\Phi^\dagger\frac{\tau^a}{2}\Phi\frac{\tau^b}{2}\right](P^\dagger\Delta P)^{ab} + \mu_2 \mathrm{Tr}\left[\Delta^\dagger t^a\Delta t^b\right](P^\dagger\Delta P)^{ab}. \end{aligned} \tag{5.2}$$

Here, t^a denotes the $\mathrm{SU}(2)$ generators in 3-dimensional representation and the matrix P is given by

$$P = \frac{1}{\sqrt{2}} \begin{pmatrix} -1 & i & 0 \\ 0 & 0 & 1 \\ 1 & i & 0 \end{pmatrix}. \tag{5.3}$$

The minima of the scalar potential is given by $\langle\phi^0\rangle = v_d/\sqrt{2}$, $\langle\chi^0\rangle = \langle\xi^0\rangle = v_t$, and $v^2 = v_d^2 + 8v_t^2 \simeq (246\text{ GeV})^2$. Using the standard convention, we define

$$\tan\beta \equiv \frac{2\sqrt{2}v_t}{v_d}. \tag{5.4}$$

The vacuum breaks the $\mathrm{SU}(2)_\mathrm{L} \times \mathrm{SU}(2)_\mathrm{R}$ invariance to the custodial $\mathrm{SU}(2)_\mathrm{V}$, under which one can construct the 5-plet $(H_5^{\pm\pm}, H_5^{\pm}, H_5^0)$, triplets $(G^\pm, G^0)$, $(H_3^\pm, H_3^0)$ and two singlet (h, H) scalars (see Table 5.1). The triplet $(G^\pm, G^0)$ denotes the would be Goldstones which

$\mathrm{SU}(2)_\mathrm{L} \times \mathrm{SU}(2)_\mathrm{R}$	$\to$	$\mathrm{SU}(2)_\mathrm{V}$				
$(\mathbf{2},\mathbf{2})$	$\to$	$\mathbf{1}$	$+$	$\mathbf{3}$		
$(\mathbf{3},\mathbf{3})$	$\to$	$\mathbf{1}$	$+$	$\mathbf{3}$	$+$	$\mathbf{5}$
		$\begin{pmatrix} h \\ H \end{pmatrix}$		$\begin{pmatrix} G^\pm \\ G^0 \end{pmatrix}$ $\begin{pmatrix} H_3^\pm \\ H_3^0 \end{pmatrix}$		$\begin{pmatrix} H_5^{\pm\pm} \\ H_5^\pm \\ H_5^0 \end{pmatrix}$

Table 5.1: *Decomposition of scalar bi-doublet $(\mathbf{2},\mathbf{2})$ and bi-triplet $(\mathbf{3},\mathbf{3})$ under the custodial $SU(2)_V$ symmetry. The two triplets under $SU(2)_V$ mix among each other due to non-zero vevs of both the bi-doublet and bi-triplet. One of the combinations of the $SU(2)_V$ triplets are eaten up to give mass to the W and Z bosons, while the orthogonal combinations remains in the physical spectrum. Two singlets can also mix through a mass-mixing, and the lightest eigenstate is identified with the observed 125 GeV scalar.*

will eventually be eaten up to give mass to the W and Z bosons. The two neutral scalars can further have a mass mixing, parametrized by an mixing angle α. With a slight abuse of notation, we shall continue to represent the mass eigenstates after diagonalization using the same symbols. The expressions for the physical scalars in terms of the original fields in Eq. (5.1) are provided in [219, 234].

5.1.2 Gauge kinetic terms

The canonical gauge kinetic terms using Φ and Δ can be written as

$$\mathcal{L}_{\text{kin}} = \frac{1}{2}\text{Tr}[(D_\mu\Phi)^\dagger(D_\mu\Phi)] + \frac{1}{2}\text{Tr}[(D_\mu\Delta)^\dagger(D_\mu\Delta)]\,, \tag{5.5}$$

where the covariant derivatives are given by

$$D_\mu\Phi = \partial_\mu\Phi + i\frac{g}{2}\tau_a W_\mu^a\Phi - i\frac{g'}{2}B_\mu\Phi\tau_3\,, \quad D_\mu\Delta = \partial_\mu\Phi + igt_a W_\mu^a\Delta - ig'B_\mu\Delta t_3\,. \tag{5.6}$$

The masses of the W and Z bosons, once Φ and Δ receive vevs, are found to be

$$M_W^2 = M_Z^2 \cos^2\theta_w = \frac{g^2}{4}(v_d^2 + 8v_t^2)\,, \tag{5.7}$$

which respects the usual tree level relation $\rho_{\rm tree} = 1$, governed by the custodial symmetry[1]. Finally, the couplings of the 125 GeV neutral Higgs boson with the weak gauge bosons, denoted by g_{hVV} where $V = W, Z$, are found to be modified with respect to their SM values as follows:

$$k_V = \frac{g_{hVV}}{g_{hVV}^{\rm SM}} = \cos\alpha\cos\beta + 2\sqrt{\frac{2}{3}}\sin\alpha\sin\beta\,. \tag{5.9}$$

5.1.3 Yukawa Lagrangian

We now concentrate on the couplings of the scalars with quarks. Since the Yukawa couplings do not respect custodial symmetry due to different hypercharge assignments for the left- and right-handed fermions, in place of bi-doublets and bi-triplets, we rather express the scalars as $2_{1/2}$, 3_0 and 3_1 representations under ${\rm SU(2)_L \times U(1)_Y}$:

$$\phi = \begin{pmatrix} \phi^+ \\ \phi^0 \end{pmatrix}, \quad \xi = \begin{pmatrix} \xi^0/\sqrt{2} & -\xi^+ \\ -\xi^- & -\xi^0/\sqrt{2} \end{pmatrix}, \quad \chi = \begin{pmatrix} \chi^+/\sqrt{2} & -\chi^{++} \\ \chi^0 & -\chi^+/\sqrt{2} \end{pmatrix}. \tag{5.10}$$

[1]The generic tree level relation for the ρ-parameter is given as

$$\rho_{\rm tree} = \frac{M_W^2}{M_Z^2\cos\theta_w^2} = \frac{\sum_i v_i^2\left[4T_i(T_i+1) - Y_i^2\right]}{\sum_i 2v_i^2 Y_i^2}\,, \tag{5.8}$$

where T_i and Y_i denote isospin and hypercharge of the $i^{\rm th}$ ${\rm SU(2)_L}$ multiplet, respectively. For the GM model, upon substituting the vevs one obtains $\rho_{\rm tree} = 1$.

The usual dimension-4 Yukawa Lagrangian is given as

$$-\mathcal{L}_{\text{Yuk}}^{(4)} = y_{ij}^{u}\bar{Q}_{Li}\phi^{c}u_{Rj} + y_{ij}^{d}\bar{Q}_{Li}\phi d_{Rj} + \text{h.c.}\,, \tag{5.11}$$

which is not expected to have any couplings involving the triplets ξ and χ for group theoretic reason.

On the other hand, the triplets can couple to the quarks through dimension-5 operators. The presence of higher dimensional Yukawa-like operators is not uncommon in a wide class of BSM theories. For example, such operators can originate when heavy vector-like fermions are integrated out [235, 236]. A broad class of composite Higgs models contain such heavy fermions [55, 56, 58]. However, instead of appealing to any specific BSM scenario, we construct independent dimension-5 operators involving the quarks with unknown $\mathcal{O}(1)$ coefficients as follows:

$$-\mathcal{L}_{\text{Yuk}}^{(5)} = \frac{c_5^u}{\Lambda}y_{ij}^{u}\bar{Q}_{Li}\chi^{\dagger}\phi u_{Rj} + \frac{c_5^d}{\Lambda}y_{ij}^{d}\bar{Q}_{Li}\chi\phi^{c}d_{Rj} + \frac{d_5^u}{\Lambda}y_{ij}^{u}\bar{Q}_{Li}\xi\phi^{c}u_{Rj} + \frac{d_5^d}{\Lambda}y_{ij}^{d}\bar{Q}_{Li}\xi\phi d_{Rj} + \text{h.c.} \tag{5.12}$$

Here Λ denotes the cut-off scale of the effective operators. We assume the coefficients of dimension-5 operators are aligned with the Yukawa couplings, following the minimal flavor violation hypothesis, to avoid strong constraints from flavor changing neutral current processes. The coefficients $c_5^{u,d}$ and $d_5^{u,d}$ are taken to be $\mathcal{O}(1)$ real numbers, whose exact values and signs depend on the microscopic details of the underlying UV theories. Here we treat them as free parameters. The real coefficients keep the 125 GeV Higgs boson as purely CP-even. The couplings of the quarks with the physical scalars are shown in Table 5.2. Note that, the couplings of the 5-plet scalars arise only at dimension-5, while those involving the triplet and the singlet Higgs bosons originate from both dimension-

Vertices	Feynman Rules
$h\bar{f}f$	$-i\frac{m_f}{v}\left[\frac{c_\alpha}{c_\beta}+s_\alpha\left(\frac{c_5^f}{\sqrt{3}}\pm\frac{d_5^f}{\sqrt{6}}\right)\frac{v}{\Lambda}\right]$
$H\bar{f}f$	$-i\frac{m_f}{v}\left[-\frac{s_\alpha}{c_\beta}+c_\alpha\left(\frac{c_5^f}{\sqrt{3}}\pm\frac{d_5^f}{\sqrt{6}}\right)\frac{v}{\Lambda}\right]$
$H_3^0\bar{f}f$	$\pm\gamma_5\frac{m_f}{v}\left[t_\beta-\frac{c_5^f}{\sqrt{2}}\frac{1}{c_\beta}\frac{v}{\Lambda}\right]$
$H_5^0\bar{f}f$	$-i\frac{m_f}{v}\left[\left(\frac{c_5^f}{\sqrt{6}}\mp\frac{d_5^f}{\sqrt{3}}\right)\frac{v}{\Lambda}\right]$
$H_3^+\bar{u}d$	$-i\frac{\sqrt{2}}{v}V_{ud}\left[\left(t_\beta-\frac{1}{c_\beta}\left(\frac{c_5^u}{2\sqrt{2}}+\frac{d_5^u}{2}\right)\frac{v}{\Lambda}\right)m_uP_L-\left(t_\beta-\frac{1}{c_\beta}\left(\frac{c_5^d}{2\sqrt{2}}-\frac{d_5^d}{2}\right)\frac{v}{\Lambda}\right)m_dP_R\right]$
$H_5^+\bar{u}d$	$i\frac{\sqrt{2}}{v}V_{ud}\left[\left(\frac{c_5^u}{2\sqrt{2}}-\frac{d_5^u}{2}\right)\frac{v}{\Lambda}m_uP_L-\left(\frac{c_5^d}{2\sqrt{2}}+\frac{d_5^d}{2}\right)\frac{v}{\Lambda}m_dP_R\right]$

Table 5.2: *The couplings of the quarks with the physical scalars are listed. The relative $\pm$ sign appearing in Feynman rules refer to up/down quarks. Also $s_\alpha(c_\alpha)\equiv\sin\alpha(\cos\alpha)$, where α is the mixing angle between the neutral scalars and $t_\beta(c_\beta)\equiv\tan\beta(\cos\beta)$.*

4 and dimension-5 operators. It is worthwhile to mention that, in both SM as well as, two Higgs doublet models the only dimension-5 operator that can be constructed is the Weinberg operator in the leptonic sector which generates neutrino Majorana masses [237]. Triplet extended scenarios, on the contrary, allow dimension-5 operators in the quark sector as well.

5.2 Flavor, electroweak and Higgs phenomenology

Before we discuss our results, it is worthwhile to recall the existing constraints in the GM model that guided us to choose our benchmark values. The dimension-5 Yukawa-like operators do not contribute to the oblique S and T parameters at one loop. Nevertheless, they constrain the triplet vev *via* the dimension-4 operators in the gauge sector [220, 234, 238]. The 125 GeV Higgs boson production and decay are also affected by the presence of dimension-5 operators. This, however, involves the mixing angle (α), which can be tuned to match the observed results [224, 238–244]. Non-observation from direct searches at LHC also restrict the masses of $H^{\pm}$ and $H^{\pm\pm}$, though the strategies involve several assumptions [242, 245–254].

Here we discuss the limits on the masses and couplings of the charged Higgs using the radiative B decay, neutral B-meson mixing and the precision measurement of the $Zb\bar{b}$ vertex. We also show the constraints on the neutral Higgs mixing angle α using the Run 2 data of the Higgs signal strength measurements at ATLAS and CMS.

5.2.1 $B \to X_s\gamma$ decay

The experimental world average for $\mathrm{Br}^{\mathrm{exp}}(B \to X_s\gamma) = (3.32 \pm 0.16) \times 10^{-4}$ [255], while $\mathrm{Br}^{\mathrm{SM}}(B \to X_s\gamma) = (3.36 \pm 0.23) \times 10^{-4}$ [256]. The branching ratio of the decay $B \to X_s\gamma$ receives large contributions from the charged Higgs couplings through the Wilson coefficient C_7^{eff}. The generic structure of the charged Higgs ($H_i^{\pm}$) couplings with the quarks can be written as

$$\mathcal{L} = \frac{\sqrt{2}}{v} V_{ud} H_i^{+} \bar{u} \left[A_u^i m_u P_L - A_d^i m_d P_R \right] d + \text{h.c.} \tag{5.13}$$

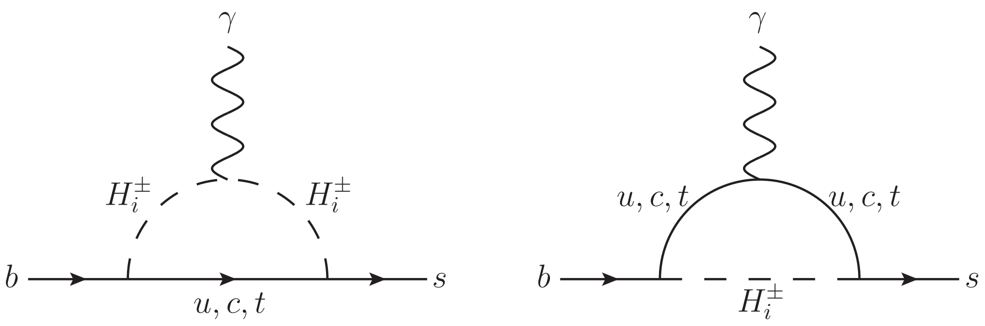

Figure 5.1: *Feynman diagrams involving the charged Higgs bosons which contribute to the amplitude of $B \to X_s\gamma$ decay.*

The new physics contributions, dominated by the top quark mass, to $C_{7,8}^{\rm eff}$ at the matching scale (~ 160 GeV [256]) is

$$\delta C_{7,8}^{\rm eff} = \sum_i \left[\frac{(A_t^i)^2}{3} F_{7,8}^{(1)}(x_i) - A_t^i A_b^i F_{7,8}^{(2)}(x_i) \right] , \tag{5.14}$$

where $x_i \equiv m_t^2/m_i^2$. Here i can take two values, 3 and 5, corresponding to the scalars $H_3^\pm$ and $H_5^\pm$. We confine ourselves to the leading order in new physics. The expressions for the functions $F_{7,8}^{(1,2)}(x_i)$ can be found in [257], while that for $A_{t,b}^i$ can be read off from Table 5.2. Following [256, 258], we have translated the limits on the branching ratio to the following range

$$-0.063 \leq \delta C_7^{\rm eff} + 0.242\, \delta C_8^{\rm eff} \leq 0.073 \,, \tag{5.15}$$

where the theoretical and experimental uncertainties are combined in quadrature. In presence of only the dimension-4 operators, the new physics part of the GM model always contributes destructively with the SM amplitude, leading to a decrease in the branching ratio. On the contrary, the dimension-5 operators may contribute constructively or destructively depending on the sign of the coefficients. Yet the prediction for the overall branching

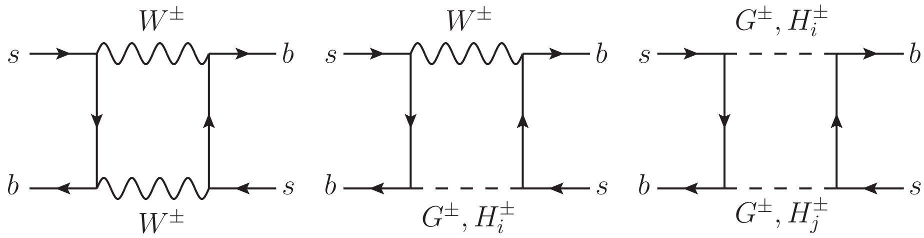

Figure 5.2: *Box diagrams contributing to the Neutral B-meson mixing.*

ratio remains reduced compared to the SM expectation, because the numerical impact of dimension-5 operators is much smaller than that of dimension-4 operators

5.2.2 Neutral B-meson mixing

For the purpose of demonstration, we show the charged Higgs contributions to the $B_s^0 - \bar{B}_s^0$ mixing, as it provides slightly stronger limits in comparison to the $B_d^0 - \bar{B}_d^0$ mixing. The main reason behind this is less uncertainties in B_s-system for both experimental measurements and the SM predictions [255]. The measured value of the mass splitting and its SM prediction in B_s-system are given as[255]

$$\Delta m_{B_s}^{\text{exp}} = (17.757 \pm 0.021)\ \text{ps}^{-1}, \quad \Delta m_{B_s}^{\text{SM}} = (18.3 \pm 2.7)\ \text{ps}^{-1}. \tag{5.16}$$

The total contributions to the mass splitting are obtained from the $W^\pm$ bosons, the Goldstones and the charged Higgs bosons ($H_3^\pm, H_5^\pm$), through the box graphs (see Fig. 5.2), whose expressions are given using the standard notations as

$$\Delta m_{B_s} = \frac{G_F^2 m_t^2}{24\pi^2}(V_{ts}^* V_{tb})^2 f_{B_s}^2 B_{B_s} m_{B_s} \eta_B I_{\text{tot}}(x_W, x_i, x_j)\,. \tag{5.17}$$

Here $x_W = m_t^2/M_W^2$, and

$$I_{\text{tot}} = I_{WW}(x_W) + \sum_{i,j}(A_t^i)^2(A_t^j)^2 I_{H_iH_j}(x_i, x_j) + 2\sum_i (A_t^i)^2 I_{WH_i}(x_W, x_i)\ . \quad (5.18)$$

The explicit expressions for the Inami-Lim functions I_{WW}, I_{WH_i} and $I_{H_iH_i}$ are given in [259, 260], while we have calculated $I_{H_iH_j}$ (with $i \neq j$) as

$$I_{H_iH_j} = x_i x_j \left[\frac{1}{(1-x_i)(1-x_j)} + \frac{\log x_i}{(x_i - x_j)(1-x_i)^2} + \frac{\log x_j}{(x_j - x_i)(1-x_j)^2}\right]. \quad (5.19)$$

After normalizing Δm_{B_s} with respect to its SM prediction, we obtain the following range at 2σ

$$0.675 \leq \frac{\Delta m_{B_s}}{\Delta m_{B_s}^{\text{SM}}} = \frac{I_{\text{tot}}(x_W, x_i, x_j)}{I_{WW}(x_W)} \leq 1.265\ . \quad (5.20)$$

Unlike in the $B \to X_s\gamma$ case, new physics contributions arising at the dimension-4 level add up constructively with the SM part in neutral meson mixing. The dimension-5 contributions, on the other hand, depend on the sign of c_5^t and d_5^t.

5.2.3 $Zb\bar{b}$ vertex

One of the most precisely measured electroweak observables is the branching ratio of the $Z \to b\bar{b}$ decay

$$R_b = \frac{\Gamma(Z \to b\bar{b})}{\Gamma(Z \to \text{hadrons})}\ , \quad (5.21)$$

where $R_b^{\text{exp}} = 0.21629 \pm 0.00066$ [261] and $R_b^{\text{SM}} = 0.21581 \pm 0.00011$ [262]. The modifications in R_b due to the charged Higgs contributions at one loop (see Fig. 5.3 for the Feynman diagrams) is given by

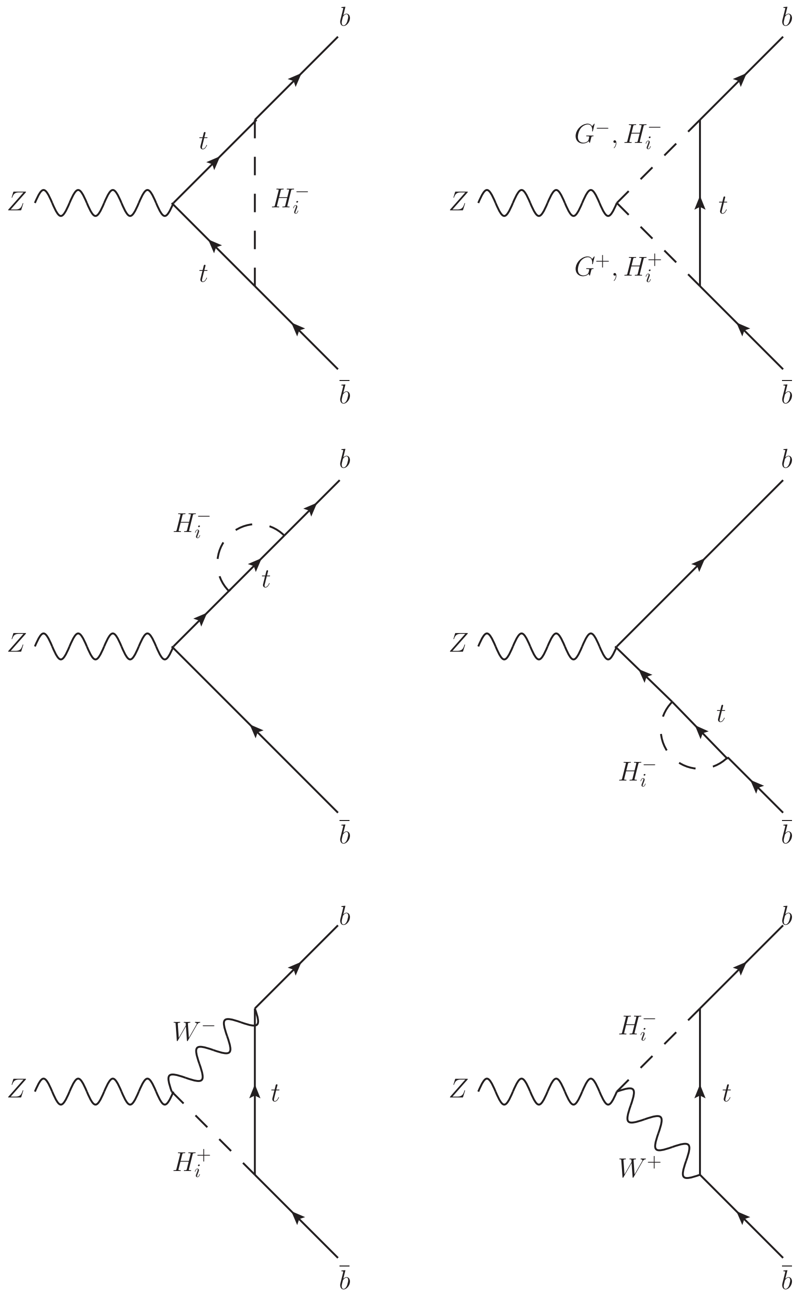

Figure 5.3: *Diagrams showing the charged Higgs contributions to the $Z \to b\bar{b}$ decay width.*

$$\delta R_b \simeq -0.7785\, \delta g^L_{\text{new}} \,. \tag{5.22}$$

Here δg^L_{new} denotes the modification in the effective $Zb_L\bar{b}_L$ coupling. It can be calculated from a combination of triangle graphs where $H^{\pm}_{3,5}$ and the charged Goldstones float inside the loop (top and middle panels in Fig. 5.3), as discussed with explicit expressions in [263, 264]. A completely new type of triangle graph, induced by the dimension-5 operators, nevertheless arises in our context. This involves the set $\{H^{\pm}_5, W^{\mp}, t\}$ inside the loop, as shown in the lower panel of Fig. 5.3 with $i = 5$. Its contribution is calculated as

$$\delta g^L_{\text{new}}(H^{\pm}_5, W^{\mp}, t) = -\frac{g^2}{16\pi^2}|V_{tb}|^2 \left(\frac{c^t_5}{2\sqrt{2}} - \frac{d^t_5}{2}\right) \frac{v}{\Lambda} s_\beta m_t^2 C_0(m_t, M_W, m_5)\,, \tag{5.23}$$

where $C_0(m_t, M_W, m_5)$ is the usual Passarino-Veltman function [265]. This new graph provides a numerically significant interference with the other contributions. Note that, a similar graph with $H^{\pm}_3$ does not exist as the $ZW^+H^-_3$ vertex is absent in the GM model. The new physics parameter space is constrained by the following 2σ range

$$-0.00086 \leq \delta R_b \leq 0.00182\,. \tag{5.24}$$

5.2.4 Combined constraints on charged Higgs

We present here the limits on the masses of the charged Higgses from the above three observables. A few benchmark values for $c^{t,b}_5$ and $d^{t,b}_5$ are chosen for the purpose of illustration and are given in Table 5.3, where the 'Set-I' simply denotes the absence of the dimension-5 operators. The left panel of Fig. 5.4 displays the constraints in the plane of the charged

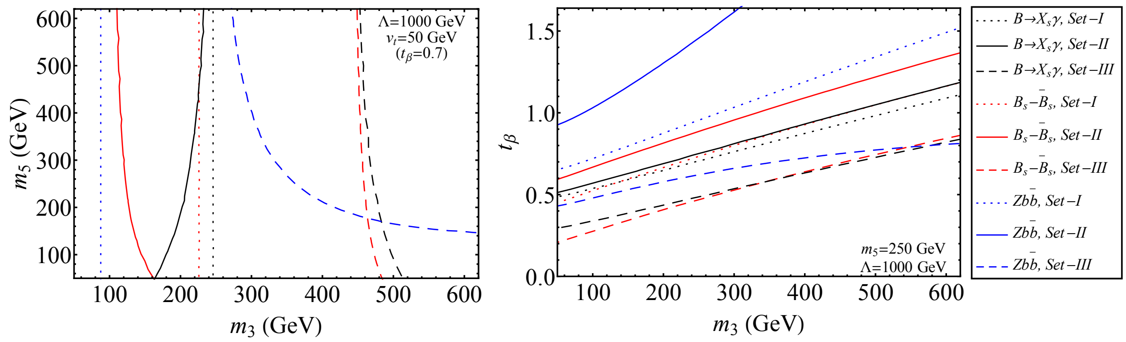

Figure 5.4: *Exclusion limits on the charged Higgs masses and the triplet vev from $B \to X_s\gamma$, $B_s^0-\bar{B}_s^0$ mixing and $Zb\bar{b}$ vertex for the different sets of benchmark parameters, as shown in Table 5.3). In the left panel, regions on the left of each curve are disfavored at 2σ, while in the right panel the regions above each curve are disfavored at 2σ. We have fixed $\Lambda = 1$ TeV, and have taken $v_t = 50$ GeV (left panel) and $m_5 = 250$ GeV (right panel).*

Set	Benchmark parameters				2σ Lower limits on m_3, m_5 (in GeV)					
					$B \to X_s\gamma$		$B_s^0 - \bar{B}_s^0$		$Zb\bar{b}$	
	c_5^t	d_5^t	c_5^b	d_5^b	m_3	m_5	m_3	m_5	m_3	m_5
					$v_t = 50$ GeV ($\tan\beta = 0.70$)					
I	0.0	0.0	0.0	0.0	250	–	225	–	85	–
II	-0.5	1.5	0.5	1.5	230	–	110	–	–	–
III	-0.5	-1.5	0.5	1.5	455	–	450	–	260	145
					$v_t = 40$ GeV ($\tan\beta = 0.52$)					
I	0.0	0.0	0.0	0.0	80	–	100	–	–	–
II	-0.5	1.5	0.5	1.5	75	–	–	–	–	–
III	-0.5	-1.5	0.5	1.5	270	–	285	–	115	50

Table 5.3: *Modified lower limits on m_3 and m_5 in presence of dimension-5 operators from the three observables for different input parameter sets. The Set-I corresponds to the purely dimension-4 case.*

Higgs masses coming from the triplet and 5-plet scalars (m_3 and m_5). The right panel shows the same limits in the $\tan\beta - m_3$ plane. We draw attention to the substantial contributions from the dimension-5 operators in comparison to the situation containing only the dimension-4 terms. The sign and magnitude of the coefficients of the new operators play a crucial rôle. In Table 5.3, we present some conservative lower limits on m_3, and in some

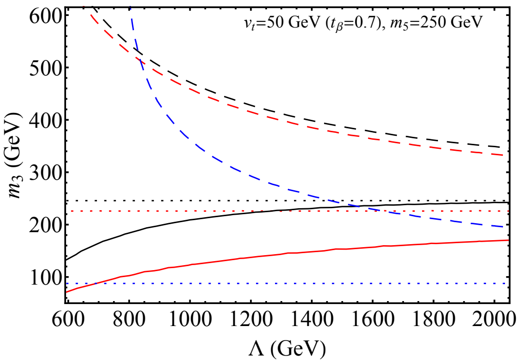

Figure 5.5: *The cut-off scale Λ is varied, fixing $v_t = 50$ GeV and $m_5 = 250$ GeV. The regions below each curve are disfavored at 2σ. The implications of different lines are as in Fig. 5.4.*

cases also on m_5, for different values of the parameters including the triplet vev. Note that, larger the triplet vev, stronger is the constraint, as expected. Reasonable constraints on m_5 arise only from $Zb\bar{b}$, due to the presence of dimension-5 operators. The situation with $B \to X_s\gamma$ has become a little tricky over the last few years [255, 266]. The experimentally measured central value and the SM prediction have moved in such a way that there exists more space to squeeze our parameters now than a few years ago. Consequently, the limits on the charged Higgs masses in the GM model from $B \to X_s\gamma$ are not as strong as before [220]. We have kept the cut-off scale $\Lambda = 1$ TeV throughout our analysis, except in Fig. 5.5 where we plotted m_3 against Λ, fixing other parameters. We emphasize that the constraints on m_3, m_5 and $\tan\beta$, *albeit* depending on the benchmark values, are both complementary as well as competitive with those obtained from oblique electroweak parameters and direct searches.

5.2.5 Constraints from Higgs signal strengths

We now discuss the limits on the $v_t - s_\alpha$ plane from the measurements of signal strengths of the 125 GeV Higgs boson at LHC. We use the Run 2 data from both CMS and ATLAS to

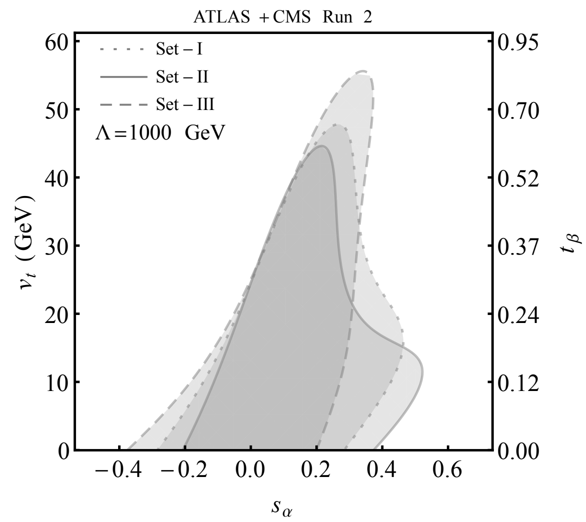

Figure 5.6: *Constraints in $v_t - s_\alpha$ plane at 2σ using the ATLAS and CMS Run 2 data is displayed. The shaded area corresponds to the allowed region. The cut-off scale Λ is fixed at 1000 GeV.*

put the limits. The hVV and $hf\bar{f}$ couplings normalized to their corresponding SM values are given by

$$k_V = c_\alpha c_\beta + 2\sqrt{\frac{2}{3}} s_\alpha s_\beta\,, \qquad k_f = \frac{c_\alpha}{c_\beta} + s_\alpha \left(\frac{c_5^f}{\sqrt{3}} \pm \frac{d_5^f}{\sqrt{6}}\right)\frac{v}{\Lambda}\,. \tag{5.25}$$

Clearly, both hVV and $hf\bar{f}$ couplings are modified even in the absence of dimension-5 operators. Therefore, Higgs signal strength measurements provide strong limits on the parameter space of the original GM model. On top of that, the dimension-5 operators in the Yukawa sector provides additional contribution to the $hf\bar{f}$ couplings, which depending on the sign and magnitude of the coefficients, may change the bounds. Using the same set of benchmark points for $c_5^{t,b}$ and $d_5^{t,b}$, as shown in Table 5.3, in Fig. 5.6 we display the limits at 95% CL in the $v_t - s_\alpha$ plane from the LHC Run 2 data. Here again, we observe the significant impact of the dimension-5 operators. In deriving these constraints we assume that the contribution of the charged Higgs bosons decouple in the $h\gamma\gamma$ decay width and falls off as $\sim v^2/m_i^2$, where $i = 3, 5$ [219]. We have further assumed that, this contribution can be neglected in comparison to that coming from dimension-5 operators provided $m_i \gg \sqrt{\Lambda v}$, which translates to $m_i \gg 500$ GeV for $\Lambda \sim 1000$ GeV. For low mass charged Higgs we expect to have more stringent constraints in comparison to what have shown in Fig. 5.6. Moreover, as shown in [244], the decoupling of the charged Higgs contribution to diphoton decay channel depends on the details of the parameters present in the scalar potential, and the limits obtained by us will change according to the decoupling behavior.

5.3 Summary

In this chapter we concentrated on triplet extended BSM scenarios from a bottom-up phenomenological approach. In particular we consider Georgi-Machacek model, which protects custodial symmetry at the tree level. Dimension-5 Yukawa-like effective operators are added in the quark sector, keeping their UV origin unspecified. Our main purpose was to demonstrate that for reasonable values of the input parameters these operators significantly modify the limits on the charged Higgs masses. In this context, we show the dimension-5 operators provide a new handle to constrain the mass of the 5-plet charged Higgs ($H_5^\pm$). We emphasize the following points regarding our analysis:

- The limits on the charged Higgs masses derived previously are not infallible once we admit higher dimensional operators and, while devising the search strategies one should not be biased by the previously existing limits.

- These operators also modify the production cross-section and branching ratios of the 125 GeV Higgs boson, which gives another way to constrain these scenarios.

Our study can be naturally extended by constructing similar operators in the leptonic sector, and importantly a new one, given by $l_L^T C i\tau_2 \chi \xi l$, together with the standard Weinberg operator $(l_L^T C i\tau_2 \phi)(\phi^T i\tau_2 l)$. A further extension can be envisaged by writing the full set of higher dimensional effective operators, in both Yukawa and gauge sectors, at the expense of introducing more parameters which would affect a large pool of observables.

CHAPTER 6

FREEZE-IN DARK MATTER MODEL

This chapter is based on the work published in the following paper:

A. Banerjee, G. Bhattacharyya, D. Chowdhury and Y. Mambrini, *Dark matter seeping through dynamic gauge kinetic mixing*, *JCAP* 1912, 009 (2019), [1905.11407].

Almost a quarter of the total energy density of the universe consists of an unknown form of matter, called the 'dark matter', whose gravitational interaction with the visible matter has only been detected till date. Among the various limitations of the SM of particle physics besides the hierarchy issue, lack of a suitable candidate for the DM is notable. In the standard lore, DM is believed to interact with its visible counterpart with non-gravitational interactions as well, however small the strength of the interaction may be. Many of the BSM scenarios, motivated otherwise, constitutes potential candidates for DM. Most popular among them is the WIMP scenario, where the DM communicates with the baryonic matter via weak interaction. The lack of any positive results in direct search experiments like XENON100 [50], LUX [51], PandaX-II [52] or more recently XENON1T [53], however, compels us to look for alternative scenarios. Combined constraints from cosmology, direct searches and accelerator based experiments have already pushed the simple BSM scenarios, like Z-portal [267–270], Higgs-portal [271–276], Z'-portal [277–283], etc., to unnatural corners of the parameter space (see [284] for recent reviews).

This situation has led to the advent of an alternative where the DM is conceived to be produced 'in' the process of progressing towards thermal equilibrium, rather than being perceived as frozen 'out' from the thermal bath. To avoid unacceptably large amount of DM production resulting in over-closure of the universe, necessitates the existence of rather feeble couplings between the dark and the visible sectors. The Feebly Interacting Massive Particle (FIMP) scenario [54, 285], thus advocated can hardly be a 'miracle' unless the small couplings can be justified from an underlying dynamics. One possibility is a mass-suppressed coupling, such as Planck scale suppressed couplings in supergravity as shown in [286–289] or suppressions arising from massive gauge bosons as mediators in SO(10) unified theories [290–292]. Similar suppressions may as well arise in massive spin-2 theories [293, 294], string theory inspired moduli portal scenarios [295] and in scenarios containing Chern-Simons type couplings [296]. A notable feature in all these constructions is a sharp temperature dependence of the DM relic density – beyond the conventional reheating temperature ($T_{\rm RH}$) – up to some maximum temperature ($T_{\rm MAX}$) accessible during the reheating process [297–303]. DM production through freeze-in mechanism may also proceed directly from the decay of inflaton [304]. Another possibility is freeze-in DM production through radiatively generated gauge kinetic mixing that we are going to discuss here. In contrary to the usual kinetic mixing with constant strengths, we demonstrate that one loop kinetic mixing, generated by integrating out some heavy vector-like fermion can act as an effective portal for freeze-in DM production [305].

6.1 Freeze-in during reheating epoch

Present day relic abundance of a DM species (χ) with mass m_χ and number density at present time $n_\chi(0)$ is defined as

$$\Omega h^2 \equiv \frac{\rho_\chi(0)}{\rho_c} = \frac{m_\chi n_\chi(0)}{\rho_c} \,. \tag{6.1}$$

Here $\rho_\chi(0)$ and $\rho_c = 8.05 \times 10^{-47}\,\mathrm{GeV}^4$ denote respectively, the energy density of the DM and the critical energy density of the universe today. The last equality indicates that the DM behave as a non-relativistic species. Evolution of the DM number density can be calculated by solving the well-known Boltzmann equation as follows:

$$\frac{\mathrm{d}n_\chi}{\mathrm{d}t} + 3H(t)n_\chi = R(T)\,, \tag{6.2}$$

where $R(T)$ denotes the effective production rate of DM and $H(T) = \sqrt{\frac{8\pi G}{3}\rho_{\mathrm{tot}}(t)}$ is the Hubble expansion rate. The total energy density of the universe at a given time receives contribution from visible matter, dark matter as well as inflaton. Requirement of structure formation in the universe necessitates that the DM relic should be fixed within the radiation dominated era. The solution of the Boltzmann equation has a non-trivial dependence on the initial conditions. In the standard freeze-out scenarios, initially the DM is assumed to be in thermal equilibrium with the visible matter due to sufficient interaction strength between the two sectors. The DM decouples from the thermal bath when the reaction rate becomes much smaller than the Hubble expansion. The number density of DM then deviates from the equilibrium distribution to produce the freeze-out relic abundance. This happens roughly around $m_\chi \sim 20T$, where T denotes the temperature of the thermal bath. On the contrary, in case of freeze-in scenario, the coupling strength of the DM with visible matter is assumed to be so small that the DM never reaches thermal equilibrium with the visible matter. Starting from zero abundance, DM would leaked-in slowly through its interaction with the visible matter to set the present day relic. Unlike the freeze-out case, the DM relic in freeze-in scenario might get fixed at a varied range of temperatures far from m_χ. Therefore, a detailed knowledge of the variation of the temperature and Hubble expansion rate at various cosmological epochs are important to determine the freeze-in relic density.

In the post-inflation cosmological backdrop we assume perturbative reheating of the universe by decay of inflaton into radiation, which quickly thermalizes among itself to fill the universe with a thermal bath. The duration of reheating crucially depends on the decay width of the inflaton. The end of the reheating is determined when the inflaton energy density goes to zero and the total energy density is dominated with radiation. A temperature ($T_{\rm RH}$) can be defined from the radiation energy density in the usual way to mark the end of the reheating epoch. However, during the onset of reheating when the inflaton energy density dominates over that of radiation, the temperature of the thermal bath can in principle be much larger than $T_{\rm RH}$. The following two equations track the evolution of the inflaton and the radiation energy densities, respectively [297, 300, 301, 306]:

$$\frac{{\rm d}\rho_\phi}{{\rm d}t} + 3H\,\rho_\phi = -\Gamma_\phi\,\rho_\phi\,, \qquad \frac{{\rm d}\rho_\gamma}{{\rm d}t} + 4H\,\rho_\gamma \approx \Gamma_\phi\,\rho_\phi\,, \tag{6.3}$$

where we have neglected the back-reaction from the interaction of DM with radiation in the evolution of the radiation energy density. We denote the mass and the decay width of the inflaton into radiation degrees of freedom using m_ϕ and Γ_ϕ, respectively. The solution of these coupled differential equations can be well approximated analytically in the limiting cases of inflaton and radiation domination. The assumption of instant thermalization of the radiation enables us to define an instantaneous temperature as $\rho_\gamma = (\pi^2 g_e/30)\, T^4$, with g_e as the number of relativistic degrees of freedom. Using the solution of Eq. (6.3), we obtain a relation between the temperature T and the dimensionless scale factor $z = a m_\phi$ as long as $T \leq T_{\rm RH}$ as [297, 301, 306]

$$T(z) \simeq \left(\frac{8^8}{3^3 5^5}\right)^{1/20} T_{\rm MAX} \left(z^{-3/2} - z^{-4}\right)^{1/4} , \tag{6.4}$$

where $T_{\rm MAX}$ is the maximum value of temperature attained during the reheating process. Clearly, during the inflaton dominated period the temperature varies as $T \propto a^{-3/8}$, which is significantly different from the usual relation $T \propto a^{-1}$ that appears during radiation dominated era. In general the relation between $T_{\rm MAX}$ and $T_{\rm RH}$ depends on the details of the inflaton sector. In the following analysis, we will take a generic choice $T_{\rm MAX} = 100\, T_{\rm RH}$ for the purpose of illustration.

Now we solve the Boltzmann Eq. (6.2), governing evolution of the freezing-in number density of DM in both inflaton ($T_{\rm MAX} \geq T \geq T_{\rm RH}$) and radiation ($T \leq T_{\rm RH}$) dominated epoch [1]. For that purpose, it is more convenient to express the evolution of n_χ in Eq. (6.2) with temperature rather than time. In the radiation dominated era the standard expression involving the Hubble rate is given by

$$\frac{\mathrm{d}}{\mathrm{d}t} = -H(T) T \frac{\mathrm{d}}{\mathrm{d}T} \quad \text{with} \;\; H(T) = \sqrt{\frac{g_e}{90}}\pi \frac{T^2}{M_P} \, . \tag{6.5}$$

The comoving number density during this epoch, which by definition does not change due to the Hubble expansion, is defined by $Y_\chi \equiv n_\chi/s \sim n_\chi a^3$, where s denotes the entropy

[1] Note that, we do not consider direct production of dark matter from inflaton decay in the present scenario [304].

density of the universe. Eq. (6.2), in terms of Y_χ during radiation domination becomes

$$\frac{\mathrm{d}Y_\chi}{\mathrm{d}T} = -\frac{R(T)}{HTs}\,, \quad \text{where} \quad s = \frac{2\pi^2}{45} g_s T^3\,. \tag{6.6}$$

We assume the energetic and entropic relativistic degrees of freedom, g_e and g_s, are equal to 106.75, and the reduced Planck mass $M_P = 2.8 \times 10^{18}$ GeV. On the other hand, for the inflaton dominated era we find [296, 307]

$$\frac{\mathrm{d}}{\mathrm{d}t} = -\frac{3}{8} H(T) T \frac{\mathrm{d}}{\mathrm{d}T} \quad \text{with} \;\; H(T) = \sqrt{\frac{5 g_{\mathrm{MAX}}^2}{72 g_{\mathrm{RH}}}} \pi \frac{T^4}{T_{\mathrm{RH}}^2 M_P}. \tag{6.7}$$

Here, g_{RH} and g_{MAX} represent the relativistic degrees of freedom at T_{RH} and T_{MAX}, respectively. Instead of the total entropy, during this epoch total number of inflaton remains approximately constant. Therefore, during the inflaton domination, the comoving yield of the DM is defined as $Y_{ID} \equiv n_\chi / n_\phi \sim n_\chi a^3$, where n_ϕ denotes the number density of the inflaton. The Boltzmann equation for the evolution of DM number density then turns out to be

$$\frac{\mathrm{d}Y_{ID}}{\mathrm{d}T} = -\frac{8}{3} \frac{R(T)}{HTn_\phi}\,, \quad \text{where,} \quad n_\phi \simeq \frac{5\pi^2 g_e^2}{96 g_{\mathrm{RH}}} \frac{T^8}{T_{\mathrm{RH}}^5}\,. \tag{6.8}$$

Note that consistency at $T = T_{\mathrm{RH}}$ demands $Y_\chi(T_{\mathrm{RH}}) s(T_{\mathrm{RH}}) = Y_{ID}(T_{\mathrm{RH}}) n_\phi(T_{\mathrm{RH}})$. Using Eqs. (6.6) and (6.8), the DM relic density is calculated by splitting it into two parts *viz.* a radiation dominated and an inflaton dominated contributions as [295, 300, 301].

$$\Omega h^2 \cong \Omega h^2_{RD} + \Omega h^2_{ID} \sim 4 \times 10^{24}\, m_\chi \left(\int_{T_0}^{T_{\mathrm{RH}}} dT \frac{R(T)}{T^6} + 1.07\, T_{\mathrm{RH}}^7 \int_{T_{\mathrm{RH}}}^{T_{\mathrm{MAX}}} dT \frac{R(T)}{T^{13}} \right), \tag{6.9}$$

where T_0 being the present day temperature. Eq. (6.9) clearly shows that DM production critically depends on how the production rate varies with the temperature. It turns out that the production of the DM will receive dominant contribution from the inflaton dominated era if the temperature dependence of the production rate follows as $R(T) \propto T^n$ with $n \geq 12$. If $R(T) \propto T^4$, only 1% of the total relic density receives contributions from the inflaton dominated era. Therefore in this case production of the majority of the DM is sensitive to the lowest available energy scales, leading to IR-dominated freeze-in. For $R(T) \propto T^8$, around 60% of DM is produced during the radiation domination. On the other hand, for $R(T) \propto T^{12}$ more than 95% of the DM is produced during the inflaton dominated epoch, leading to UV freeze-in of the DM.

6.2 Freeze-in *via* kinetic mixing portal

Here we demonstrate that kinetic mixing portal can be employed to produce DM through freeze-in mechanism. Portals of kinetic mixing with constant strengths have often been used in the literature in the context of various UV complete scenarios [308–311] to motivate DM production [312–315]. However, the major challenge is to justify the smallness of the mixing parameter, required for freeze-in scenario. We assume the existence of a spin-1 mediator Z' coupled to a fermionic DM χ while keeping the SM sector neutral with respect to it. The Z' can arise from gauging a $\mathrm{U}(1)'$ and may receive a mass ($M_{Z'}$) by Stückelberg or some dark Higgs mechanism. The Lagrangian of the dark sector consisting of a massive Z' is then given by

$$\mathcal{L}_{\text{dark}} = -\frac{1}{4} Z'^{\mu\nu} Z'_{\mu\nu} + \frac{1}{2} M_{Z'}^2 Z'^{\mu} Z'_{\mu} + \bar{\chi}(i\not{D} - m_\chi)\chi \,, \tag{6.10}$$

where $\not{D} = \not{\partial} + i g_D q_\chi \not{Z}'$ and $Z'_{\mu\nu} = \partial_\mu Z'_\nu - \partial_\nu Z'_\mu$ is the field strength of Z'. Following the principle of gauge invariance, tree level kinetic mixing term between the dark $\mathrm{U}(1)'$ and the hypercharge $\mathrm{U}(1)_\mathrm{Y}$ can be written as

$$\mathcal{L}_{\text{mix}} = -\frac{\delta}{2} B^{\mu\nu} Z'_{\mu\nu}, \tag{6.11}$$

B_μ being the gauge field associated with the hypercharge. The literature is rich in studies where the δ is a free parameter, in general small to avoid overproduction of dark matter in freeze-out or freeze-in scenarios, while respecting direct detection constraints. This smallness corresponds to a tuning arising from some UV dynamics. In particular, a UV realization of vanishing tree level kinetic mixing has been envisaged in the literature [309] if either of the two $\mathrm{U}(1)$ factors transcends from a non-Abelian group. Radiative effects, however, will give rise to finite logarithmic corrections to the kinetic mixing [308]. Here we illustrate two alternate possibilities to account for a small mixing parameter. First, we resort to *clockwork* mechanism to generate a tiny tree level kinetic mixing. Next we show that the kinetic mixing portal between a dark $\mathrm{U}(1)'$ and hypercharge $\mathrm{U}(1)_\mathrm{Y}$, generated by loops of some heavy vector-like fermion exhibits a strong temperature dependence (we call it 'dynamic mixing'), and can efficiently produce dark matter in the early stages of the reheating. The extreme smallness of the coupling is guaranteed in this case by the suppression arising from the heaviness of the loop fermion together with the loop factor.

6.2.1 Tiny kinetic mixing *à la* clockwork mechanism

The Clockwork mechanism furnishes a sophisticated way to generate small couplings at the low energy without resorting to any significant tuning in the UV. The framework can easily be generalized from scalars to fermions and vector bosons and even to gravitons [316,

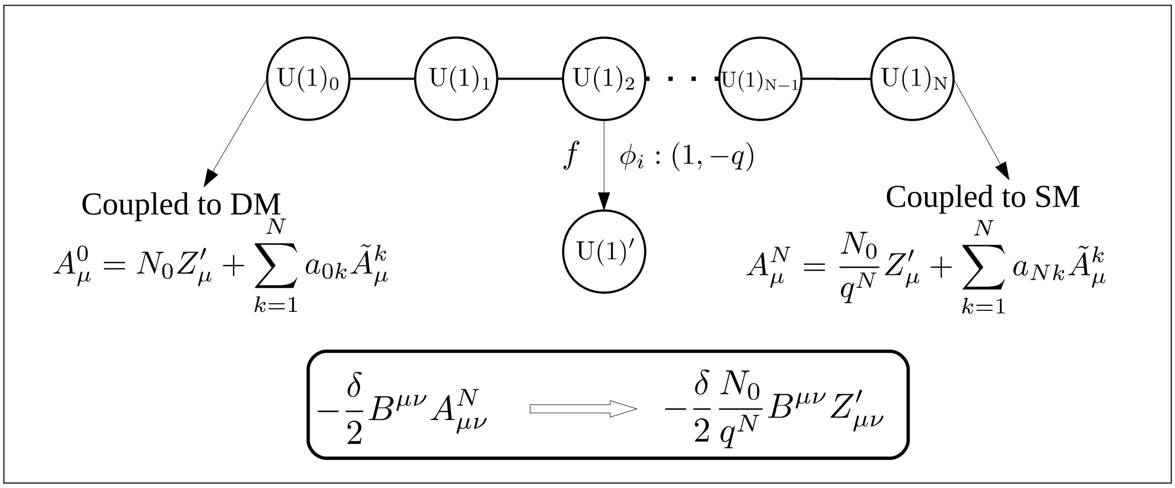

Figure 6.1: *Clockwork mechanism for generating tiny kinetic mixing.*

317]. The clockwork mechanism has a wide range of applications in scenarios that warrant small couplings, for example, axion physics [318–323], dark matter scenarios [324–327], inflation [328–330], neutrino mass and flavour hierarchy [331–337], relaxion models [338–340] etc. In our context, the clockwork setup consists of $N+1$ gauged $\mathrm{U}(1)$ symmetries, each of which are broken spontaneously to a single unbroken $\mathrm{U}(1)$, at a very high scale (f). The spontaneous breaking is facilitated by vevs of N scalar link fields [319]. These scalar fields are charged under two neighboring sites with charges $(1, -q)$, respectively. The Lagrangian involving $N+1$ gauge fields below the symmetry breaking scale f is given by

$$\mathcal{L} = -\sum_{k=0}^{N} \frac{1}{4} F^k_{\mu\nu} F^{k\mu\nu} + \sum_{k=0}^{N-1} \frac{g_c^2 f^2}{2} \left(A^k_\mu - q A^{k+1}_\mu\right)^2 . \tag{6.12}$$

The mass matrix for the gauge bosons takes a tri-diagonal form [319], common for all clockwork scenarios. After the diagonalization to the mass basis, N massive gauge bosons ($\tilde{A}^k_\mu$) with masses of the order of $g_c f$ are produced, while keeping one massless gauge boson (Z'_μ) corresponding to the unbroken $\mathrm{U}(1)$. We can identify the latter with the dark $\mathrm{U}(1)'$. Note that, the mass of the Z' can be generated at much lower scales through mechanism indicated earlier, independent of the clockwork sector. The expressions for the gauge fields at the $N^{\rm th}$ site (A_μ^N) and at the zeroth site (A_μ^0) in terms of the mass basis are given as

$$A_\mu^N = \frac{N_0}{q^N} Z'_\mu + \sum_{k=1}^{N} a_{Nk} \tilde{A}_\mu^k, \qquad A_\mu^0 = N_0 Z'_\mu + \sum_{k=1}^{N} a_{0k} \tilde{A}_\mu^k \,, \tag{6.13}$$

where N_0 is an $\mathcal{O}(1)$ constant and a_{jk} denotes the elements of rotation matrix with $\mathcal{O}(1)$ values. As shown in Fig. 6.1, the DM is assumed to couple to the clockwork setup at the zeroth site, while B_μ has a dimension-4 kinetic mixing with A_μ^N only. Clearly, due to the clockwork mechanism, the Z' will have geometrically suppressed tree level mixing with B_μ as given by [319, 341, 342]

$$\delta \sim \frac{\mathcal{O}(1)}{q^N}. \tag{6.14}$$

To provide a numerical estimate, we take $q = 3$ and $N = 20$ to find $\delta \sim \mathcal{O}(10^{-10})$. Note that, the other heavy clockwork modes ($\tilde{A}_\mu^k$), inspite of having large mixing with B_μ has negligible contribution to dark matter phenomenology due to their large mass. Therefore, we can safely integrate out these heavy modes keeping only Z' as relevant dynamic gauge field coming from the clockwork framework.

6.2.2 Emergence of dynamic gauge kinetic mixing

The second possible avenue, that we present here is freeze-in DM production through radiatively generated gauge kinetic mixing. In what follows, we assume that the two Abelian sectors dominantly communicate through some hybrid fermionic mediators. We will neglect the tree level (contact) mixing in our framework to study the effect of the radiatively generated kinetic mixing. A possible realistic UV setup which leads to tiny contact mixing may arise from a clockwork mechanism, as eluded in the previous section. We assume the

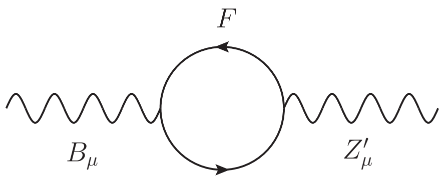

Figure 6.2: *One loop graph for kinetic mixing.*

hybrid mediators are a set of heavy fermions F_j, which are vector-like under both the $\mathrm{U}(1)'$ and the $\mathrm{U}(1)_\mathrm{Y}$. The Lagrangian of the hybrid sector is given by

$$\mathcal{L}_{\text{hybrid}} = \sum_j^{N_F} \bar{F}_j (i\not{\partial} - m_j - g' Q'_j \not{B} - g_D Q_{Dj} \not{Z}') F_j \,, \tag{6.15}$$

where N_F is the number of hybrid fermions and we assume that $m_j \gg M_{Z'}$. For simplicity and without lack of generalities, we consider a minimal scenario with $N_F = 1$, $m_j = m_F$, $Q'_j = Q'$ and $Q_{Dj} = Q_D$. In the context of a clockwork-like UV realization, the hybrid mediator with mass $m_F \ll f$, is assumed to couple to the clockwork setup only at the zeroth site, which implies that Z' will see both the hybrid mediator and the DM with $\mathcal{O}(1)$ interaction strength. Now we compute the gauge kinetic mixing generated by this fermion at energy scales below m_F.

Once the heavy hybrid fermion is integrated out, an effective kinetic mixing is generated at one loop for processes occurring at scales below m_F. Note that, the one loop mixed vacuum polarization diagram, as shown in Fig. 6.2, contains a logarithmically divergent piece. Since the mixing term corresponds to a marginal gauge invariant operator, even if we have neglected the tree level mixing as mentioned previously, a dimension-4 counterterm exists in the absence of any forbidding symmetry, to take care of the divergence. The

Lorentz structure of the one loop contribution is

$$i\Pi^{\mu\nu}_{Z'B}(p^2) = i\Pi_{Z'B}(p^2)\left(p^2\eta^{\mu\nu} - p^\mu p^\nu\right) . \tag{6.16}$$

The full analytic expression for $\Pi_{Z'B}$, calculated using the dimensional regularization scheme, is given in terms of $r \equiv p^2/4m_F^2$ with μ as the renormalization scale as

$$\begin{aligned}\Pi_{Z'B}(p^2) = &-\frac{(g'Q')(g_DQ_D)}{12\pi^2}\left[\frac{1}{\hat{\epsilon}} + \log\left(\frac{\mu^2}{m_F^2}\right) + \frac{5}{3} + \frac{1}{r}\right.\\ &\left. + \sqrt{1-\frac{1}{r}}\left(1+\frac{1}{2r}\right)\log\left(1-2r+2\sqrt{r(r-1)}\right)\right] ,\end{aligned} \tag{6.17}$$

where

$$\frac{1}{\hat{\epsilon}} \equiv \frac{1}{\epsilon} - \gamma_E + \log 4\pi\,, \qquad d = 4-2\epsilon\,,$$

and $\gamma_E \simeq 0.577$ is the Euler-Mascheroni constant. In the limit $p^2 \ll m_F^2$ or equivalently $r \to 0$, $\Pi_{Z'B}$ becomes

$$\Pi_{Z'B}(p^2) \simeq -\frac{(g'Q')(g_DQ_D)}{12\pi^2}\left[\frac{1}{\hat{\epsilon}} + \log\left(\frac{\mu^2}{m_F^2}\right) + \frac{p^2}{5m_F^2} + \mathcal{O}\left(\frac{p^4}{m_F^4}\right)\right] . \tag{6.18}$$

The renormalized kinetic mixing for $p^2 \ll m_F^2$ is then given as

$$\delta_{\text{ren}}(p^2) = \Pi_{Z'B}(p^2) - \delta_{\text{CT}}\,, \tag{6.19}$$

where δ_{CT} denotes the counterterm. Recall that g' and g_D have usual logarithmic running triggered by the standard and dark degrees of freedom, respectively, nevertheless, we fix them to constant values, as the effect of their running is numerically insignificant for our purpose. The natural renormalization prescription we employ to determine the counterterm is that at large distance ($p^2 \to 0$) the mixing vanishes to keep the quantum electrodynamics totally uncontaminated. This implies that

$$\delta_{\text{ren}}(0) = \Pi_{Z'B}(0) - \delta_{\text{CT}} = 0\,, \tag{6.20}$$

and it follows consequently

$$\delta_{\text{ren}}(p^2) = \Pi_{Z'B}(p^2) - \Pi_{Z'B}(0) \simeq -\frac{(g'Q')(g_D Q_D)}{60\pi^2}\frac{p^2}{m_F^2} + \mathcal{O}\left(\frac{p^4}{m_F^4}\right)\,. \tag{6.21}$$

The expression given above is reminiscent of the origin of Lamb shift in quantum electrodynamics. The logarithmic correction in addition to the divergent piece, is also absorbed by the counterterm. On the contrary, in momentum independent renormalization schemes (*e.g.* $\overline{\text{MS}}$ scheme) one can set $\mu = m_F$ to implement the decoupling of heavy hybrid particles in the loop [343], leading to identical result as given in Eq. (6.21). Note that, if either of the $\mathrm{U}(1)$ symmetries has a non-Abelian parentage in the UV [308, 309], one loop divergence would be canceled in the absence of any counterterm, as well as any tree level mixing. However, this specific scenario would keep the momentum dependent mixing sub-leading in comparison to the logarithmic contribution. Therefore, instead of appealing to this usual UV realization of embedding one of the $\mathrm{U}(1)$ factors into a non-Abelian group, we alluded to the presence of a clockwork mechanism at the UV to promote the relevance of the momentum dependent portal. At low energy the loop contribution can also be envisaged through the following dimension-6 operator

$$\mathcal{O}^{(6)}_{Z'B} = \frac{1}{\Lambda_{\text{eff}}^2} B_{\mu\nu} \Box Z'^{\mu\nu}, \quad \text{with} \quad \frac{1}{\Lambda_{\text{eff}}^2} = \frac{(g'Q')(g_D Q_D)}{60\pi^2}\frac{1}{m_F^2}\,. \tag{6.22}$$

The effective kinetic mixing below m_F is of the order $\mathcal{O}(p^2/m_F^2)$ suppressed by a loop factor. Additionally, thanks to the explicit momentum dependence involved, the strength of mixing depends on the energy and dynamics of the process under consideration. These two attributes make the dynamic kinetic mixing an efficient portal for UV-dominated freeze-in production of DM.

6.3 Dark matter production

We now describe the freeze-in production mechanism of DM through the kinetic mixing portal. Two main production channels involved are *(i)* $f\bar{f} \to \chi\bar{\chi}$ and *(ii)* $H^\dagger H \to \chi\bar{\chi}$, where f and H denote the SM fermions and Higgs doublet, respectively. We will provide a comparison between the efficiency of constant and dynamic kinetic mixing as a portal for freeze-in DM production.

6.3.1 Production rate

The expression for the DM production rate in the freeze-in scenario, defined in Eq. (6.2), is given as

$$R(T) = \alpha \left(g' g_D q_\chi\right)^2 T \int_{4m_\chi^2}^{\infty} ds \sqrt{s - 4m_\chi^2}\, K_1\left(\frac{\sqrt{s}}{T}\right) \delta_{\text{ren}}^2(s) \frac{s(s + 2m_\chi^2)}{(s - M_{Z'}^2)^2 + M_{Z'}^2 \Gamma_{Z'}^2}\,, \tag{6.23}$$

where $K_1(x)$ is the modified Bessel function of the second kind and $\delta_{\text{ren}}(s)$ denotes strength of kinetic mixing. For constant mixing, $\delta_{\text{ren}}(s)$ can be replaced by a constant free parameter δ, while its expression for the dynamic mixing scenario can be read off from Eq. (6.21). The coefficient α for the production channels $f\bar{f} \to \chi\bar{\chi}$ and $H^\dagger H \to \chi\bar{\chi}$ are, respectively given by

$$\alpha_{f\bar{f}\to\chi\bar{\chi}} = \frac{1}{96\pi^5}\sum_f \left(v_f^2 + a_f^2\right)\,, \quad \alpha_{H^\dagger H\to\chi\bar{\chi}} = \frac{1}{768\pi^5}\,. \tag{6.24}$$

Here v_f and a_f are the vector and axial-vector couplings of the SM fermions with B_μ. For quarks in the initial state, an additional factor in α, due to the number of colors ($N_c = 3$) should be taken into account. The decay width of Z' to the SM particles are negligible compared to that to the DM,because of the smallness of kinetic mixing. The expression for the decay width of Z' to a pair of DM is found to be

$$\Gamma_{Z'} = \frac{g_D^2 q_\chi^2}{12\pi} M_{Z'}\left(1 + \frac{2m_\chi^2}{M_{Z'}^2}\right)\sqrt{1 - \frac{4m_\chi^2}{M_{Z'}^2}}\,. \tag{6.25}$$

We have performed full numerical computation of the rate using the CUBA package [344]. However, for the brevity of understanding, we present below the generic structure of the production rates for three distinct ranges of $M_{Z'}$ and assuming $m_\chi \ll T$. We also assume $\Gamma_{Z'} \ll M_{Z'}$ while presenting the analytic expressions for the approximate rates. The temperature dependence of the production rates for the dynamic ($R(T)$) as well as constant ($R_\delta(T)$) kinetic mixing cases can be estimated in the above mentioned regimes as

$$R(T) = \frac{\mathcal{C}}{(4\pi)^4}\times\begin{cases} \dfrac{T^8}{m_F^4}\,, \\ \dfrac{M_{Z'}^8 T}{m_F^4 \Gamma_{Z'}} K_1\left(\dfrac{M_{Z'}}{T}\right), \\ \dfrac{T^{12}}{m_F^4 M_{Z'}^4}\,, \end{cases} \quad R_\delta(T) = \mathcal{C}'\times\begin{cases} \delta^2 T^4\,, & (M_{Z'} \ll T) \\ \dfrac{\delta^2 M_{Z'}^4 T}{\Gamma_{Z'}} K_1\left(\dfrac{M_{Z'}}{T}\right), & (M_{Z'} \sim T) \\ \delta^2 \dfrac{T^8}{M_{Z'}^4}\,. & (M_{Z'} \gg T) \end{cases} \tag{6.26}$$

Numerical constants $\mathcal{C}$ and $\mathcal{C}'$ for the production channels $f\bar{f} \to \chi\bar{\chi}$ and $H^\dagger H \to \chi\bar{\chi}$ are displayed in Table 6.1.

For a set of benchmark values of parameters, the DM production rate as a function of

$\mathcal{C}$	$f\bar{f} \to \chi\bar{\chi}$	$H^\dagger H \to \chi\bar{\chi}$
$M_{Z'} \ll T$	$\dfrac{1568 g'^4 \beta^2}{675\pi^5}$	$\dfrac{16 g'^4 \beta^2}{225\pi^5}$
$M_{Z'} \sim T$	$\dfrac{49 g'^4 \beta^2}{16200\pi^4}$	$\dfrac{g'^4 \beta^2}{10800\pi^4}$
$M_{Z'} \gg T$	$\dfrac{401408 g'^4 \beta^2}{45\pi^5}$	$\dfrac{4096 g'^4 \beta^2}{15\pi^5}$

$\mathcal{C}'$	$f\bar{f} \to \chi\bar{\chi}$	$H^\dagger H \to \chi\bar{\chi}$
$M_{Z'} \ll T$	$\dfrac{49 g'^2 \beta'^2}{288\pi^5}$	$\dfrac{g'^2 \beta'^2}{192\pi^5}$
$M_{Z'} \sim T$	$\dfrac{49 g'^2 \beta'^2}{1152\pi^4}$	$\dfrac{g'^2 \beta'^2}{768\pi^4}$
$M_{Z'} \gg T$	$\dfrac{98 g'^2 \beta'^2}{3\pi^5}$	$\dfrac{g'^2 \beta'^2}{\pi^5}$

Table 6.1: *Expressions for the coefficients $\mathcal{C}$ and $\mathcal{C}'$, where $\beta \equiv g_D^2 q_\chi Q' Q_D$ and $\beta' \equiv g_D q_\chi$.*

the variable $x \equiv M_{Z'}/T$ is shown in Fig. 6.3 (solid curves for dynamic mixing case). For simplicity, we set $g_D^2 q_\chi Q' Q_D = 1$ (see Eqs. (6.10) and (6.15)), $m_F = 10^{13}$ GeV, and $M_{Z'} = 10^{10}$ GeV. From left to right in the solid curves, we fix $m_\chi = 10^{12}$, 10^{10}, 10^9, and 10^4 GeV (cyan, brown, blue, and black), respectively. From the expressions of the approximate rates in Eq.(6.26), one can intuitively understand the different regimes of the DM production, as shown in Fig. 6.3. The rate shows a pronounced temperature dependence and in general falls as the universe cools down. In the small $x \ll 1$ (large T) limit, the temperature of the thermal bath is much higher than the mass of the mediator, and hence the rate is governed by the light mediator approximation ($M_{Z'} \ll T$). In large $x \gg 1$ (small T) regime, on the other hand, sufficient temperature is not available in the bath to produce Z' on-shell, as indicated by the region dictated by the heavy mediator approximation ($M_{Z'} \gg T$). However, if the bath temperature is around the Z' mass ($x \sim 1$), dark matter production is going through the on-shell Z' decay leading to s-channel resonance enhancement. Thus, the Z'-pole effects can be observed around $x \sim 1$ and the rate of production of the DM is governed by the narrow width approximation ($M_{Z'} \sim T$). Moreover, once the temperature falls below m_χ, rate drops exponentially due to the Boltzmann suppression ($\propto e^{-m_\chi/T}$). The colored vertical lines, in the Fig. 6.3, mark $T = m_\chi$ for four different values of the

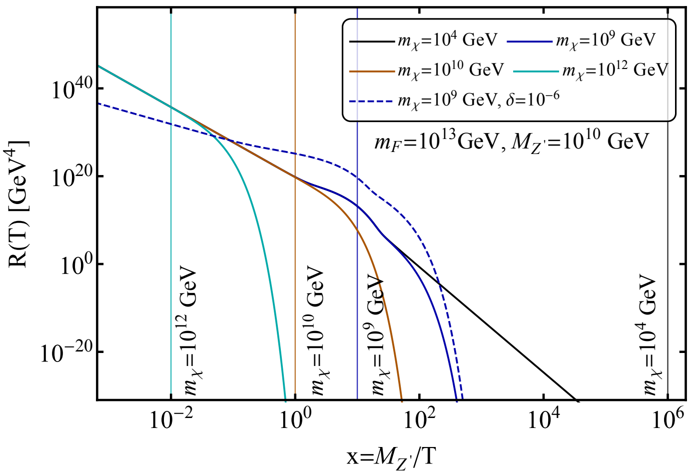

Figure 6.3: *DM production rate for both dynamic (solid curves) and constant (dashed curve) kinetic mixing portals are shown.*

DM masses. For $m_\chi = 10^{12}$ GeV and 10^{10} GeV, Boltzmann suppression predates the Z' pole, and hence resonance enhancement around $x \sim 1$ is absent for these cases.

We also compare the DM production rates as found with dynamic mixing with that using a tree level constant kinetic mixing[2] portal (dashed blue curve) for $m_\chi = 10^9$ GeV and kinetic mixing parameter $\delta = 10^{-6}$, in the Fig. 6.3. The comparison indicates that in the case of constant mixing, as the temperature decreases, rate falls at a slower pace than for the dynamic mixing. This aspect can be accounted by noting the relative suppressions in the production rates between the dynamic and constant mixing cases, given in Eq. (6.26). Therefore, while the dynamic portal will produce the DM mostly at early times leading to a UV freeze-in, the production will take place for a prolonged duration for the constant mixing case, depending on the strength of the mixing parameter.

[2]Strictly speaking, δ, as defined in Eq. (6.11), runs logarithmically being proportional to itself. However, for the purpose of comparison, we treat δ to be a constant, as the numerical effect of its running on the DM production is insignificant.

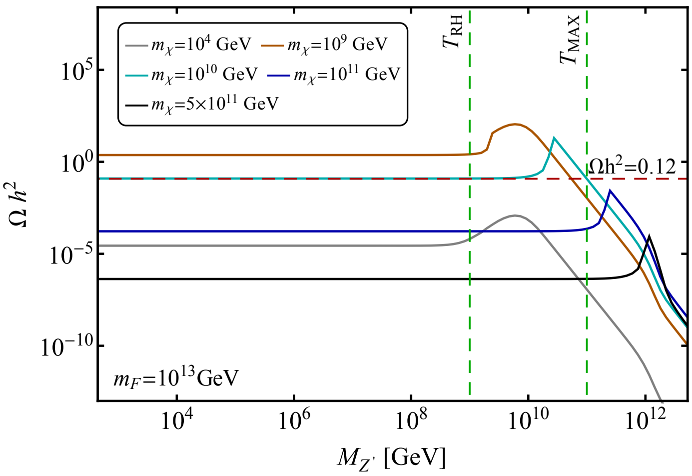

Figure 6.4: *Dependence of DM relic abundance on Z' mass for dynamic portal.*

6.3.2 Relic abundance

Now we calculate the DM relic abundance, and examine the consequences of matching it with the observed $\Omega h^2 \sim 0.12$ on the parameter space of the model. In Fig. 6.4, we display the dependence of Ωh^2 on $M_{Z'}$ for different values of m_χ (colored solid lines). In the light mediator regime ($M_{Z'} \ll T_{\rm RH}$), Ωh^2 is independent to $M_{Z'}$ as the relic density saturates at a much higher temperature. However, in the $T_{\rm RH} \lesssim M_{Z'} \lesssim T_{\rm MAX}$ region the relic abundance increases due to s-channel resonance when $M_{Z'} \simeq 2m_\chi$. When we consider heavier Z' its on-shell production from the thermal bath gets suppressed which causes a fall in the Ωh^2. Once $M_{Z'} \gg T_{\rm MAX}$ the density falls at a faster rate. Recalling $\Omega h^2 \propto m_\chi n_\chi$, we follow that for relatively smaller values of m_χ the relic density grows with increasing m_χ (gray and brown curves). In contrast, we observe a fall in Ωh^2 once $m_\chi > T_{\rm RH}$ (cyan, blue and black curves) due to a severe phase space suppression in n_χ.

In Fig. 6.5, we display the contours of $\Omega h^2 = 0.12$ in the $M_{Z'} - m_\chi$ plane for both dynamic and constant kinetic mixing portals. We first discuss the dynamic kinetic mixing results for two representative choices of $m_F = 5\times 10^{12}$ GeV (gray) and 10^{13} GeV (brown), respectively. Each choice of m_F corresponds to a contour of $m_\chi n_\chi = \mathrm{constant}$, which implies that lighter (heavier) DM needs to be produced in large (small) number. In particular, the right (left)-hand branch of the contour is associated with less (more) DM production. For low $M_{Z'}$ ($\ll T_{\text{RH}}$) the contour is independent of $M_{Z'}$ as explained earlier in the context of Fig. 6.4. When $M_{Z'} \sim T_{\text{RH}}$, excess DM production due to s-channel resonance is compensated as the left-handed branch of the contour (which was so long vertical) turns towards smaller values of m_χ. The contour cannot continue indefinitely towards increasingly smaller m_χ as n_χ needs to be appropriately balanced by arranging a lighter mediator (*i.e.* small $M_{Z'}$), which in turn weakens the dynamic portal ($\propto M_{Z'}^2/m_F^2$). This explains the upper left edge of the contour. Then the contour turns right towards larger m_χ requiring monotonically increasing $M_{Z'}$ to keep $m_\chi n_\chi =$ constant. Finally beyond certain values of m_χ and $M_{Z'}$, the DM production is insufficient to reproduce the observed $\Omega h2$, as indicated by the upper right edge of the contour. We also observe that the contour for $m_F = 10^{13}$ GeV is contained within that of $m_F = 5\times 10^{12}$ GeV, because larger (smaller) m_F implies weaker (stronger) kinetic mixing ($\propto 1/m_F^2$). To justify the viability of the above discussion, we now make a quantitative estimate of the required smallness of the contact term, compared to the p^2-dependent term for different regions of parameter space in Fig. 6.5. Comparing between $R(T)$ and $R_\delta(T)$ in Eq. (6.26) we find the condition to render the effects of the contact term insignificant as

$$\delta \ll \frac{1}{16\pi^2}\frac{T^2}{m_F^2}. \tag{6.27}$$

Since the relic abundance gets saturated at or above $T \sim m_\chi$, for $M_{Z'} \ll T_{\text{RH}}$, $m_\chi \sim 10^6$ GeV and $m_F \sim 10^{12}$ GeV we estimate $\delta \ll 10^{-14}$ is required, to be neglected safely. On

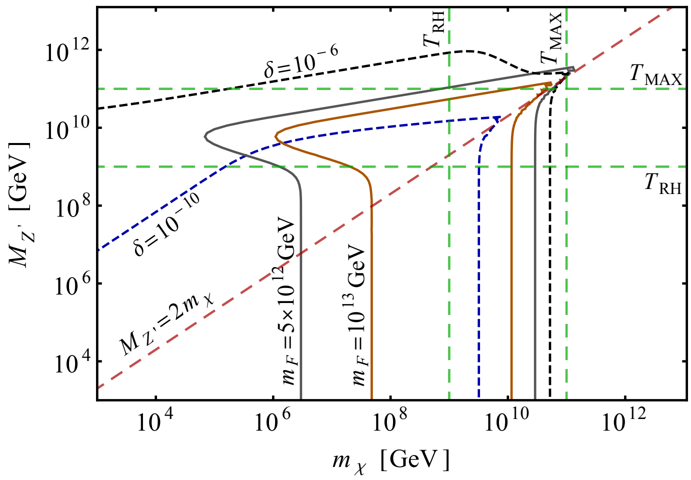

Figure 6.5: *Contours of* $\Omega h^2 = 0.12$ *for both dynamic (brown and gray solid curves) and constant (black and blue dashed curves) mixing portals are displayed.*

the other hand, for $M_{Z'} \geq T_{\rm RH}$ the condition fairly relaxes to $\delta \ll 10^{-8}$.

For comparison, we have performed the same analysis with constant kinetic mixing for $\delta = 10^{-6}$ (black dashed), and 10^{-10} (blue dashed). The main difference with the dynamic portal case is the absence of additional powers of temperature involved in the dynamics. For a given value of δ, the vertical line is absent in the left-hand side as a large $M_{Z'}$ is required to counterbalance the DM over production. Larger δ requires heavier Z' to reproduce the relic abundance. For $\delta = 10^{-6}$, when m_χ crosses $T_{\rm RH}$, Boltzmann suppression shows up as a dip. This happens because in the constant mixing scenario the production of DM occurs almost entirely in the radiation dominated era, while in the dynamic mixing case additional powers of T is responsible for DM production even in the inflaton dominated period ($T_{\rm RH} < T < T_{\rm MAX}$). For $\delta = 10^{-10}$, once $M_{Z'}$ crosses $T_{\rm RH}$ the slope of the contour changes accordingly to adjust $m_\chi n_\chi =$ constant.

6.4 Summary

In this chapter we consider freeze-in production of DM in the early stage of the reheating epoch.

- We have identified a scale-dependent portal for freezing-in DM production, created through one loop gauge kinetic mixing between a dark $\mathrm{U}(1)'$ and hypercharge $\mathrm{U}(1)_{\mathrm{Y}}$ by integrating out a very heavy vector-like fermion. The requirement of preserving quantum electrodynamics at large distances ensures the strength of this mixing strongly dependent on the energy of the process involved.
- The strong temperature sensitivity of the mixing allows the dark matter to be produced through the 'UV freeze-in' mechanism mostly during the early stage of reheating era.
- We have demonstrated the difference of this scenario from freeze-in DM production through constant kinetic mixing.

Although the 'freeze-in' mechanism was primarily advocated to justify the continued absence of evidence in DM direct searches, it is time to put serious thoughts on any possible, however far-fetched, tests of such scenarios. For instance, possible future detection of gravitational waves, generated if the $\mathrm{U}(1)'$ breaking is associated with first order phase transition [345–347], may indicate towards a Z' mass range far beyond the reach of any future colliders, thus shedding some light on the DM portal. An interesting corollary would be to employ the concept of this dynamic kinetic mixing in a 'freeze-out' scenario, *albeit* with a different parameter range.

APPENDIX A

SO(5) AND SO(6) GENERATORS

The explicit expressions for the generators of SO(5) in the fundamental representation are as follows:

$$
\begin{aligned}
(T^a_{L,R})_{ij} &= -\frac{i}{2}\left[\frac{1}{2}\epsilon^{abc}(\delta^b_i\delta^c_j - \delta^b_j\delta^c_i) \pm (\delta^a_i\delta^4_j - \delta^a_j\delta^4_i)\right], && \text{(A.1)}\\
(T^{\hat{a}})_{ij} &= -\frac{i}{\sqrt{2}}(\delta^{\hat{a}}_i\delta^5_j - \delta^{\hat{a}}_j\delta^5_i)\,, && \text{(A.2)}
\end{aligned}
$$

where i, j runs from 1 to 5. The generators $T^a_{L,R}$ span the $\mathrm{SO}(4) \simeq \mathrm{SU}(2)_L \times \mathrm{SU}(2)_R$ subgroup, with a running from 1 to 3, while the four generators $T^{\hat{a}}$ span the coset $\mathrm{SO}(5)/\mathrm{SO}(4)$.

In case of $\mathrm{SO}(6)$, in addition to the above ten generators, five more spanning the $\mathrm{SO}(6)/\mathrm{SO}(5)$ coset space are given by

$$
(\hat{T}^{\hat{\alpha}})_{ij} = -\frac{i}{\sqrt{2}}(\delta^{\hat{\alpha}}_i\delta^6_j - \delta^{\hat{\alpha}}_j\delta^6_i)\,. \tag{A.3}
$$

Note that for $\mathrm{SO}(6)$ generators, i, j runs from 1 to 6.

APPENDIX B

FERMION EMBEDDINGS

B.1 $\mathrm{SO}(5)/\mathrm{SO}(4)$ Coset

Fundamental $\mathbf{5}$, adjoint $\mathbf{10}$ and symmetric $\mathbf{14}$ representations of $\mathrm{SO}(5)$ can be decomposed under the unbroken $\mathrm{SO}(4) \equiv \mathrm{SU}(2)_{\mathrm{L}} \times \mathrm{SU}(2)_{\mathrm{R}}$ as:

$$\begin{aligned} \mathbf{5} &= \mathbf{1}+\mathbf{4} = (\mathbf{1},\mathbf{1})+(\mathbf{2},\mathbf{2})\,, \\ \mathbf{10} &= \mathbf{4}+\mathbf{6} = (\mathbf{2},\mathbf{2})+(\mathbf{3},\mathbf{1})+(\mathbf{1},\mathbf{3})\,, \qquad \text{(B.1)} \\ \mathbf{14} &= \mathbf{1}+\mathbf{4}+\mathbf{9} = (\mathbf{1},\mathbf{1})+(\mathbf{2},\mathbf{2})+(\mathbf{3},\mathbf{3})\,. \qquad \text{(B.2)} \end{aligned}$$

We embed t_L into the $(\mathbf{2},\mathbf{2})$'s to tame non-standard corrections to the $Zb\bar{b}$ vertex under control, while t_R is embedded into $(\mathbf{1},\mathbf{1})$. The embeddings of the top quarks into incomplete multiplets of $\mathbf{5}$ and $\mathbf{14}$ are shown below:

$$Q_L^5 = \left(\Psi_{(2,2)},0\right)^T\,, \quad T_R^5 = \left(0,0,0,0,t_R\right)^T\,, \qquad \text{(B.3)}$$

and

$$Q_L^{14} = \left(\begin{array}{c|c} 0_{4\times4} & \frac{\Psi^T_{(2,2)}}{\sqrt{2}} \\ \hline \frac{\Psi_{(2,2)}}{\sqrt{2}} & 0 \end{array}\right), \quad T_R^{14} = \left(\begin{array}{c|c} -\frac{t_R}{2\sqrt{5}} I_4 & 0_{4\times1} \\ \hline 0_{1\times4} & 4\frac{t_R}{2\sqrt{5}} \end{array}\right), \tag{B.4}$$

where

$$\Psi_{(2,2)} = \frac{1}{\sqrt{2}}(ib_L, b_L, it_L, -t_L). \tag{B.5}$$

B.2 $\mathrm{SO}(6)/\mathrm{SO}(5)$ Coset

Decomposition of different representations of $\mathrm{SO}(6)$, under the maximal subgroup $\mathrm{SO}(6) \supset \mathrm{SO}(4) \times \mathrm{SO}(2) \simeq \mathrm{SU}(2)_L \times \mathrm{SU}(2)_R \times \mathrm{U}(1)_\eta$ are as follows:

$$\begin{aligned} \mathbf{6}_0 &= (\mathbf{2},\mathbf{2})_0 + (\mathbf{1},\mathbf{1})_2 + (\mathbf{1},\mathbf{1})_{-2}\,, \\ \mathbf{15}_0 &= (\mathbf{1},\mathbf{1})_0 + (\mathbf{2},\mathbf{2})_2 + (\mathbf{2},\mathbf{2})_{-2} + (\mathbf{3},\mathbf{1})_0 + (\mathbf{1},\mathbf{3})_0\,, \\ \mathbf{20'}_0 &= (\mathbf{1},\mathbf{1})_0 + (\mathbf{1},\mathbf{1})_4 + \mathbf{1},\mathbf{1})_{-4} + (\mathbf{2},\mathbf{2})_2 + (\mathbf{2},\mathbf{2})_{-2} + (\mathbf{3},\mathbf{3})_0\,, \end{aligned} \tag{B.6}$$

where the subscripts denote charges under $\mathrm{U}(1)_\eta$. Embedding of t_L and t_R in the above representations are given by

$$Q_L^6 = \left(\Psi_{(2,2)}, 0, 0\right)^T\,, \qquad T_R^6 = (0,0,0,0,0,t_R)^T\,, \tag{B.7}$$

$$Q_L^{15} = \left(\begin{array}{c|cc} 0_{4\times4} & 0 & \frac{\Psi^T_{(2,2)}}{\sqrt{2}} \\ \hline \begin{matrix} 0 \\ -\frac{\Psi_{(2,2)}}{\sqrt{2}} \end{matrix} & \multicolumn{2}{c}{0_{2\times2}} \end{array}\right), \quad T_R^{15} = \left(\begin{array}{cc|cc|c} 0 & -i\frac{t_R}{2} & \multicolumn{2}{c|}{0_{2\times2}} & \\ i\frac{t_R}{2} & 0 & & & \\ \cline{1-4} \multicolumn{2}{c|}{0_{2\times2}} & 0 & i\frac{t_R}{2} & 0_{4\times2} \\ & & -i\frac{t_R}{2} & 0 & \\ \hline \multicolumn{4}{c|}{0_{2\times4}} & 0_{2\times2} \end{array}\right), \tag{B.8}$$

and

$$Q_L^{20} = \left(\begin{array}{c|c} 0_{4\times 4} & 0 \quad \frac{\Psi^T_{(2,2)}}{\sqrt{2}} \\ \hline \begin{array}{c} 0 \\ \frac{\Psi_{(2,2)}}{\sqrt{2}} \end{array} & 0_{2\times 2} \end{array}\right) , \quad T_R^{20} = \left(\begin{array}{c|c} -\frac{t_R}{2\sqrt{3}} I_4 & 0_{4\times 2} \\ \hline 0_{2\times 4} & \frac{t_R}{\sqrt{3}} I_2 \end{array}\right) . \tag{B.9}$$

Here again, $\Psi_{(2,2)}$ is given by Eq. (B.5).

APPENDIX C

DETAILS OF FORM FACTORS

Detailed expressions of the form factors for different models in terms of the masses and decay constants of the lightest resonances, in the Euclidean space, are shown (for calculations, see [101]).

C.1 $\mathrm{SO}(5)/\mathrm{SO}(4)$ Coset

$\mathbf{MCHM_{5_L-5_R}}$

$$\left.\begin{aligned}
\Pi_0^L &= 1 + \frac{|F_4^L|^2}{q^2+m_{Q_4}^2} \\
\Pi_1^L &= \frac{1}{2}\left(\frac{|F_1^L|^2}{q^2+m_{Q_1}^2} - \frac{|F_4^L|^2}{q^2+m_{Q_4}^2}\right) \\
\Pi_0^R &= 1 + \frac{|F_1^R|^2}{q^2+m_{Q_1}^2}, \\
\Pi_1^R &= \frac{|F_4^R|^2}{q^2+m_{Q_4}^2} - \frac{|F_1^R|^2}{q^2+m_{Q_1}^2}, \\
\Pi_1^{LR} &= \frac{\sqrt{5}}{2}\frac{F_4^L F_4^{R*} m_{Q_4}}{q^2+m_{Q_4}^2} - \frac{1}{\sqrt{2}}\frac{F_1^L F_1^{R*} m_{Q_1}}{q^2+m_{Q_1}^2}
\end{aligned}\right\} \tag{C.1}$$

$\mathbf{MCHM_{14_L-14_R}}$

$$\left.\begin{aligned}
\Pi_0^L &= 1+\frac{|F_4^L|^2}{q^2+m_{Q_4}^2},\\
\Pi_1^L &= \left(\frac{5}{4}\frac{|F_1^L|^2}{q^2+m_{Q_1}^2}-\frac{5}{2}\frac{|F_4^L|^2}{q^2+m_{Q_4}^2}+\frac{5}{4}\frac{|F_9^L|^2}{q^2+m_{Q_9}^2}\right),\\
\Pi_2^L &= \left(-\frac{5}{4}\frac{|F_1^L|^2}{q^2+m_{Q_1}^2}+2\frac{|F_4^L|^2}{q^2+m_{Q_4}^2}-\frac{3}{4}\frac{|F_9^L|^2}{q^2+m_{Q_9}^2}\right),\\
\Pi_0^R &= 1+\frac{|F_1^R|^2}{q^2+m_{Q_1}^2},\\
\Pi_1^R &= \left(\frac{5}{2}\frac{|F_4^R|^2}{q^2+m_{Q_4}^2}-\frac{5}{2}\frac{|F_1^R|^2}{q^2+m_{Q_1}^2}\right),\\
\Pi_2^R &= \left(\frac{25}{16}\frac{|F_1^R|^2}{q^2+m_{Q_1}^2}-\frac{5}{2}\frac{|F_4^R|^2}{q^2+m_{Q_4}^2}+\frac{15}{16}\frac{|F_9^R|^2}{q^2+m_{Q_9}^2}\right),\\
\Pi_1^{LR} &= -\frac{\sqrt{5}}{2}\left(\frac{F_1^L F_1^{R*} m_{Q_1}}{q^2+m_{Q_1}^2}-\frac{F_4^L F_4^{R*} m_{Q_4}}{q^2+m_{Q_4}^2}\right),\\
\Pi_2^{LR} &= -\left(-\frac{5\sqrt{5}}{8}\frac{F_1^L F_1^{R*} m_{Q_1}}{q^2+m_{Q_1}^2}+\sqrt{5}\frac{F_4^L F_4^{R*} m_{Q_4}}{q^2+m_{Q_4}^2}-\frac{3\sqrt{5}}{8}\frac{F_9^L F_9^{R*} m_{Q_9}}{q^2+m_{Q_9}^2}\right).
\end{aligned}\right\} \tag{C.2}$$

$\mathbf{MCHM_{14_L-5_R}}$

$$\left.\begin{aligned}
\Pi_0^L &= 1+\frac{|F_4^L|^2}{q^2+m_{Q_4}^2},\\
\Pi_1^L &= \frac{5}{4}\frac{|F_1^L|^2}{q^2+m_{Q_1}^2}-\frac{5}{2}\frac{|F_4^L|^2}{q^2+m_{Q_4}^2}+\frac{5}{4}\frac{|F_9^L|^2}{q^2+m_{Q_9}^2},\\
\Pi_2^L &= 2\frac{|F_4^L|^2}{q^2+m_{Q_4}^2}-\frac{5}{4}\frac{|F_1^L|^2}{q^2+m_{Q_1}^2}-\frac{3}{4}\frac{|F_9^L|^2}{q^2+m_{Q_9}^2},\\
\Pi_0^R &= 1+\frac{|F_1^R|^2}{q^2+m_{Q_1}^2},\\
\Pi_1^R &= \frac{|F_4^R|^2}{q^2+m_{Q_4}^2}-\frac{|F_1^R|^2}{q^2+m_{Q_1}^2},\\
\Pi_1^{LR} &= \frac{1}{\sqrt{2}}\frac{F_4^L F_4^{R*} m_{Q_4}}{q^2+m_{Q_4}^2}-\frac{\sqrt{5}}{2}\frac{F_1^L F_1^{R*} m_{Q_1}}{q^2+m_{Q_1}^2},\\
\Pi_2^{LR} &= \frac{\sqrt{5}}{2}\frac{F_1^L F_1^{R*} m_{Q_1}}{q^2+m_{Q_1}^2}-\sqrt{2}\frac{F_4^L F_4^{R*} m_{Q_4}}{q^2+m_{Q_4}^2}.
\end{aligned}\right\} \tag{C.3}$$

$\mathbf{MCHM_{5_L-14_R}}$

$$\left.\begin{aligned}
\Pi_0^L &= 1+\frac{|F_4^L|^2}{q^2+m_{Q_4}^2}\\
\Pi_1^L &= \frac{1}{2}\left(\frac{|F_1^L|^2}{q^2+m_{Q_1}^2}-\frac{|F_4^L|^2}{q^2+m_{Q_4}^2}\right)\\
\Pi_0^R &= 1+\frac{|F_1^R|^2}{q^2+m_{Q_1}^2}\\
\Pi_1^R &= \frac{5}{2}\left(\frac{|F_4^R|^2}{q^2+m_{Q_4}^2}-\frac{|F_1^R|^2}{q^2+m_{Q_1}^2}\right)\\
\Pi_2^R &= \frac{25}{16}\frac{|F_1^R|^2}{q^2+m_{Q_1}^2}-\frac{5}{2}\frac{|F_4^R|^2}{q^2+m_{Q_4}^2}+\frac{15}{16}\frac{|F_9^R|^2}{q^2+m_{Q_9}^2}\\
\Pi_1^{LR} &= \frac{\sqrt{5}}{2}\frac{F_4^L F_4^{R*} m_{Q_4}}{q^2+m_{Q_4}^2}-\frac{1}{\sqrt{2}}\frac{F_1^L F_1^{R*} m_{Q_1}}{q^2+m_{Q_1}^2}\\
\Pi_2^{LR} &= \frac{5\sqrt{2}}{8}\frac{F_1^L F_1^{R*} m_{Q_1}}{q^2+m_{Q_1}^2}-\frac{\sqrt{5}}{2}\frac{F_4^L F_4^{R*} m_{Q_4}}{q^2+m_{Q_4}^2}
\end{aligned}\right\} \tag{C.4}$$

C.2 $\mathbf{SO(6)/SO(5)}$ Coset

$\mathbf{NMCHM_{6_L-6_R}}$

$$\left.\begin{aligned}
\Pi_0^L &= 1+\frac{|F_5^L|^2}{q^2+m_{Q_5}^2}\\
\Pi_1^L &= \frac{1}{2}\left(\frac{|F_1^L|^2}{q^2+m_{Q_1}^2}-\frac{|F_5^L|^2}{q^2+m_{Q_5}^2}\right)\\
\Pi_0^R &= 1+\frac{|F_1^R|^2}{q^2+m_{Q_1}^2},\\
\Pi_1^R &= \frac{|F_5^R|^2}{q^2+m_{Q_5}^2}-\frac{|F_1^R|^2}{q^2+m_{Q_1}^2},\\
\Pi_1^{LR} &= \frac{\sqrt{5}}{2}\frac{F_5^L F_5^{R*} m_{Q_5}}{q^2+m_{Q_5}^2}-\frac{1}{\sqrt{2}}\frac{F_1^L F_1^{R*} m_{Q_1}}{q^2+m_{Q_1}^2}
\end{aligned}\right\} \tag{C.5}$$

APPENDIX D

EXPRESSIONS FOR Π-FUNCTIONS, Δ_t, AND Δ_t^η FOR $\mathbf{SO(6)/SO(5)}$ COSET

The Π-functions for $\mathrm{SO}(6)/\mathrm{SO}(5)$ coset are shown for different representations in Table D.1. The $\mathrm{NMCHM}_{15_\mathrm{L}-1_\mathrm{R}}$ case is omitted because it cannot generate a Yukawa term in the Lagrangian.

Models	$\Pi_{t_L}(h,\eta)$	$\Pi_{t_R}(h,\eta)$	$\Pi_{t_L t_R}(h,\eta)$
$\mathrm{NMCHM}_{6_\mathrm{L}-1_\mathrm{R}}$	$\Pi_0^L + \Pi_1^L \frac{h^2}{f^2}$	Π_0^R	$\Pi_1^{LR} \frac{h}{f}$
$\mathrm{NMCHM}_{6_\mathrm{L}-6_\mathrm{R}}$	$\Pi_0^L + \Pi_1^L \frac{h^2}{f^2}$	$\Pi_0^R + \Pi_1^R \frac{h^2}{f^2} + \Pi_\eta^R \frac{\eta^2}{f^2}$	$\Pi_1^{LR} \frac{h}{f} \sqrt{1 - \frac{h^2}{f^2} - \frac{\eta^2}{f^2}}$
$\mathrm{NMCHM}_{6_\mathrm{L}-15_\mathrm{R}}$	$\Pi_0^L + \Pi_1^L \frac{h^2}{f^2}$	$\Pi_0^R + \Pi_1^R \frac{h^2}{f^2}$	$\Pi_1^{LR} \frac{h}{f}$
$\mathrm{NMCHM}_{6_\mathrm{L}-20_\mathrm{R}}$	$\Pi_0^L + \Pi_1^L \frac{h^2}{f^2}$	$\Pi_0^R + \Pi_1^R \frac{h^2}{f^2} + \Pi_2^R \frac{h^4}{f^4}$	$\frac{h}{f} \left(\Pi_1^{LR} + \Pi_2^{LR} \frac{h^2}{f^2} \right)$
$\mathrm{NMCHM}_{15_\mathrm{L}-6_\mathrm{R}}$	$\Pi_0^L + \Pi_1^L \frac{h^2}{f^2} + \Pi_\eta^L \frac{\eta^2}{f^2}$	$\Pi_0^R + \Pi_1^R \frac{h^2}{f^2} + \Pi_\eta^R \frac{\eta^2}{f^2}$	$\Pi_1^{LR} \frac{h}{f}$

(Table continued to page 136)

(Table D.1: continued from page 135)

Models	$\Pi_{t_L}(h,\eta)$	$\Pi_{t_R}(h,\eta)$	$\Pi_{t_L t_R}(h,\eta)$
$\mathrm{NMCHM}_{15_\mathrm{L}-15_\mathrm{R}}$	$\Pi_0^L+\Pi_1^L\frac{h^2}{f^2}+\Pi_\eta^L\frac{\eta^2}{f^2}$	$\Pi_0^R+\Pi_1^R\frac{h^2}{f^2}$	$\Pi_1^{LR}\frac{h}{f}\sqrt{1-\frac{h^2}{f^2}-\frac{\eta^2}{f^2}}$
$\mathrm{NMCHM}_{15_\mathrm{L}-20_\mathrm{R}}$	$\Pi_0^L+\Pi_1^L\frac{h^2}{f^2}+\Pi_\eta^L\frac{\eta^2}{f^2}$	$\Pi_0^R+\Pi_1^R\frac{h^2}{f^2}+\Pi_2^R\frac{h^4}{f^4}$	$\Pi_1^{LR}\frac{h}{f}\sqrt{1-\frac{h^2}{f^2}-\frac{\eta^2}{f^2}}$
$\mathrm{NMCHM}_{20_\mathrm{L}-1_\mathrm{R}}$	$\Pi_0^L+\Pi_1^L\frac{h^2}{f^2}+\Pi_2^L\frac{h^4}{f^4}$ $+\Pi_\eta^L\frac{\eta^2}{f^2}+\Pi_{h\eta}^L\frac{h^2}{f^2}\frac{\eta^2}{f^2}$	Π_0^R	$\Pi_1^{LR}\frac{h}{f}\sqrt{1-\frac{h^2}{f^2}-\frac{\eta^2}{f^2}}$
$\mathrm{NMCHM}_{20_\mathrm{L}-6_\mathrm{R}}$	$\Pi_0^L+\Pi_1^L\frac{h^2}{f^2}+\Pi_2^L\frac{h^4}{f^4}$ $+\Pi_\eta^L\frac{\eta^2}{f^2}+\Pi_{h\eta}^L\frac{h^2}{f^2}\frac{\eta^2}{f^2}$	$\Pi_0^R+\Pi_1^R\frac{h^2}{f^2}+\Pi_\eta^R\frac{\eta^2}{f^2}$	$\frac{h}{f}\Big(\Pi_1^{LR}$ $+\Pi_2^{LR}\frac{h^2}{f^2}+\Pi_\eta^{LR}\frac{\eta^2}{f^2}\Big)$
$\mathrm{NMCHM}_{20_\mathrm{L}-15_\mathrm{R}}$	$\Pi_0^L+\Pi_1^L\frac{h^2}{f^2}+\Pi_2^L\frac{h^4}{f^4}$ $+\Pi_\eta^L\frac{\eta^2}{f^2}+\Pi_{h\eta}^L\frac{h^2}{f^2}\frac{\eta^2}{f^2}$	$\Pi_0^R+\Pi_1^R\frac{h^2}{f^2}$	$\Pi_1^{LR}\frac{h}{f}\sqrt{1-\frac{h^2}{f^2}-\frac{\eta^2}{f^2}}$
$\mathrm{NMCHM}_{20_\mathrm{L}-20_\mathrm{R}}$	$\Pi_0^L+\Pi_1^L\frac{h^2}{f^2}+\Pi_2^L\frac{h^4}{f^4}$ $+\Pi_\eta^L\frac{\eta^2}{f^2}+\Pi_{h\eta}^L\frac{h^2}{f^2}\frac{\eta^2}{f^2}$	$\Pi_0^R+\Pi_1^R\frac{h^2}{f^2}+\Pi_2^R\frac{h^4}{f^4}$	$\frac{h}{f}\sqrt{1-\frac{h^2}{f^2}-\frac{\eta^2}{f^2}}$ $\left(\Pi_1^{LR}+\Pi_2^{LR}\frac{h^2}{f^2}\right)$

Table D.1: *List of Π-functions for different representations (upto dimension* **20***) of next-to-minimal model.*

The expressions for Δ_t and Δ_t^η, as defined in Eq. (4.18), in terms of the form factors, for different $\mathrm{SO}(6)$ representations are presented in Table D.2.

Models		Coupling Modifiers
$\mathrm{NMCHM}_{6_\mathrm{L}-1_\mathrm{R}}$	Δ_t	$-\left(\frac{\Pi_1^L}{\Pi_0^L}+\frac{1}{2}\right)$
	Δ_t^η	0
$\mathrm{NMCHM}_{6_\mathrm{L}-6_\mathrm{R}}$	Δ_t	$-\left(1+\frac{\Pi_\eta^R}{\Pi_0^R}\chi\right)^{-1}\left[\frac{\Pi_1^L}{\Pi_0^L}+\frac{\Pi_1^R}{\Pi_0^R}+\frac{3}{2}+\left(\frac{\Pi_1^L}{\Pi_0^L}\frac{\Pi_\eta^R}{\Pi_0^R}+\frac{1}{2}\frac{\Pi_\eta^R}{\Pi_0^R}\right)\chi\right]$
	Δ_t^η	$\left(1+\frac{\Pi_\eta^R}{\Pi_0^R}\right)\left(1+\frac{\Pi_\eta^R}{\Pi_0^R}\chi\right)^{-1}\sqrt{\frac{\chi}{1-\chi}}$

(Table continued to page 137)

(Table D.2: continued from page 136)

Models		Coupling Modifiers
$\mathrm{NMCHM}_{6_\mathrm{L}-15_\mathrm{R}}$	Δ_t	$-\left[\frac{\Pi_1^L}{\Pi_0^L}+\frac{\Pi_1^R}{\Pi_0^R}+\frac{1}{2}\right]$
	Δ_t^η	0
$\mathrm{NMCHM}_{6_\mathrm{L}-20_\mathrm{R}}$	Δ_t	$\left[2\frac{\Pi_2^{LR}}{\Pi_1^{LR}}-\frac{\Pi_1^L}{\Pi_0^L}-\frac{\Pi_1^R}{\Pi_0^R}-\frac{1}{2}\right]$
	Δ_t^η	0
$\mathrm{NMCHM}_{15_\mathrm{L}-6_\mathrm{R}}$	Δ_t	$-\left(1+\frac{\Pi_\eta^L}{\Pi_0^L}\chi\right)^{-1}\left(1+\frac{\Pi_\eta^R}{\Pi_0^R}\chi\right)^{-1}\left[\frac{\Pi_1^L}{\Pi_0^L}+\frac{\Pi_1^R}{\Pi_0^R}+\frac{1}{2}\right.$ $\left.-\left(\frac{1}{2}\frac{\Pi_\eta^L}{\Pi_0^L}+\frac{1}{2}\frac{\Pi_\eta^R}{\Pi_0^R}-\frac{\Pi_1^L}{\Pi_0^L}\frac{\Pi_\eta^R}{\Pi_0^R}-\frac{\Pi_1^R}{\Pi_0^R}\frac{\Pi_\eta^L}{\Pi_0^L}\right)\chi-\frac{3}{2}\frac{\Pi_\eta^L}{\Pi_0^L}\frac{\Pi_\eta^R}{\Pi_0^R}\chi^2\right]$
	Δ_t^η	$(1-\chi)\left(1+\frac{\Pi_\eta^L}{\Pi_0^L}\chi\right)^{-1}\left(1+\frac{\Pi_\eta^R}{\Pi_0^R}\chi\right)^{-1}\left[\frac{\Pi_\eta^L}{\Pi_0^L}+\frac{\Pi_\eta^R}{\Pi_0^R}+2\frac{\Pi_\eta^L}{\Pi_0^L}\frac{\Pi_\eta^R}{\Pi_0^R}\chi\right]\sqrt{\frac{\chi}{1-\chi}}$
$\mathrm{NMCHM}_{15_\mathrm{L}-15_\mathrm{R}}$	Δ_t	$-\left(1+\frac{\Pi_\eta^L}{\Pi_0^L}\chi\right)^{-1}\left[\frac{\Pi_1^L}{\Pi_0^L}+\frac{\Pi_1^R}{\Pi_0^R}+\frac{3}{2}+\left(\frac{1}{2}\frac{\Pi_\eta^L}{\Pi_0^L}+\frac{\Pi_\eta^L}{\Pi_0^L}\frac{\Pi_1^R}{\Pi_0^R}\right)\chi\right]$
	Δ_t^η	$\left(1+\frac{\Pi_\eta^L}{\Pi_0^L}\right)\left(1+\frac{\Pi_\eta^L}{\Pi_0^L}\chi\right)^{-1}\sqrt{\frac{\chi}{1-\chi}}$
$\mathrm{NMCHM}_{15_\mathrm{L}-20_\mathrm{R}}$	Δ_t	$-\left(1+\frac{\Pi_\eta^L}{\Pi_0^L}\chi\right)^{-1}\left[\frac{\Pi_1^L}{\Pi_0^L}+\frac{\Pi_1^R}{\Pi_0^R}+\frac{3}{2}+\left(\frac{1}{2}\frac{\Pi_\eta^L}{\Pi_0^L}+\frac{\Pi_\eta^L}{\Pi_0^L}\frac{\Pi_1^R}{\Pi_0^R}\right)\chi\right]$
	Δ_t^η	$\left(1+\frac{\Pi_\eta^L}{\Pi_0^L}\right)\left(1+\frac{\Pi_\eta^L}{\Pi_0^L}\chi\right)^{-1}\sqrt{\frac{\chi}{1-\chi}}$
$\mathrm{NMCHM}_{20_\mathrm{L}-1_\mathrm{R}}$	Δ_t	$-\left(1+\frac{\Pi_\eta^L}{\Pi_0^L}\chi\right)^{-1}\left[\frac{\Pi_1^L}{\Pi_0^L}+\frac{3}{2}+\left(\frac{1}{2}\frac{\Pi_\eta^L}{\Pi_0^L}+\frac{\Pi_{h\eta}^L}{\Pi_0^L}\right)\chi\right]$
	Δ_t^η	$\left(1+\frac{\Pi_\eta^L}{\Pi_0^L}\right)\left(1+\frac{\Pi_\eta^L}{\Pi_0^L}\chi\right)^{-1}\sqrt{\frac{\chi}{1-\chi}}$

(Table continued to page 138)

(Table D.2: continued from page 137)

Models		Coupling Modifiers
$\mathrm{NMCHM}_{20_\mathrm{L}-6_\mathrm{R}}$	Δ_t	$\begin{aligned}&\left(1+\frac{\Pi^L_\eta}{\Pi^L_0}\chi\right)^{-1}\left(1+\frac{\Pi^R_\eta}{\Pi^R_0}\chi\right)^{-1}\left(1+\frac{\Pi^{LR}_\eta}{\Pi^{LR}_1}\chi\right)^{-1}\Big[2\frac{\Pi^{LR}_2}{\Pi^{LR}_1}-\frac{\Pi^L_1}{\Pi^L_0}-\frac{\Pi^R_1}{\Pi^R_0}-\frac{1}{2}\\&+\Big(\frac{1}{2}\frac{\Pi^L_\eta}{\Pi^L_0}+\frac{1}{2}\frac{\Pi^R_\eta}{\Pi^R_0}-\frac{5}{2}\frac{\Pi^{LR}_\eta}{\Pi^{LR}_1}-\frac{\Pi^L_{h\eta}}{\Pi^L_0}+2\frac{\Pi^{LR}_2}{\Pi^{LR}_1}\frac{\Pi^L_\eta}{\Pi^L_0}+2\frac{\Pi^{LR}_2}{\Pi^{LR}_1}\frac{\Pi^R_\eta}{\Pi^R_0}-\frac{\Pi^L_1}{\Pi^L_0}\frac{\Pi^R_\eta}{\Pi^R_0}\\&-\frac{\Pi^R_1}{\Pi^R_0}\frac{\Pi^L_\eta}{\Pi^L_0}-\frac{\Pi^L_1}{\Pi^L_0}\frac{\Pi^{LR}_\eta}{\Pi^{LR}_1}-\frac{\Pi^R_1}{\Pi^R_0}\frac{\Pi^{LR}_\eta}{\Pi^{LR}_1}\Big)\chi+\Big(\frac{3}{2}\frac{\Pi^L_\eta}{\Pi^L_0}\frac{\Pi^R_\eta}{\Pi^R_0}-\frac{3}{2}\frac{\Pi^L_\eta}{\Pi^L_0}\frac{\Pi^{LR}_\eta}{\Pi^{LR}_1}-\frac{3}{2}\frac{\Pi^R_\eta}{\Pi^R_0}\frac{\Pi^{LR}_\eta}{\Pi^{LR}_1}\\&-\frac{\Pi^L_{h\eta}}{\Pi^L_0}\frac{\Pi^R_\eta}{\Pi^R_0}-\frac{\Pi^L_{h\eta}}{\Pi^L_0}\frac{\Pi^{LR}_\eta}{\Pi^{LR}_1}+2\frac{\Pi^{LR}_2}{\Pi^{LR}_1}\frac{\Pi^L_\eta}{\Pi^L_0}\frac{\Pi^R_\eta}{\Pi^R_0}-\frac{\Pi^R_1}{\Pi^R_0}\frac{\Pi^L_\eta}{\Pi^L_0}\frac{\Pi^{LR}_\eta}{\Pi^{LR}_1}-\frac{\Pi^L_1}{\Pi^L_0}\frac{\Pi^R_\eta}{\Pi^R_0}\frac{\Pi^{LR}_\eta}{\Pi^{LR}_1}\Big)\chi^2\\&+\Big(-\frac{1}{2}\frac{\Pi^L_\eta}{\Pi^L_0}\frac{\Pi^R_\eta}{\Pi^R_0}\frac{\Pi^{LR}_\eta}{\Pi^{LR}_1}-\frac{\Pi^L_{h\eta}}{\Pi^L_0}\frac{\Pi^R_\eta}{\Pi^R_0}\frac{\Pi^{LR}_\eta}{\Pi^{LR}_1}\Big)\chi^3\Big]\end{aligned}$
	Δ_t^η	$\begin{aligned}&-(1-\chi)\left(1+\frac{\Pi^L_\eta}{\Pi^L_0}\chi\right)^{-1}\left(1+\frac{\Pi^R_\eta}{\Pi^R_0}\chi\right)^{-1}\left(1+\frac{\Pi^{LR}_\eta}{\Pi^{LR}_1}\chi\right)^{-1}\\&\left[2\frac{\Pi^{LR}_\eta}{\Pi^{LR}_1}-\frac{\Pi^L_\eta}{\Pi^L_0}-\frac{\Pi^R_\eta}{\Pi^R_0}+\left(\frac{\Pi^L_\eta}{\Pi^L_0}\frac{\Pi^{LR}_\eta}{\Pi^{LR}_1}+\frac{\Pi^R_\eta}{\Pi^R_0}\frac{\Pi^{LR}_\eta}{\Pi^{LR}_1}-2\frac{\Pi^L_\eta}{\Pi^L_0}\frac{\Pi^R_\eta}{\Pi^R_0}\right)\chi\right]\sqrt{\frac{\chi}{1-\chi}}\end{aligned}$
$\mathrm{NMCHM}_{20_\mathrm{L}-15_\mathrm{R}}$	Δ_t	$-\left(1+\frac{\Pi^L_\eta}{\Pi^L_0}\chi\right)^{-1}\left[\frac{\Pi^L_1}{\Pi^L_0}+\frac{\Pi^R_1}{\Pi^R_0}+\frac{3}{2}+\left(\frac{1}{2}\frac{\Pi^L_\eta}{\Pi^L_0}+\frac{\Pi^L_{h\eta}}{\Pi^L_0}+\frac{\Pi^L_\eta}{\Pi^L_0}\frac{\Pi^R_1}{\Pi^R_0}\right)\chi\right]$
	Δ_t^η	$\left(1+\frac{\Pi^L_\eta}{\Pi^L_0}\right)\left(1+\frac{\Pi^L_\eta}{\Pi^L_0}\chi\right)^{-1}\sqrt{\frac{\chi}{1-\chi}}$
$\mathrm{NMCHM}_{20_\mathrm{L}-20_\mathrm{R}}$	Δ_t	$\begin{aligned}&\left(1+\frac{\Pi^L_\eta}{\Pi^L_0}\chi\right)^{-1}\Big[2\frac{\Pi^{LR}_2}{\Pi^{LR}_1}-\frac{\Pi^L_1}{\Pi^L_0}-\frac{\Pi^R_1}{\Pi^R_0}-\frac{3}{2}\\&+\left(2\frac{\Pi^{LR}_2}{\Pi^{LR}_1}\frac{\Pi^L_\eta}{\Pi^L_0}-\frac{\Pi^R_1}{\Pi^R_0}\frac{\Pi^L_\eta}{\Pi^L_0}-\frac{1}{2}\frac{\Pi^L_\eta}{\Pi^L_0}-\frac{\Pi^L_{h\eta}}{\Pi^L_0}\right)\chi\Big]\end{aligned}$
	Δ_t^η	$\left(1+\frac{\Pi^L_\eta}{\Pi^L_0}\right)\left(1+\frac{\Pi^L_\eta}{\Pi^L_0}\chi\right)^{-1}\sqrt{\frac{\chi}{1-\chi}}$

Table D.2: *Expressions for* Δ_t *and* Δ_t^η *for different representations of* $\mathrm{SO}(6)$ *in which top quark is embedded.*

BIBLIOGRAPHY

[1] ATLAS collaboration, G. Aad et al., *Observation of a new particle in the search for the Standard Model Higgs boson with the ATLAS detector at the LHC*, *Phys. Lett.* **B716** (2012) 1–29, [1207.7214].

[2] CMS collaboration, S. Chatrchyan et al., *Observation of a new boson at a mass of 125 GeV with the CMS experiment at the LHC*, *Phys. Lett.* **B716** (2012) 30–61, [1207.7235].

[3] G. F. Giudice, G. Isidori, A. Salvio and A. Strumia, *Softened Gravity and the Extension of the Standard Model up to Infinite Energy*, *JHEP* **02** (2015) 137, [1412.2769].

[4] SNO collaboration, Q. Ahmad et al., *Measurement of the rate of $\nu_e + d \to p + p + e^-$ interactions produced by ^8B solar neutrinos at the Sudbury Neutrino Observatory*, *Phys. Rev. Lett.* **87** (2001) 071301, [nucl-ex/0106015].

[5] K2K collaboration, E. Aliu et al., *Evidence for muon neutrino oscillation in an accelerator-based experiment*, *Phys. Rev. Lett.* **94** (2005) 081802, [hep-ex/0411038].

[6] SUPER-KAMIOKANDE collaboration, J. Hosaka et al., *Solar neutrino measurements in super-Kamiokande-I*, *Phys. Rev. D* **73** (2006) 112001, [hep-ex/0508053].

[7] MINOS collaboration, D. Michael et al., *Observation of muon neutrino disappearance with the MINOS detectors and the NuMI neutrino beam*, *Phys. Rev. Lett.* **97** (2006) 191801, [hep-ex/0607088].

[8] F. Zwicky, *Die Rotverschiebung von extragalaktischen Nebeln*, *Helv. Phys. Acta* **6** (1933) 110–127.

[9] SUPERNOVA SEARCH TEAM collaboration, A. G. Riess et al., *Observational evidence from supernovae for an accelerating universe and a cosmological constant*, *Astron. J.* **116** (1998) 1009–1038, [astro-ph/9805201].

[10] M. Markevitch, A. H. Gonzalez, D. Clowe, A. Vikhlinin, L. David, W. Forman et al., *Direct constraints on the dark matter self-interaction cross-section from the merging galaxy cluster 1E0657-56*, *Astrophys. J.* **606** (2004) 819–824, [astro-ph/0309303].

[11] PLANCK collaboration, N. Aghanim et al., *Planck 2018 results. VI. Cosmological parameters*, 1807.06209.

[12] A. Sakharov, *Violation of CP Invariance, C asymmetry, and baryon asymmetry of the universe*, *Sov. Phys. Usp.* **34** (1991) 392–393.

[13] C. J. Copi, D. N. Schramm and M. S. Turner, *Big bang nucleosynthesis and the baryon density of the universe*, *Science* **267** (1995) 192–199, [astro-ph/9407006].

[14] PLANCK collaboration, P. Ade et al., *Planck 2015 results. XIII. Cosmological parameters*, *Astron. Astrophys.* **594** (2016) A13, [1502.01589].

[15] G. 't Hooft, *Naturalness, chiral symmetry, and spontaneous chiral symmetry breaking*, *NATO Sci. Ser. B* **59** (1980) 135–157.

[16] H. P. Nilles, *Supersymmetry, Supergravity and Particle Physics*, *Phys. Rept.* **110** (1984) 1–162.

[17] H. E. Haber and G. L. Kane, *The Search for Supersymmetry: Probing Physics Beyond the Standard Model*, *Phys. Rept.* **117** (1985) 75–263.

[18] M. Sohnius, *Introducing Supersymmetry*, *Phys. Rept.* **128** (1985) 39–204.

[19] J. D. Lykken, *Introduction to supersymmetry*, in *Fields, strings and duality. Proceedings, Summer School, Theoretical Advanced Study Institute in Elementary Particle Physics, TASI'96, Boulder, USA, June 2-28, 1996*, pp. 85–153, 1996. hep-th/9612114.

[20] M. Drees, *An Introduction to supersymmetry*, in *Inauguration Conference of the Asia Pacific Center for Theoretical Physics (APCTP)*, 11, 1996. hep-ph/9611409.

[21] S. P. Martin, *A Supersymmetry primer*, hep-ph/9709356.

[22] D. B. Kaplan and H. Georgi, *SU(2) $\times$ U(1) Breaking by Vacuum Misalignment*, *Phys. Lett.* **B136** (1984) 183–186.

[23] D. B. Kaplan, H. Georgi and S. Dimopoulos, *Composite Higgs Scalars*, *Phys. Lett.* **136B** (1984) 187–190.

[24] M. J. Dugan, H. Georgi and D. B. Kaplan, *Anatomy of a Composite Higgs Model*, *Nucl. Phys.* **B254** (1985) 299–326.

[25] N. Arkani-Hamed, A. Cohen, E. Katz, A. Nelson, T. Gregoire and J. G. Wacker, *The Minimal moose for a little Higgs*, *JHEP* **08** (2002) 021, [hep-ph/0206020].

[26] N. Arkani-Hamed, A. G. Cohen, E. Katz and A. E. Nelson, *The Littlest Higgs*, *JHEP* **07** (2002) 034, [hep-ph/0206021].

[27] M. Schmaltz and D. Tucker-Smith, *Little Higgs review*, *Ann. Rev. Nucl. Part. Sci.* **55** (2005) 229–270, [hep-ph/0502182].

[28] M. Perelstein, *Little Higgs models and their phenomenology*, *Prog. Part. Nucl. Phys.* **58** (2007) 247–291, [hep-ph/0512128].

[29] I. Antoniadis, *A Possible new dimension at a few TeV*, *Phys. Lett. B* **246** (1990) 377–384.

[30] Y. Hosotani, *Dynamical Mass Generation by Compact Extra Dimensions*, *Phys. Lett. B* **126** (1983) 309–313.

[31] L. Randall and R. Sundrum, *A Large mass hierarchy from a small extra dimension*, *Phys. Rev. Lett.* **83** (1999) 3370–3373, [hep-ph/9905221].

[32] M. Kubo, C. Lim and H. Yamashita, *The Hosotani mechanism in bulk gauge theories with an orbifold extra space S**1 / Z(2)*, *Mod. Phys. Lett. A* **17** (2002) 2249–2264, [hep-ph/0111327].

[33] Z. Chacko, H.-S. Goh and R. Harnik, *The Twin Higgs: Natural electroweak breaking from mirror symmetry*, *Phys. Rev. Lett.* **96** (2006) 231802, [hep-ph/0506256].

[34] N. Craig, A. Katz, M. Strassler and R. Sundrum, *Naturalness in the Dark at the LHC*, *JHEP* **07** (2015) 105, [1501.05310].

[35] N. Craig, S. Knapen and P. Longhi, *Neutral Naturalness from Orbifold Higgs Models*, *Phys. Rev. Lett.* **114** (2015) 061803, [1410.6808].

[36] G. Burdman, Z. Chacko, R. Harnik, L. de Lima and C. B. Verhaaren, *Colorless Top Partners, a 125 GeV Higgs, and the Limits on Naturalness*, *Phys. Rev. D* **91** (2015) 055007, [1411.3310].

[37] S. Weinberg, *Implications of Dynamical Symmetry Breaking*, *Phys. Rev. D* **13** (1976) 974–996.

[38] L. Susskind, *Dynamics of Spontaneous Symmetry Breaking in the Weinberg-Salam Theory*, *Phys. Rev. D* **20** (1979) 2619–2625.

[39] C. T. Hill and E. H. Simmons, *Strong Dynamics and Electroweak Symmetry Breaking*, *Phys. Rept.* **381** (2003) 235–402, [hep-ph/0203079].

[40] K. Lane, *Two Lectures on Technicolor*, hep-ph/0202255.

[41] R. Chivukula, *Lectures on technicolor and compositeness*, in *Theoretical Advanced Study Institute in Elementary Particle Physics (TASI 2000): Flavor Physics for the Millennium*, pp. 731–772, 6, 2000. hep-ph/0011264.

[42] ALEPH, CDF, D0, DELPHI, L3, OPAL, SLD, LEP Electroweak Working Group, Tevatron Electroweak Working Group, SLD Electroweak Working Group, SLD Heavy Flavor Group collaboration, *Precision Electroweak Measurements and Constraints on the Standard Model*, 0911.2604.

[43] V. Agrawal, S. M. Barr, J. F. Donoghue and D. Seckel, *Viable range of the mass scale of the standard model*, *Phys. Rev. D* **57** (1998) 5480–5492, [hep-ph/9707380].

[44] P. W. Graham, D. E. Kaplan and S. Rajendran, *Cosmological Relaxation of the Electroweak Scale*, *Phys. Rev. Lett.* **115** (2015) 221801, [1504.07551].

[45] R. S. Gupta, Z. Komargodski, G. Perez and L. Ubaldi, *Is the Relaxion an Axion?*, *JHEP* **02** (2016) 166, [1509.00047].

[46] A. Hook and G. Marques-Tavares, *Relaxation from particle production*, *JHEP* **12** (2016) 101, [1607.01786].

[47] N. Arkani-Hamed, T. Cohen, R. T. D'Agnolo, A. Hook, H. D. Kim and D. Pinner, *Solving the Hierarchy Problem at Reheating with a Large Number of Degrees of Freedom*, *Phys. Rev. Lett.* **117** (2016) 251801, [1607.06821].

[48] M. Srednicki, R. Watkins and K. A. Olive, *Calculations of Relic Densities in the Early Universe*, *Nucl. Phys. B* **310** (1988) 693.

[49] P. Gondolo and G. Gelmini, *Cosmic abundances of stable particles: Improved analysis*, *Nucl. Phys. B* **360** (1991) 145–179.

[50] XENON100 collaboration, E. Aprile et al., *Dark Matter Results from 225 Live Days of XENON100 Data*, *Phys. Rev. Lett.* **109** (2012) 181301, [1207.5988].

[51] LUX collaboration, D. S. Akerib et al., *Results from a search for dark matter in the complete LUX exposure*, *Phys. Rev. Lett.* **118** (2017) 021303, [1608.07648].

[52] PANDAX-II collaboration, X. Cui et al., *Dark Matter Results From 54-Ton-Day Exposure of PandaX-II Experiment*, *Phys. Rev. Lett.* **119** (2017) 181302, [1708.06917].

[53] XENON collaboration, E. Aprile et al., *Dark Matter Search Results from a One Ton-Year Exposure of XENON1T*, *Phys. Rev. Lett.* **121** (2018) 111302, [1805.12562].

[54] L. J. Hall, K. Jedamzik, J. March-Russell and S. M. West, *Freeze-In Production of FIMP Dark Matter*, *JHEP* **03** (2010) 080, [0911.1120].

[55] R. Contino, *The Higgs as a Composite Nambu-Goldstone Boson*, in *Physics of the large and the small, TASI 09, proceedings of the Theoretical Advanced Study Institute in Elementary Particle Physics, Boulder, Colorado, USA, 1-26 June 2009*, pp. 235–306, 2011. 1005.4269. DOI.

[56] G. Panico and A. Wulzer, *The Composite Nambu-Goldstone Higgs*, *Lect. Notes Phys.* **913** (2016) pp.1–316, [1506.01961].

[57] C. Csaki, C. Grojean and J. Terning, *Alternatives to an Elementary Higgs*, *Rev. Mod. Phys.* **88** (2016) 045001, [1512.00468].

[58] C. Csaki and P. Tanedo, *Beyond the Standard Model*, in *Proceedings, 2013 European School of High-Energy Physics (ESHEP 2013): Paradfurdo, Hungary, June 5-18, 2013*, pp. 169–268, 2015. 1602.04228. DOI.

[59] G. F. Giudice, C. Grojean, A. Pomarol and R. Rattazzi, *The Strongly-Interacting Light Higgs*, *JHEP* **06** (2007) 045, [hep-ph/0703164].

[60] H. Georgi, *Effective field theory and electroweak radiative corrections*, *Nucl. Phys. B* **363** (1991) 301–325.

[61] R. Barbieri, A. Pomarol, R. Rattazzi and A. Strumia, *Electroweak symmetry breaking after LEP-1 and LEP-2*, *Nucl. Phys. B* **703** (2004) 127–146, [hep-ph/0405040].

[62] S. R. Coleman, J. Wess and B. Zumino, *Structure of phenomenological Lagrangians. 1.*, *Phys. Rev.* **177** (1969) 2239–2247.

[63] C. G. Callan, Jr., S. R. Coleman, J. Wess and B. Zumino, *Structure of phenomenological Lagrangians. 2.*, *Phys. Rev.* **177** (1969) 2247–2250.

[64] S. R. Coleman and E. J. Weinberg, *Radiative Corrections as the Origin of Spontaneous Symmetry Breaking*, *Phys. Rev.* **D7** (1973) 1888–1910.

[65] S. Dimopoulos and L. Susskind, *Mass without scalars*, *Nuclear Physics B* **155** (1979) 237 – 252.

[66] T. Appelquist and L. C. R. Wijewardhana, *Chiral hierarchies and chiral perturbations in technicolor theories*, *Phys. Rev. D* **35** (Jan, 1987) 774–777.

[67] T. Appelquist and L. C. R. Wijewardhana, *Chiral hierarchies from slowly running couplings in technicolor theories*, *Phys. Rev. D* **36** (Jul, 1987) 568–580.

[68] T. Appelquist, D. Karabali and L. C. R. Wijewardhana, *Chiral hierarchies and flavor-changing neutral currents in hypercolor*, *Phys. Rev. Lett.* **57** (Aug, 1986) 957–960.

[69] E. Eichten and K. D. Lane, *Dynamical Breaking of Weak Interaction Symmetries*, *Phys. Lett. B* **90** (1980) 125–130.

[70] D. B. Kaplan, *Flavor at SSC energies: A New mechanism for dynamically generated fermion masses*, *Nucl. Phys.* **B365** (1991) 259–278.

[71] R. Contino and A. Pomarol, *Holography for fermions*, *JHEP* **11** (2004) 058, [hep-th/0406257].

[72] Y. Grossman and M. Neubert, *Neutrino masses and mixings in nonfactorizable geometry*, *Phys. Lett. B* **474** (2000) 361–371, [hep-ph/9912408].

[73] T. Gherghetta and A. Pomarol, *Bulk fields and supersymmetry in a slice of AdS*, *Nucl. Phys. B* **586** (2000) 141–162, [hep-ph/0003129].

[74] S. J. Huber and Q. Shafi, *Fermion masses, mixings and proton decay in a Randall-Sundrum model*, *Phys. Lett. B* **498** (2001) 256–262, [hep-ph/0010195].

[75] S. J. Huber, *Flavor violation and warped geometry*, *Nucl. Phys. B* **666** (2003) 269–288, [hep-ph/0303183].

[76] K. Agashe, G. Perez and A. Soni, *Flavor structure of warped extra dimension models*, *Phys. Rev. D* **71** (2005) 016002, [hep-ph/0408134].

[77] K. Agashe, G. Perez and A. Soni, *B-factory signals for a warped extra dimension*, *Phys. Rev. Lett.* **93** (2004) 201804, [hep-ph/0406101].

[78] D. T. Murnane, *The landscape of composite Higgs models*. PhD thesis, Adelaide U., 2019.

[79] A. Pomarol and F. Riva, *The Composite Higgs and Light Resonance Connection*, *JHEP* **08** (2012) 135, [1205.6434].

[80] J. M. Maldacena, *The Large N limit of superconformal field theories and supergravity*, *Int. J. Theor. Phys.* **38** (1999) 1113–1133, [hep-th/9711200].

[81] Y. Hosotani, *Dynamical Gauge Symmetry Breaking as the Casimir Effect*, *Phys. Lett. B* **129** (1983) 193–197.

[82] C. Scrucca, M. Serone, L. Silvestrini and A. Wulzer, *Gauge Higgs unification in orbifold models*, *JHEP* **02** (2004) 049, [hep-th/0312267].

[83] R. Chivukula, D. A. Dicus, H.-J. He and S. Nandi, *Unitarity of the higher dimensional standard model*, *Phys. Lett. B* **562** (2003) 109–117, [hep-ph/0302263].

[84] R. Chivukula, E. H. Simmons, H.-J. He, M. Kurachi and M. Tanabashi, *Ideal fermion delocalization in five dimensional gauge theories*, *Phys. Rev. D* **72** (2005) 095013, [hep-ph/0509110].

[85] G. Panico, M. Serone and A. Wulzer, *A Model of electroweak symmetry breaking from a fifth dimension*, *Nucl. Phys. B* **739** (2006) 186–207, [hep-ph/0510373].

[86] R. Contino, Y. Nomura and A. Pomarol, *Higgs as a holographic pseudoGoldstone boson*, *Nucl. Phys.* **B671** (2003) 148–174, [hep-ph/0306259].

[87] R. Contino, L. Da Rold and A. Pomarol, *Light custodians in natural composite Higgs models*, *Phys. Rev.* **D75** (2007) 055014, [hep-ph/0612048].

[88] K. Agashe, R. Contino and A. Pomarol, *The Minimal composite Higgs model*, *Nucl. Phys.* **B719** (2005) 165–187, [hep-ph/0412089].

[89] N. Arkani-Hamed, A. G. Cohen and H. Georgi, *(De)constructing dimensions*, *Phys. Rev. Lett.* **86** (2001) 4757–4761, [hep-th/0104005].

[90] C. T. Hill, S. Pokorski and J. Wang, *Gauge Invariant Effective Lagrangian for Kaluza-Klein Modes*, *Phys. Rev. D* **64** (2001) 105005, [hep-th/0104035].

[91] N. Arkani-Hamed, A. G. Cohen and H. Georgi, *Electroweak symmetry breaking from dimensional deconstruction*, *Phys. Lett. B* **513** (2001) 232–240, [hep-ph/0105239].

[92] H. Georgi, *Vector Realization of Chiral Symmetry*, *Nucl. Phys. B* **331** (1990) 311–330.

[93] S. De Curtis, M. Redi and A. Tesi, *The 4D Composite Higgs*, *JHEP* **04** (2012) 042, [1110.1613].

[94] G. Panico and A. Wulzer, *The Discrete Composite Higgs Model*, *JHEP* **09** (2011) 135, [1106.2719].

[95] R. Contino, D. Marzocca, D. Pappadopulo and R. Rattazzi, *On the effect of resonances in composite Higgs phenomenology*, *JHEP* **10** (2011) 081, [1109.1570].

[96] A. Azatov and J. Galloway, *Light Custodians and Higgs Physics in Composite Models*, *Phys. Rev.* **D85** (2012) 055013, [1110.5646].

[97] O. Matsedonskyi, G. Panico and A. Wulzer, *Light Top Partners for a Light Composite Higgs*, *JHEP* **01** (2013) 164, [1204.6333].

[98] D. Marzocca, M. Serone and J. Shu, *General Composite Higgs Models*, *JHEP* **08** (2012) 013, [1205.0770].

[99] G. Panico, M. Redi, A. Tesi and A. Wulzer, *On the Tuning and the Mass of the Composite Higgs*, *JHEP* **03** (2013) 051, [1210.7114].

[100] M. Carena, L. Da Rold and E. Pontón, *Minimal Composite Higgs Models at the LHC*, *JHEP* **06** (2014) 159, [1402.2987].

[101] M. Montull, F. Riva, E. Salvioni and R. Torre, *Higgs Couplings in Composite Models*, *Phys. Rev.* **D88** (2013) 095006, [1308.0559].

[102] A. Carmona and F. Goertz, *A naturally light Higgs without light Top Partners*, *JHEP* **05** (2015) 002, [1410.8555].

[103] C. Niehoff, P. Stangl and D. M. Straub, *Direct and indirect signals of natural composite Higgs models*, *JHEP* **01** (2016) 119, [1508.00569].

[104] S. Kanemura, K. Kaneta, N. Machida, S. Odori and T. Shindou, *Single and double production of the Higgs boson at hadron and lepton colliders in minimal composite Higgs models*, *Phys. Rev.* **D94** (2016) 015028, [1603.05588].

[105] M. B. Gavela, K. Kanshin, P. A. N. Machado and S. Saa, *The linearâĂŞnon-linear frontier for the Goldstone Higgs*, *Eur. Phys. J.* **C76** (2016) 690, [1610.08083].

[106] D. Liu, I. Low and C. E. M. Wagner, *Modification of Higgs Couplings in Minimal Composite Models*, *Phys. Rev.* **D96** (2017) 035013, [1703.07791].

[107] E. Witten, *Baryons in the 1/n Expansion*, *Nucl. Phys. B* **160** (1979) 57–115.

[108] B. Bellazzini, C. Csaki, J. Hubisz, J. Serra and J. Terning, *Composite Higgs Sketch*, *JHEP* **11** (2012) 003, [1205.4032].

[109] K. Agashe, R. Contino, L. Da Rold and A. Pomarol, *A Custodial symmetry for $Zb\bar{b}$*, *Phys. Lett.* **B641** (2006) 62–66, [hep-ph/0605341].

[110] S. Weinberg, *Precise relations between the spectra of vector and axial vector mesons*, *Phys. Rev. Lett.* **18** (1967) 507–509.

[111] P. R. Archer, *Fine Tuning in the Holographic Minimal Composite Higgs Model*, 1403.8048.

[112] J. Barnard and M. White, *Collider constraints on tuning in composite Higgs models*, *JHEP* **10** (2015) 072, [1507.02332].

[113] C. Csaki, T. Ma and J. Shu, *Maximally Symmetric Composite Higgs Models*, *Phys. Rev. Lett.* **119** (2017) 131803, [1702.00405].

[114] J. Barnard, D. Murnane, M. White and A. G. Williams, *Constraining fine tuning in Composite Higgs Models with partially composite leptons*, *JHEP* **09** (2017) 049, [1703.07653].

[115] D. Pappadopulo, A. Thamm and R. Torre, *A minimally tuned composite Higgs model from an extra dimension*, *JHEP* **07** (2013) 058, [1303.3062].

[116] ATLAS COLLABORATION collaboration, *Search for new physics using events with b-jets and a pair of same charge leptons in 3.2 fb^{-1} of pp collisions at $\sqrt{s} = 13$ TeV with the ATLAS detector*, Tech. Rep. ATLAS-CONF-2016-032, CERN, Geneva, Jun, 2016.

[117] T. Gherghetta, B. von Harling, A. D. Medina and M. A. Schmidt, *The Scale-Invariant NMSSM and the 126 GeV Higgs Boson*, *JHEP* **02** (2013) 032, [1212.5243].

[118] F. Brummer, S. Kraml and S. Kulkarni, *Anatomy of maximal stop mixing in the MSSM*, *JHEP* **08** (2012) 089, [1204.5977].

[119] K. Agashe and R. Contino, *The Minimal composite Higgs model and electroweak precision tests*, *Nucl. Phys.* **B742** (2006) 59–85, [hep-ph/0510164].

[120] J. Barnard, T. Gherghetta, A. Medina and T. S. Ray, *Radiative corrections to the composite Higgs mass from a gluon partner*, *JHEP* **10** (2013) 055, [1307.4778].

[121] A. Carmona and F. Goertz, *Composite Taus and Higgs Decays*, *PoS* **EPS-HEP2013** (2013) 267, [1310.3825].

[122] C. Csáki, T. Ma and J. Shu, *Trigonometric Parity for Composite Higgs Models*, *Phys. Rev. Lett.* **121** (2018) 231801, [1709.08636].

[123] C. Csáki, T. Ma, J. Shu and J.-H. Yu, *Emergence of Maximal Symmetry*, *Phys. Rev. Lett.* **124** (2020) 241801, [1810.07704].

[124] B. Gripaios, A. Pomarol, F. Riva and J. Serra, *Beyond the Minimal Composite Higgs Model*, *JHEP* **04** (2009) 070, [0902.1483].

[125] J. Galloway, J. A. Evans, M. A. Luty and R. A. Tacchi, *Minimal Conformal Technicolor and Precision Electroweak Tests*, *JHEP* **10** (2010) 086, [1001.1361].

[126] J. Mrazek, A. Pomarol, R. Rattazzi, M. Redi, J. Serra and A. Wulzer, *The Other Natural Two Higgs Doublet Model*, *Nucl. Phys.* **B853** (2011) 1–48, [1105.5403].

[127] M. Chala, *$h \to \gamma\gamma$ excess and Dark Matter from Composite Higgs Models*, *JHEP* **01** (2013) 122, [1210.6208].

[128] E. Bertuzzo, T. S. Ray, H. de Sandes and C. A. Savoy, *On Composite Two Higgs Doublet Models*, *JHEP* **05** (2013) 153, [1206.2623].

[129] M. Chala, G. Nardini and I. Sobolev, *Unified explanation for dark matter and electroweak baryogenesis with direct detection and gravitational wave signatures*, *Phys. Rev.* **D94** (2016) 055006, [1605.08663].

[130] C. Cai, G. Cacciapaglia and H.-H. Zhang, *Vacuum alignment in a composite 2HDM*, *JHEP* **01** (2019) 130, [1805.07619].

[131] A. Agugliaro, G. Cacciapaglia, A. Deandrea and S. De Curtis, *Vacuum misalignment and pattern of scalar masses in the SU(5)/SO(5) composite Higgs model*, *JHEP* **02** (2019) 089, [1808.10175].

[132] M. Redi and A. Tesi, *Implications of a Light Higgs in Composite Models*, *JHEP* **10** (2012) 166, [1205.0232].

[133] J. Serra, *Beyond the Minimal Top Partner Decay*, *JHEP* **09** (2015) 176, [1506.05110].

[134] M. Low, A. Tesi and L.-T. Wang, *A pseudoscalar decaying to photon pairs in the early LHC Run 2 data*, *JHEP* **03** (2016) 108, [1512.05328].

[135] H. Cai, T. Flacke and M. Lespinasse, *A composite scalar hint from di-boson resonances?*, 1512.04508.

[136] A. Arbey, G. Cacciapaglia, H. Cai, A. Deandrea, S. Le Corre and F. Sannino, *Fundamental Composite Electroweak Dynamics: Status at the LHC*, *Phys. Rev.* **D95** (2017) 015028, [1502.04718].

[137] C. Niehoff, P. Stangl and D. M. Straub, *Electroweak symmetry breaking and collider signatures in the next-to-minimal composite Higgs model*, *JHEP* **04** (2017) 117, [1611.09356].

[138] M. Golterman and Y. Shamir, *Effective potential in ultraviolet completions for composite Higgs models*, *Phys. Rev. D* **97** (2018) 095005, [1707.06033].

[139] T. Alanne, N. Bizot, G. Cacciapaglia and F. Sannino, *Classification of NLO operators for composite Higgs models*, *Phys. Rev. D* **97** (2018) 075028, [1801.05444].

[140] D. Murnane, M. J. White and A. G. Williams, *Exploring Fine-tuning of the Next-to-Minimal Composite Higgs Model*, *JHEP* **04** (2019) 076, [1810.08355].

[141] L. Bian, Y. Wu and K.-P. Xie, *Electroweak phase transition with composite Higgs models: calculability, gravitational waves and collider searches*, *JHEP* **12** (2019) 028, [1909.02014].

[142] S. De Curtis, L. Delle Rose and G. Panico, *Composite Dynamics in the Early Universe*, *JHEP* **12** (2019) 149, [1909.07894].

[143] M. Frigerio, A. Pomarol, F. Riva and A. Urbano, *Composite Scalar Dark Matter*, *JHEP* **07** (2012) 015, [1204.2808].

[144] D. Marzocca and A. Urbano, *Composite Dark Matter and LHC Interplay*, *JHEP* **07** (2014) 107, [1404.7419].

[145] N. Fonseca, R. Zukanovich Funchal, A. Lessa and L. Lopez-Honorez, *Dark Matter Constraints on Composite Higgs Models*, *JHEP* **06** (2015) 154, [1501.05957].

[146] M. Kim, S. J. Lee and A. Parolini, *WIMP Dark Matter in Composite Higgs Models and the Dilaton Portal*, 1602.05590.

[147] J. R. Espinosa, B. Gripaios, T. Konstandin and F. Riva, *Electroweak Baryogenesis in Non-minimal Composite Higgs Models*, *JCAP* **1201** (2012) 012, [1110.2876].

[148] E. Katz, A. E. Nelson and D. G. E. Walker, *The Intermediate Higgs*, *JHEP* **08** (2005) 074, [hep-ph/0504252].

[149] J. Barnard, T. Gherghetta and T. S. Ray, *UV descriptions of composite Higgs models without elementary scalars*, *JHEP* **02** (2014) 002, [1311.6562].

[150] G. Ferretti and D. Karateev, *Fermionic UV completions of Composite Higgs models*, *JHEP* **03** (2014) 077, [1312.5330].

[151] G. Cacciapaglia and F. Sannino, *Fundamental Composite (Goldstone) Higgs Dynamics*, *JHEP* **04** (2014) 111, [1402.0233].

[152] A. Agugliaro, O. Antipin, D. Becciolini, S. De Curtis and M. Redi, *UV complete composite Higgs models*, *Phys. Rev. D* **95** (2017) 035019, [1609.07122].

[153] J. Galloway, A. L. Kagan and A. Martin, *A UV complete partially composite-pNGB Higgs*, *Phys. Rev. D* **95** (2017) 035038, [1609.05883].

[154] A. Banerjee, G. Bhattacharyya and T. S. Ray, *Improving Fine-tuning in Composite Higgs Models*, *Phys. Rev.* **D96** (2017) 035040, [1703.08011].

[155] D. Buarque Franzosi, G. Cacciapaglia, H. Cai, A. Deandrea and M. Frandsen, *Vector and Axial-vector resonances in composite models of the Higgs boson*, *JHEP* **11** (2016) 076, [1605.01363].

[156] M. Chaichian, A. Datta, K. Huitu and Z.-h. Yu, *Radion and Higgs mixing at the LHC*, *Phys. Lett.* **B524** (2002) 161–169, [hep-ph/0110035].

[157] D. Dominici, B. Grzadkowski, J. F. Gunion and M. Toharia, *The Scalar sector of the Randall-Sundrum model*, *Nucl. Phys.* **B671** (2003) 243–292, [hep-ph/0206192].

[158] N. Desai, U. Maitra and B. Mukhopadhyaya, *An updated analysis of radion-higgs mixing in the light of LHC data*, *JHEP* **10** (2013) 093, [1307.3765].

[159] K. S. Babu, C. F. Kolda and J. March-Russell, *Implications of generalized Z - Z-prime mixing*, *Phys. Rev.* **D57** (1998) 6788–6792, [hep-ph/9710441].

[160] H. Georgi, D. B. Kaplan and L. Randall, *Manifesting the Invisible Axion at Low-energies*, *Phys. Lett.* **B169** (1986) 73–78.

[161] K. S. Jeong, Y. Shoji and M. Yamaguchi, *Singlet-Doublet Higgs Mixing and Its Implications on the Higgs mass in the PQ-NMSSM*, *JHEP* **09** (2012) 007, [1205.2486].

[162] K. Agashe, R. Contino and R. Sundrum, *Top compositeness and precision unification*, *Phys. Rev. Lett.* **95** (2005) 171804, [hep-ph/0502222].

[163] A. Falkowski, F. Riva and A. Urbano, *Higgs at last*, *JHEP* **11** (2013) 111, [1303.1812].

[164] R. Barbieri, B. Bellazzini, V. S. Rychkov and A. Varagnolo, *The Higgs boson from an extended symmetry*, *Phys. Rev.* **D76** (2007) 115008, [0706.0432].

[165] ATLAS, CMS collaboration, G. Aad et al., *Measurements of the Higgs boson production and decay rates and constraints on its couplings from a combined ATLAS and CMS analysis of the LHC pp collision data at $\sqrt{s} = 7$ and 8 TeV*, *JHEP* **08** (2016) 045, [1606.02266].

[166] CMS collaboration, *Projected Performance of an Upgraded CMS Detector at the LHC and HL-LHC: Contribution to the Snowmass Process*, in *Proceedings,*

Community Summer Study 2013: Snowmass on the Mississippi (CSS2013): Minneapolis, MN, USA, July 29-August 6, 2013, 2013. 1307.7135.

[167] *Projections for measurements of Higgs boson signal strengths and coupling parameters with the ATLAS detector at a HL-LHC*, Tech. Rep. ATL-PHYS-PUB-2014-016, CERN, Geneva, Oct, 2014.

[168] G. J. Gounaris and F. M. Renard, *Remarkable signals of t_R compositeness*, 1611.02426.

[169] F. M. Renard, *$t_{L,R}$ inclusive distributions as tests of top compositeness*, 1701.03382.

[170] A. Banerjee, G. Bhattacharyya, N. Kumar and T. S. Ray, *Constraining Composite Higgs Models using LHC data*, *JHEP* **03** (2018) 062, [1712.07494].

[171] A. Banerjee and G. Bhattacharyya, *Probing the Higgs boson through Yukawa force*, 2006.01164.

[172] V. Sanz and J. Setford, *Composite Higgs Models after Run 2*, *Adv. High Energy Phys.* **2018** (2018) 7168480, [1703.10190].

[173] R. Contino, M. Ghezzi, C. Grojean, M. Muhlleitner and M. Spira, *Effective Lagrangian for a light Higgs-like scalar*, *JHEP* **07** (2013) 035, [1303.3876].

[174] M. Hashimoto, *Revisiting vectorlike quark models with enhanced top Yukawa coupling*, *Phys. Rev.* **D96** (2017) 035020, [1704.02615].

[175] S. Jana and S. Nandi, *New Physics Scale from Higgs Observables with Effective Dimension-6 Operators*, *Phys. Lett. B* **783** (2018) 51–58, [1710.00619].

[176] G. Cacciapaglia, A. Deandrea, G. Drieu La Rochelle and J.-B. Flament, *Higgs couplings beyond the Standard Model*, *JHEP* **03** (2013) 029, [1210.8120].

[177] A. Azatov, C. Grojean, A. Paul and E. Salvioni, *Resolving gluon fusion loops at current and future hadron colliders*, *JHEP* **09** (2016) 123, [1608.00977].

[178] M. Frigerio, J. Serra and A. Varagnolo, *Composite GUTs: models and expectations at the LHC*, *JHEP* **06** (2011) 029, [1103.2997].

[179] J. Barnard, T. Gherghetta, T. S. Ray and A. Spray, *The Unnatural Composite Higgs*, *JHEP* **01** (2015) 067, [1409.7391].

[180] W. Buchmuller and D. Wyler, *Effective Lagrangian Analysis of New Interactions and Flavor Conservation*, *Nucl. Phys.* **B268** (1986) 621–653.

[181] K. Hagiwara, S. Ishihara, R. Szalapski and D. Zeppenfeld, *Low-energy effects of new interactions in the electroweak boson sector*, *Phys. Rev.* **D48** (1993) 2182–2203.

[182] B. Grzadkowski, M. Iskrzynski, M. Misiak and J. Rosiek, *Dimension-Six Terms in the Standard Model Lagrangian*, *JHEP* **10** (2010) 085, [1008.4884].

[183] A. Azatov, R. Contino and J. Galloway, *Model-Independent Bounds on a Light Higgs*, *JHEP* **04** (2012) 127, [1202.3415].

[184] J. Ellis and T. You, *Updated Global Analysis of Higgs Couplings*, *JHEP* **06** (2013) 103, [1303.3879].

[185] M. B. Einhorn and J. Wudka, *Higgs-Boson Couplings Beyond the Standard Model*, *Nucl. Phys. B* **877** (2013) 792–806, [1308.2255].

[186] A. Pomarol and F. Riva, *Towards the Ultimate SM Fit to Close in on Higgs Physics*, *JHEP* **01** (2014) 151, [1308.2803].

[187] J. Ellis, V. Sanz and T. You, *Complete Higgs Sector Constraints on Dimension-6 Operators*, *JHEP* **07** (2014) 036, [1404.3667].

[188] J. de Blas, M. Ciuchini, E. Franco, D. Ghosh, S. Mishima, M. Pierini et al., *Global Bayesian Analysis of the Higgs-boson Couplings*, *Nucl. Part. Phys. Proc.* **273-275** (2016) 834–840, [1410.4204].

[189] J. Bernon, B. Dumont and S. Kraml, *Status of Higgs couplings after run 1 of the LHC*, *Phys. Rev. D* **90** (2014) 071301, [1409.1588].

[190] I. Brivio and M. Trott, *The Standard Model as an Effective Field Theory*, *Phys. Rept.* **793** (2019) 1–98, [1706.08945].

[191] S. Bar-Shalom and A. Soni, *Universally enhanced light-quarks Yukawa couplings paradigm*, *Phys. Rev. D* **98** (2018) 055001, [1804.02400].

[192] J. Ellis, C. W. Murphy, V. Sanz and T. You, *Updated Global SMEFT Fit to Higgs, Diboson and Electroweak Data*, *JHEP* **06** (2018) 146, [1803.03252].

[193] G. Buchalla, O. Cata and C. Krause, *A Systematic Approach to the SILH Lagrangian*, *Nucl. Phys. B* **894** (2015) 602–620, [1412.6356].

[194] M. Chala, G. Durieux, C. Grojean, L. de Lima and O. Matsedonskyi, *Minimally extended SILH*, *JHEP* **06** (2017) 088, [1703.10624].

[195] G. Buchalla, O. Cata, A. Celis and C. Krause, *Fitting Higgs Data with Nonlinear Effective Theory*, *Eur. Phys. J.* **C76** (2016) 233, [1511.00988].

[196] M. Cepeda et al., *Report from Working Group 2*, *CERN Yellow Rep. Monogr.* **7** (2019) 221–584, [1902.00134].

[197] LHC Higgs Cross Section Working Group collaboration, J. R. Andersen et al., *Handbook of LHC Higgs Cross Sections: 3. Higgs Properties*, 1307.1347.

[198] LHC Higgs Cross Section Working Group collaboration, D. de Florian et al., *Handbook of LHC Higgs Cross Sections: 4. Deciphering the Nature of the Higgs Sector*, 1610.07922.

[199] J. de Blas, O. Eberhardt and C. Krause, *Current and Future Constraints on Higgs Couplings in the Nonlinear Effective Theory*, *JHEP* **07** (2018) 048, [1803.00939].

[200] ATLAS collaboration, G. Aad et al., *Combined measurements of Higgs boson production and decay using up to* 80 *fb*$^{-1}$ *of proton-proton collision data at* $\sqrt{s} =$ *13 TeV collected with the ATLAS experiment*, *Phys. Rev.* **D101** (2020) 012002, [1909.02845].

[201] CMS collaboration, *Combined Higgs boson production and decay measurements with up to 137 fb-1 of proton-proton collision data at sqrts = 13 TeV*, Tech. Rep. CMS-PAS-HIG-19-005, CERN, Geneva, 2020.

[202] M. Ciuchini, E. Franco, S. Mishima and L. Silvestrini, *Electroweak Precision Observables, New Physics and the Nature of a 126 GeV Higgs Boson*, *JHEP* **08** (2013) 106, [1306.4644].

[203] J. de Blas, M. Ciuchini, E. Franco, S. Mishima, M. Pierini, L. Reina et al., *Electroweak precision observables and Higgs-boson signal strengths in the*

Standard Model and beyond: present and future, *JHEP* **12** (2016) 135, [1608.01509].

[204] CMS collaboration, A. M. Sirunyan et al., *Observation of* $\mathrm{t\bar{t}}H$ *production*, *Phys. Rev. Lett.* **120** (2018) 231801, [1804.02610].

[205] ATLAS collaboration, M. Aaboud et al., *Observation of Higgs boson production in association with a top quark pair at the LHC with the ATLAS detector*, *Phys. Lett.* **B784** (2018) 173–191, [1806.00425].

[206] CMS collaboration, A. M. Sirunyan et al., *Observation of Higgs boson decay to bottom quarks*, *Phys. Rev. Lett.* **121** (2018) 121801, [1808.08242].

[207] ATLAS collaboration, M. Aaboud et al., *Observation of* $H \to b\bar{b}$ *decays and* VH *production with the ATLAS detector*, *Phys. Lett.* **B786** (2018) 59–86, [1808.08238].

[208] J. L. Diaz-Cruz, J. Hernandez-Sanchez and J. J. Toscano, *An Effective Lagrangian description of charged Higgs decays* $H^+ \to W^+\gamma$*,* W^+Z *and* $W^+ h_0$, *Phys. Lett.* **B512** (2001) 339–348, [hep-ph/0106001].

[209] Y. Kikuta, Y. Okada and Y. Yamamoto, *Structure of dimension-six derivative interactions in pseudo Nambu-Goldstone N Higgs doublet models*, *Phys. Rev.* **D85** (2012) 075021, [1111.2120].

[210] Y. Kikuta and Y. Yamamoto, *Derivative interactions and perturbative UV contributions in N Higgs Doublet Models*, *Eur. Phys. J.* **C76** (2016) 297, [1510.05540].

[211] A. Crivellin, M. Ghezzi and M. Procura, *Effective Field Theory with Two Higgs Doublets*, *JHEP* **09** (2016) 160, [1608.00975].

[212] S. Karmakar and S. Rakshit, *Higher dimensional operators in 2HDM*, *JHEP* **10** (2017) 048, [1707.00716].

[213] A. Banerjee, G. Bhattacharyya and N. Kumar, *Impact of Yukawa-like dimension-five operators on the Georgi-Machacek model*, *Phys. Rev.* **D99** (2019) 035028, [1901.01725].

[214] H. Georgi and M. Machacek, *DOUBLY CHARGED HIGGS BOSONS*, *Nucl. Phys.* **B262** (1985) 463–477.

[215] M. S. Chanowitz and M. Golden, *Higgs Boson Triplets With M (W) = M (Z) $\cos\theta\omega$*, *Phys. Lett.* **165B** (1985) 105–108.

[216] J. F. Gunion, R. Vega and J. Wudka, *Higgs triplets in the standard model*, *Phys. Rev.* **D42** (1990) 1673–1691.

[217] M. Aoki and S. Kanemura, *Unitarity bounds in the Higgs model including triplet fields with custodial symmetry*, *Phys. Rev.* **D77** (2008) 095009, [0712.4053].

[218] C.-W. Chiang and K. Yagyu, *Testing the custodial symmetry in the Higgs sector of the Georgi-Machacek model*, *JHEP* **01** (2013) 026, [1211.2658].

[219] K. Hartling, K. Kumar and H. E. Logan, *The decoupling limit in the Georgi-Machacek model*, *Phys. Rev.* **D90** (2014) 015007, [1404.2640].

[220] K. Hartling, K. Kumar and H. E. Logan, *Indirect constraints on the Georgi-Machacek model and implications for Higgs boson couplings*, *Phys. Rev.* **D91** (2015) 015013, [1410.5538].

[221] C.-W. Chiang and T. Yamada, *Electroweak phase transition in GeorgiâĂŞMachacek model*, *Phys. Lett.* **B735** (2014) 295–300, [1404.5182].

[222] C.-W. Chiang, S. Kanemura and K. Yagyu, *Novel constraint on the parameter space of the Georgi-Machacek model with current LHC data*, *Phys. Rev.* **D90** (2014) 115025, [1407.5053].

[223] H. E. Logan and V. Rentala, *All the generalized Georgi-Machacek models*, *Phys. Rev.* **D92** (2015) 075011, [1502.01275].

[224] C.-W. Chiang, A.-L. Kuo and T. Yamada, *Searches of exotic Higgs bosons in general mass spectra of the Georgi-Machacek model at the LHC*, *JHEP* **01** (2016) 120, [1511.00865].

[225] J. Chang, C.-R. Chen and C.-W. Chiang, *Higgs boson pair productions in the Georgi-Machacek model at the LHC*, *JHEP* **03** (2017) 137, [1701.06291].

[226] C. Degrande, K. Hartling and H. E. Logan, *Scalar decays to $\gamma\gamma$, $Z\gamma$, and $W\gamma$ in the Georgi-Machacek model*, *Phys. Rev.* **D96** (2017) 075013, [1708.08753].

[227] S. Blasi, S. De Curtis and K. Yagyu, *Effects of custodial symmetry breaking in the Georgi-Machacek model at high energies*, *Phys. Rev.* **D96** (2017) 015001, [1704.08512].

[228] A. Biswas, D. K. Ghosh, S. K. Patra and A. Shaw, *$b \to c\ell\nu$ anomalies in light of extended scalar sectors*, *Int. J. Mod. Phys. A* **34** (2019) 1950112, [1801.03375].

[229] B. Keeshan, H. E. Logan and T. Pilkington, *Custodial symmetry violation in the Georgi-Machacek model*, 1807.11511.

[230] N. Ghosh, S. Ghosh and I. Saha, *Charged Higgs boson searches in the Georgi-Machacek model at the LHC*, *Phys. Rev.* **D101** (2020) 015029, [1908.00396].

[231] N. Chakrabarty, I. Chakraborty and D. K. Ghosh, *Fingerprinting the contribution of colored scalars to the* $H^+W^-Z(\gamma)$ *vertex*, 2003.01105.

[232] A. Ismail, H. E. Logan and Y. Wu, *Updated constraints on the Georgi-Machacek model from LHC Run 2*, 2003.02272.

[233] A. Ismail, B. Keeshan, H. E. Logan and Y. Wu, *A benchmark for LHC searches for low-mass custodial fiveplet scalars in the Georgi-Machacek model*, 2003.05536.

[234] C.-W. Chiang, A.-L. Kuo and K. Yagyu, *Enhancements of weak gauge boson scattering processes at the CERN LHC*, *JHEP* **10** (2013) 072, [1307.7526].

[235] E. Coluccio Leskow, T. A. W. Martin and A. de la Puente, *Vector-like quarks with a scalar triplet*, *Phys. Lett.* **B743** (2015) 366–376, [1409.3579].

[236] M. Chala, M. Ramos and M. Spannowsky, *Gravitational wave and collider probes of a triplet Higgs sector with a low cutoff*, *Eur. Phys. J. C* **79** (2019) 156, [1812.01901].

[237] S. Weinberg, *Baryon and Lepton Nonconserving Processes*, *Phys. Rev. Lett.* **43** (1979) 1566–1570.

[238] S. Kanemura, M. Kikuchi and K. Yagyu, *Probing exotic Higgs sectors from the precise measurement of Higgs boson couplings*, *Phys. Rev.* **D88** (2013) 015020, [1301.7303].

[239] H. E. Logan and M.-A. Roy, *Higgs couplings in a model with triplets*, *Phys. Rev.* **D82** (2010) 115011, [1008.4869].

[240] G. Belanger, B. Dumont, U. Ellwanger, J. F. Gunion and S. Kraml, *Global fit to Higgs signal strengths and couplings and implications for extended Higgs sectors*, *Phys. Rev.* **D88** (2013) 075008, [1306.2941].

[241] C.-W. Chiang and K. Tsumura, *Properties and searches of the exotic neutral Higgs bosons in the Georgi-Machacek model*, *JHEP* **04** (2015) 113, [1501.04257].

[242] B. Li, Z.-L. Han and Y. Liao, *Higgs production at future e^+e colliders in the Georgi-Machacek model*, *JHEP* **02** (2018) 007, [1710.00184].

[243] C.-W. Chiang, G. Cottin and O. Eberhardt, *Global fits in the Georgi-Machacek model*, *Phys. Rev. D* **99** (2019) 015001, [1807.10660].

[244] D. Das and I. Saha, *Cornering variants of the Georgi-Machacek model using Higgs precision data*, *Phys. Rev.* **D98** (2018) 095010, [1811.00979].

[245] J.-Y. Cen, J.-H. Chen, X.-G. He, G. Li, J.-Y. Su and W. Wang, *Searching for a charged Higgs boson with both $H^\pm W^\mp Z$ and $H^\pm tb$ couplings at the LHC*, *JHEP* **01** (2019) 148, [1811.00910].

[246] ATLAS collaboration, G. Aad et al., *Search for a Charged Higgs Boson Produced in the Vector-Boson Fusion Mode with Decay $H^\pm \to W^\pm Z$ using pp Collisions at $\sqrt{s} = 8$âĂĽâĂĽTeV with the ATLAS Experiment*, *Phys. Rev. Lett.* **114** (2015) 231801, [1503.04233].

[247] CMS collaboration, A. M. Sirunyan et al., *Search for Charged Higgs Bosons Produced via Vector Boson Fusion and Decaying into a Pair of W and Z Bosons*

Using pp Collisions at $\sqrt{s} = 13$ TeV, Phys. Rev. Lett. **119** (2017) 141802, [1705.02942].

[248] C.-W. Chiang, T. Nomura and K. Tsumura, *Search for doubly charged Higgs bosons using the same-sign diboson mode at the LHC*, Phys. Rev. **D85** (2012) 095023, [1202.2014].

[249] C. Englert, E. Re and M. Spannowsky, *Pinning down Higgs triplets at the LHC*, Phys. Rev. **D88** (2013) 035024, [1306.6228].

[250] C.-W. Chiang, S. Kanemura and K. Yagyu, *Phenomenology of the Georgi-Machacek model at future electron-positron colliders*, Phys. Rev. **D93** (2016) 055002, [1510.06297].

[251] H. Sun, X. Luo, W. Wei and T. Liu, *Searching for the doubly-charged Higgs bosons in the Georgi-Machacek model at the electron-proton colliders*, Phys. Rev. **D96** (2017) 095003, [1710.06284].

[252] CMS COLLABORATION collaboration, *A search for doubly-charged Higgs boson production in three and four lepton final states at $\sqrt{s} = 13$ TeV*, Tech. Rep. CMS-PAS-HIG-16-036, CERN, Geneva, 2017.

[253] ATLAS collaboration, M. Aaboud et al., *Search for doubly charged Higgs boson production in multi-lepton final states with the ATLAS detector using protonâĂŞproton collisions at $\sqrt{s} = 13$ TeV*, Eur. Phys. J. **C78** (2018) 199, [1710.09748].

[254] ATLAS collaboration, M. Aaboud et al., *Search for doubly charged scalar bosons*

decaying into same-sign W boson pairs with the ATLAS detector, Eur. Phys. J. C **79** (2019) 58, [1808.01899].

[255] HFLAV collaboration, Y. Amhis et al., *Averages of b-hadron, c-hadron, and τ-lepton properties as of summer 2016*, Eur. Phys. J. **C77** (2017) 895, [1612.07233].

[256] M. Misiak et al., *Updated NNLO QCD predictions for the weak radiative B-meson decays*, Phys. Rev. Lett. **114** (2015) 221801, [1503.01789].

[257] M. Ciuchini, G. Degrassi, P. Gambino and G. F. Giudice, *Next-to-leading QCD corrections to $B \to X_s\gamma$: Standard model and two Higgs doublet model*, Nucl. Phys. **B527** (1998) 21–43, [hep-ph/9710335].

[258] Q.-Y. Hu, X.-Q. Li and Y.-D. Yang, *$B^0 \to K^{*0}\mu^+\mu^-$ decay in the Aligned Two-Higgs-Doublet Model*, Eur. Phys. J. **C77** (2017) 190, [1612.08867].

[259] F. Mahmoudi and O. Stal, *Flavor constraints on the two-Higgs-doublet model with general Yukawa couplings*, Phys. Rev. **D81** (2010) 035016, [0907.1791].

[260] L. F. Abbott, P. Sikivie and M. B. Wise, *Constraints on Charged Higgs Couplings*, Phys. Rev. **D21** (1980) 1393.

[261] ALEPH, DELPHI, L3, OPAL, SLD, LEP Electroweak Working Group, SLD Electroweak Group, SLD Heavy Flavour Group collaboration, S. Schael et al., *Precision electroweak measurements on the Z resonance*, Phys. Rept. **427** (2006) 257–454, [hep-ex/0509008].

[262] J. Haller, A. Hoecker, R. Kogler, K. MÃűnig, T. Peiffer and J. Stelzer, *Update of the global electroweak fit and constraints on two-Higgs-doublet models*, *Eur. Phys. J.* **C78** (2018) 675, [1803.01853].

[263] H. E. Haber and H. E. Logan, *Radiative corrections to the $Zb\bar{b}$ vertex and constraints on extended Higgs sectors*, *Phys. Rev.* **D62** (2000) 015011, [hep-ph/9909335].

[264] H. E. Logan, *Radiative corrections to the $Zb\bar{b}$ vertex and constraints on extended Higgs sectors*. PhD thesis, UC, Santa Cruz, 1999. hep-ph/9906332.

[265] G. Passarino and M. J. G. Veltman, *One Loop Corrections for e+ e- Annihilation Into mu+ mu- in the Weinberg Model*, *Nucl. Phys.* **B160** (1979) 151–207.

[266] Heavy Flavor Averaging Group (HFAG) collaboration, Y. Amhis et al., *Averages of b-hadron, c-hadron, and τ-lepton properties as of summer 2014*, 1412.7515.

[267] J. Ellis, A. Fowlie, L. Marzola and M. Raidal, *Statistical Analyses of Higgs- and Z-Portal Dark Matter Models*, *Phys. Rev.* **D97** (2018) 115014, [1711.09912].

[268] G. Arcadi, Y. Mambrini and F. Richard, *Z-portal dark matter*, *JCAP* **1503** (2015) 018, [1411.2985].

[269] J. Kearney, N. Orlofsky and A. Pierce, *Z boson mediated dark matter beyond the effective theory*, *Phys. Rev.* **D95** (2017) 035020, [1611.05048].

[270] M. Escudero, A. Berlin, D. Hooper and M.-X. Lin, *Toward (Finally!) Ruling Out Z and Higgs Mediated Dark Matter Models*, *JCAP* **1612** (2016) 029, [1609.09079].

[271] J. A. Casas, D. G. Cerdeño, J. M. Moreno and J. Quilis, *Reopening the Higgs portal for single scalar dark matter*, *JHEP* **05** (2017) 036, [1701.08134].

[272] A. Djouadi, O. Lebedev, Y. Mambrini and J. Quevillon, *Implications of LHC searches for Higgs–portal dark matter*, *Phys. Lett.* **B709** (2012) 65–69, [1112.3299].

[273] A. Djouadi, A. Falkowski, Y. Mambrini and J. Quevillon, *Direct Detection of Higgs-Portal Dark Matter at the LHC*, *Eur. Phys. J.* **C73** (2013) 2455, [1205.3169].

[274] O. Lebedev, H. M. Lee and Y. Mambrini, *Vector Higgs-portal dark matter and the invisible Higgs*, *Phys. Lett.* **B707** (2012) 570–576, [1111.4482].

[275] Y. Mambrini, *Higgs searches and singlet scalar dark matter: Combined constraints from XENON 100 and the LHC*, *Phys. Rev.* **D84** (2011) 115017, [1108.0671].

[276] C. Gross, O. Lebedev and Y. Mambrini, *Non-Abelian gauge fields as dark matter*, *JHEP* **08** (2015) 158, [1505.07480].

[277] A. Alves, S. Profumo and F. S. Queiroz, *The dark Z' portal: direct, indirect and collider searches*, *JHEP* **04** (2014) 063, [1312.5281].

[278] O. Lebedev and Y. Mambrini, *Axial dark matter: The case for an invisible Z*, *Phys. Lett.* **B734** (2014) 350–353, [1403.4837].

[279] G. Arcadi, Y. Mambrini, M. H. G. Tytgat and B. Zaldivar, *Invisible Z' and dark matter: LHC vs LUX constraints*, *JHEP* **03** (2014) 134, [1401.0221].

[280] E. Dudas, L. Heurtier, Y. Mambrini and B. Zaldivar, *Extra U(1), effective operators, anomalies and dark matter*, *JHEP* **11** (2013) 083, [1307.0005].

[281] E. Dudas, Y. Mambrini, S. Pokorski and A. Romagnoni, *Extra U(1) as natural source of a monochromatic gamma ray line*, *JHEP* **10** (2012) 123, [1205.1520].

[282] Y. Mambrini, *The ZZ' kinetic mixing in the light of the recent direct and indirect dark matter searches*, *JCAP* **1107** (2011) 009, [1104.4799].

[283] Y. Mambrini, *The Kinetic dark-mixing in the light of CoGENT and XENON100*, *JCAP* **1009** (2010) 022, [1006.3318].

[284] G. Arcadi, M. Dutra, P. Ghosh, M. Lindner, Y. Mambrini, M. Pierre et al., *The waning of the WIMP? A review of models, searches, and constraints*, *Eur. Phys. J.* **C78** (2018) 203, [1703.07364].

[285] X. Chu, T. Hambye and M. H. G. Tytgat, *The Four Basic Ways of Creating Dark Matter Through a Portal*, *JCAP* **1205** (2012) 034, [1112.0493].

[286] K. Benakli, Y. Chen, E. Dudas and Y. Mambrini, *Minimal model of gravitino dark matter*, *Phys. Rev.* **D95** (2017) 095002, [1701.06574].

[287] E. Dudas, Y. Mambrini and K. Olive, *Case for an EeV Gravitino*, *Phys. Rev. Lett.* **119** (2017) 051801, [1704.03008].

[288] E. Dudas, T. Gherghetta, K. Kaneta, Y. Mambrini and K. A. Olive, *Gravitino decay in high scale supersymmetry with R -parity violation*, *Phys. Rev.* **D98** (2018) 015030, [1805.07342].

[289] E. Dudas, T. Gherghetta, Y. Mambrini and K. A. Olive, *Inflation and High-Scale Supersymmetry with an EeV Gravitino*, *Phys. Rev.* **D96** (2017) 115032, [1710.07341].

[290] Y. Mambrini, N. Nagata, K. A. Olive, J. Quevillon and J. Zheng, *Dark matter and gauge coupling unification in nonsupersymmetric SO(10) grand unified models*, *Phys. Rev.* **D91** (2015) 095010, [1502.06929].

[291] Y. Mambrini, K. A. Olive, J. Quevillon and B. Zaldivar, *Gauge Coupling Unification and Nonequilibrium Thermal Dark Matter*, *Phys. Rev. Lett.* **110** (2013) 241306, [1302.4438].

[292] Y. Mambrini, N. Nagata, K. A. Olive and J. Zheng, *Vacuum Stability and Radiative Electroweak Symmetry Breaking in an SO(10) Dark Matter Model*, *Phys. Rev.* **D93** (2016) 111703, [1602.05583].

[293] N. Bernal, M. Dutra, Y. Mambrini, K. Olive, M. Peloso and M. Pierre, *Spin-2 Portal Dark Matter*, *Phys. Rev.* **D97** (2018) 115020, [1803.01866].

[294] M. Garny, A. Palessandro, M. Sandora and M. S. Sloth, *Theory and Phenomenology of Planckian Interacting Massive Particles as Dark Matter*, *JCAP* **1802** (2018) 027, [1709.09688].

[295] D. Chowdhury, E. Dudas, M. Dutra and Y. Mambrini, *Moduli Portal Dark Matter*, *Phys. Rev.* **D99** (2019) 095028, [1811.01947].

[296] G. Bhattacharyya, M. Dutra, Y. Mambrini and M. Pierre, *Freezing-in dark matter through a heavy invisible ZâĂš*, *Phys. Rev.* **D98** (2018) 035038, [1806.00016].

[297] M. A. G. Garcia, Y. Mambrini, K. A. Olive and M. Peloso, *Enhancement of the Dark Matter Abundance Before Reheating: Applications to Gravitino Dark Matter*, *Phys. Rev.* **D96** (2017) 103510, [1709.01549].

[298] M. A. G. Garcia and M. A. Amin, *Prethermalization production of dark matter*, *Phys. Rev.* **D98** (2018) 103504, [1806.01865].

[299] I. Baldes, D. Chowdhury and M. H. Tytgat, *Forays into the dark side of the swamp*, *Phys. Rev. D* **100** (2019) 095009, [1907.06663].

[300] N. Bernal, F. Elahi, C. Maldonado and J. Unwin, *Ultraviolet Freeze-in and Non-Standard Cosmologies*, *JCAP* **11** (2019) 026, [1909.07992].

[301] M. Dutra, *Origins for dark matter particles : from the "WIMP miracle" to the "FIMP wonder"*. PhD thesis, Orsay, LPT, 2019.

[302] N. Bernal, A. Donini, M. G. Folgado and N. Rius, *Kaluza-Klein FIMP Dark Matter in Warped Extra-Dimensions*, 2004.14403.

[303] N. Bernal, J. Rubio and H. VeermÃd'e, *Boosting Ultraviolet Freeze-in in NO Models*, 2004.13706.

[304] K. Kaneta, Y. Mambrini and K. A. Olive, *Radiative production of nonthermal dark matter*, *Phys. Rev.* **D99** (2019) 063508, [1901.04449].

[305] A. Banerjee, G. Bhattacharyya, D. Chowdhury and Y. Mambrini, *Dark matter seeping through dynamic gauge kinetic mixing*, *JCAP* **12** (2019) 009, [1905.11407].

[306] G. F. Giudice, E. W. Kolb and A. Riotto, *Largest temperature of the radiation era and its cosmological implications*, *Phys. Rev.* **D64** (2001) 023508, [hep-ph/0005123].

[307] A. Mazumdar and B. Zaldivar, *Quantifying the reheating temperature of the universe*, *Nucl. Phys.* **B886** (2014) 312–327, [1310.5143].

[308] B. Holdom, *Two U(1)'s and Epsilon Charge Shifts*, *Phys. Lett.* **166B** (1986) 196–198.

[309] K. R. Dienes, C. F. Kolda and J. March-Russell, *Kinetic mixing and the supersymmetric gauge hierarchy*, *Nucl. Phys.* **B492** (1997) 104–118, [hep-ph/9610479].

[310] S. A. Abel, M. D. Goodsell, J. Jaeckel, V. V. Khoze and A. Ringwald, *Kinetic Mixing of the Photon with Hidden U(1)s in String Phenomenology*, *JHEP* **07** (2008) 124, [0803.1449].

[311] M. Goodsell, J. Jaeckel, J. Redondo and A. Ringwald, *Naturally Light Hidden Photons in LARGE Volume String Compactifications*, *JHEP* **11** (2009) 027, [0909.0515].

[312] D. Feldman, B. Kors and P. Nath, *Extra-weakly Interacting Dark Matter*, *Phys. Rev.* **D75** (2007) 023503, [hep-ph/0610133].

[313] Z. Kang, T. Li, T. Liu, C. Tong and J. M. Yang, *Light Dark Matter from the $U(1)_X$ Sector in the NMSSM with Gauge Mediation*, *JCAP* **1101** (2011) 028, [1008.5243].

[314] X. Chu, Y. Mambrini, J. Quevillon and B. Zaldivar, *Thermal and non-thermal production of dark matter via Z'-portal(s)*, *JCAP* **1401** (2014) 034, [1306.4677].

[315] Y. Mambrini, *The ZZ' kinetic mixing in the light of the recent direct and indirect dark matter searches*, *JCAP* **1107** (2011) 009, [1104.4799].

[316] G. F. Giudice, Y. Kats, M. McCullough, R. Torre and A. Urbano, *Clockwork/linear dilaton: structure and phenomenology*, *JHEP* **06** (2018) 009, [1711.08437].

[317] D. K. Hong, D. H. Kim and C. S. Shin, *Clockwork graviton contributions to muon $g-2$*, *Phys. Rev.* **D97** (2018) 035014, [1706.09376].

[318] D. E. Kaplan and R. Rattazzi, *Large field excursions and approximate discrete symmetries from a clockwork axion*, *Phys. Rev.* **D93** (2016) 085007, [1511.01827].

[319] G. F. Giudice and M. McCullough, *A Clockwork Theory*, *JHEP* **02** (2017) 036, [1610.07962].

[320] R. Coy, M. Frigerio and M. Ibe, *Dynamical Clockwork Axions*, *JHEP* **10** (2017) 002, [1706.04529].

[321] P. Agrawal, J. Fan, M. Reece and L.-T. Wang, *Experimental Targets for Photon Couplings of the QCD Axion*, *JHEP* **02** (2018) 006, [1709.06085].

[322] A. J. Long, *Cosmological Aspects of the Clockwork Axion*, *JHEP* **07** (2018) 066, [1803.07086].

[323] Q. Bonnefoy, *Topics beyond the Standard Model : axions, supersymmetry, string theory*. PhD thesis, U. Paris-Saclay, 2019.

[324] T. Hambye, D. Teresi and M. H. G. Tytgat, *A Clockwork WIMP*, *JHEP* **07** (2017) 047, [1612.06411].

[325] J. Kim and J. McDonald, *Clockwork Higgs portal model for freeze-in dark matter*, *Phys. Rev.* **D98** (2018) 023533, [1709.04105].

[326] J. Kim and J. Mcdonald, *Freeze-In Dark Matter from a sub-Higgs Mass Clockwork Sector via the Higgs Portal*, *Phys. Rev. D* **98** (2018) 123503, [1804.02661].

[327] A. Goudelis, K. A. Mohan and D. Sengupta, *Clockworking FIMPs*, 1807.06642.

[328] K. Choi, H. Kim and S. Yun, *Natural inflation with multiple sub-Planckian axions*, *Phys. Rev.* **D90** (2014) 023545, [1404.6209].

[329] A. Kehagias and A. Riotto, *Clockwork Inflation*, *Phys. Lett.* **B767** (2017) 73–80, [1611.03316].

[330] S. H. Im, H. P. Nilles and A. Trautner, *Exploring extra dimensions through inflationary tensor modes*, *JHEP* **03** (2018) 004, [1707.03830].

[331] A. Ibarra, A. Kushwaha and S. K. Vempati, *Clockwork for Neutrino Masses and Lepton Flavor Violation*, *Phys. Lett.* **B780** (2018) 86–92, [1711.02070].

[332] K. M. Patel, *Clockwork mechanism for flavor hierarchies*, *Phys. Rev.* **D96** (2017) 115013, [1711.05393].

[333] R. Alonso, A. Carmona, B. M. Dillon, J. F. Kamenik, J. Martin Camalich and J. Zupan, *A clockwork solution to the flavor puzzle*, *JHEP* **10** (2018) 099, [1807.09792].

[334] A. Banerjee, S. Ghosh and T. S. Ray, *Clockworked VEVs and Neutrino Mass*, *JHEP* **11** (2018) 075, [1808.04010].

[335] T. Kitabayashi, *Scalar clockwork and flavor neutrino mass matrix*, 2003.06550.

[336] F. Abreu de Souza and G. von Gersdorff, *A Random Clockwork of Flavor*, *JHEP* **02** (2020) 186, [1911.08476].

[337] T. Kitabayashi, *Clockwork origin of neutrino mixings*, *Phys. Rev. D* **100** (2019) 035019, [1904.12516].

[338] K. Choi and S. H. Im, *Realizing the relaxion from multiple axions and its UV completion with high scale supersymmetry*, *JHEP* **01** (2016) 149, [1511.00132].

[339] T. Flacke, C. Frugiuele, E. Fuchs, R. S. Gupta and G. Perez, *Phenomenology of relaxion-Higgs mixing*, *JHEP* **06** (2017) 050, [1610.02025].

[340] O. Davidi, R. S. Gupta, G. Perez, D. Redigolo and A. Shalit, *The hierarchion, a relaxion addressing the Standard Model's hierarchies*, *JHEP* **08** (2018) 153, [1806.08791].

[341] H. M. Lee, *Gauged $U(1)$ clockwork theory*, *Phys. Lett.* **B778** (2018) 79–87, [1708.03564].

[342] T. Gherghetta, J. Kersten, K. Olive and M. Pospelov, *Evaluating the price of tiny kinetic mixing*, *Phys. Rev. D* **100** (2019) 095001, [1909.00696].

[343] A. V. Manohar, *Effective field theories*, *Lect. Notes Phys.* **479** (1997) 311–362, [hep-ph/9606222].

[344] T. Hahn, *CUBA: A Library for multidimensional numerical integration*, *Comput. Phys. Commun.* **168** (2005) 78–95, [hep-ph/0404043].

[345] J. Jaeckel, V. V. Khoze and M. Spannowsky, *Hearing the signal of dark sectors with gravitational wave detectors*, *Phys. Rev.* **D94** (2016) 103519, [1602.03901].

[346] P. S. B. Dev and A. Mazumdar, *Probing the Scale of New Physics by Advanced LIGO/VIRGO*, *Phys. Rev.* **D93** (2016) 104001, [1602.04203].

[347] T. Hasegawa, N. Okada and O. Seto, *Gravitational waves from the minimal gauged $U(1)_{B-L}$ model*, *Phys. Rev. D* **99** (2019) 095039, [1904.03020].

ABBREVIATIONS

BSM	Beyond Standard Model
C-W	Coleman-Weinberg
DM	Dark matter
EWSB	Electroweak symmetry breaking
FIMP	Feebly interacting massive particle
HL-LHC	High Luminosity Large Hadron Collider
LEP	Large Electron Positron collider
LHC	Large Hadron Collider
MCHM	Minimal composite Higgs model
NGB	Nambu-Goldstone boson
NMCHM	Next-to-minimal composite Higgs model
pNGB	pseudo Nambu-Goldstone boson
QCD	Quantum Chromodynamics
QED	Quantum Electrodynamics
SM	Standard Model
vev	Vacuum expectation value
WIMP	Weakly interacting massive particle

Thesis Highlight

Name of the Student: Avik Banerjee

Name of the CI/OCC: Saha Institute of Nuclear Physics, Kolkata

Enrolment No.: PHYS05201504020

Thesis Title: Composite Higgs and Physics Beyond the Standard Model

Discipline: Physical Sciences **Sub-Area of Discipline:** High Energy Physics Phenomenology

Date of viva voce: November 19, 2020

The Standard Model (SM) of particle physics, despite its all glories and success suffers from various limitations–both on the theoretical and observational grounds. In this thesis, we address one of the major theoretical limitation, namely the stability of the weak scale using a composite Higgs setup. In addition, we discuss a model of freeze-in dark matter (DM) scenario to explain the observed relic abundance of non-baryonic matter in the universe. The composite Higgs framework, where the Higgs originates as a pseudo Nambu-Goldstone boson of a spontaneously broken global symmetry in some strongly interacting sector, has two major phenomenological consequences. First, this scenario predicts the existence of non-standard spin-1 particles as well as additional colored fermions also known as top-partners, which can in principle be searched at the Large Hadron Collider (LHC). We explore the connection between a light Higgs boson and a light top-partner resonance, which is somewhat in tension with the present LHC data, in such models. We suggest a possible avenue to depart from such strong correlations in a next-to-minimal setup using the mechanism of level repulsion between the doublet Higgs boson and an additional scalar signlet, as shown in

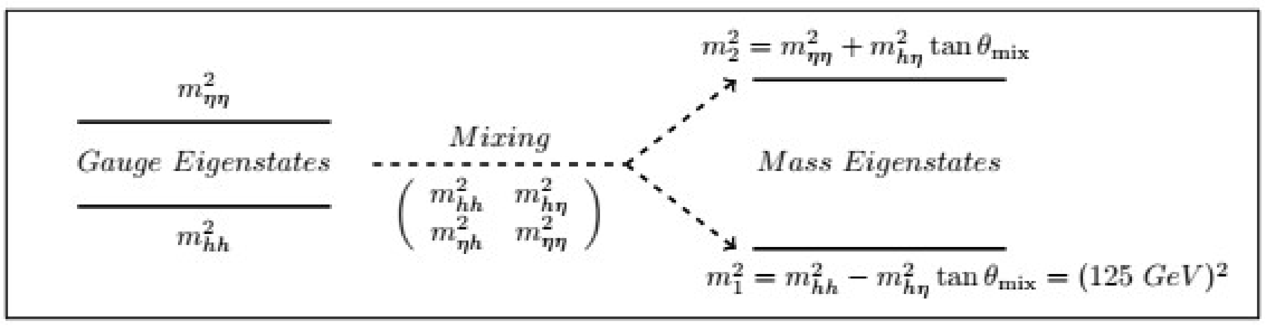

Figure 1. Level repulsion mechanism between a doublet Higgs boson and a singlet scalar state in the next-to-minimal composite Higgs model can lift the strong connection between the light Higgs and light top-partners.

Figure 1. Another noteworthy implication of the composite Higgs setup involve the modification of the Higgs couplings with other SM particles, from their SM reference values. We have systematically studied these modifications in various composite Higgs frameworks and constrained the relevant parameter space using the current Higgs data. We have also explored the Georgi-Machacek model composed of doublet and triplet Higgs bosons and investigated its phenomenology in the presence of higher dimensional operators. Motivated by the scarcity of any experimental signature probing the nature of the DM, we explore a scenario by extending the SM with a gauged U(1) symmetry, where instead of freezing-out from the thermal bath, the DM is frozen 'in' the early universe. We identify an energy dependent portal interaction between the visible matter and DM enabling 'UV freeze-in' of DM during the inflaton dominated epoch of reheating.